AN ABSTRACT OF THE DISSERTATION OF

<u>Xuemei Wan</u> for the degree of <u>Doctor of Philosophy</u> in <u>Pharmaceutical Sciences </u>presented on<u> June 1, 2018.</u>

Title: <u>Natural Products as Pharmacological Tools to probe Mitochondrial and Secretory Function in Cancer Cells</u>

Abstract approved:

_____

Jane E. Ishmael

Cancer is the second leading cause of death in the United States. To date, over 60% of current anticancer drugs were inspired by the discovery of chemical structure from nature, commonly known as a natural product. This work represents the biological characterization of several marine natural product compounds and their use as pharmacological tools to study mitochondrial and secretory functions in human cancer cells. The natural product mandelalide A was recently found to be a direct inhibitor of ATP synthase. We revealed that mandelalide A induces transient activation of the AMP-activated protein kinase pathway in an LKB1-dependent manner in several human cancer cells. Mandelalide A induces a synergistic affect in combination with first-line antitumor agents erlotinib and paclitaxel on EGFR mutant non-small cell lung cancer cells. Another new class of cytotoxic marine natural products, coibamide A and apratoxin A, were found to use autophagy-related protein 5 (ATG5) to promote cell death signaling. Mouse embryonic fibroblasts (MEFs) with a functional autophagy pathway were more sensitive to these rare natural product compounds which are inhibitors of the secretory pathway. The secretory pathway is a potentially novel, and future target for cancer therapy. We developed a workflow for discovery of new secretion inhibitors by combining a functional Gluc secretion assay with recognized cell viability assays. We used this workflow to identify 6 small molecules out of 3906 screened, and characterized the inhibitory activity of coibamide A in this screen. Using a cellular thermal shift assay, we identified the translocon protein Sec61 alpha as a direct binding target of coibamide A. We discovered that the resident

endoplasmic reticulum (ER) chaperone protein glucose regulated protein 78 (GRP78) is a critical, indirect target of coibamide A. High basal expression of GRP78 and distribution to cellular compartment outside the ER has been increasingly associated with human cancers. We identified upregulation of GRP78 expression in canine osteosarcoma cells and investigated the use of an anti-cancer drug OSU-03012 to target GPR78 overexpression in these cells. In summary, we concluded that activation of AMPK pathway by mandelalide A-like compounds, and inhibition of secretory function or secretory client proteins by coibamide A-like compounds could be beneficial as therapeutical strategies in cancer treatment.

Natural Products as Pharmacological Tools to probe Mitochondrial and
Secretory Function in Cancer Cells

by
Xuemei Wan

A DISSERTATION

submitted to

Oregon State University

in partial fulfillment of

the requirements for the

degree of

Doctor of Philosophy

Presented June 1, 2018
Commencement June 2018

<u>Doctor of Philosophy</u> dissertation of <u>Xuemei Wan</u> presented on <u>June 1, 2018</u>

APPROVED:

_____

Major Professor, representing Pharmaceutical Sciences

_____

Dean of the College of Pharmacy

_____

Dean of the Graduate School

I understand that my dissertation will become part of the permanent collection of Oregon State University libraries. My signature below authorizes release of my dissertation to any reader upon request.

_____

Xuemei Wan, Author

ACKNOWLEDGEMENTS

CONTRIBUTION OF AUTHORS

Dr. Jane E. Ishmael contributed to research design, data analysis, writing and editing. Xuemei Wan performed and managed experiments. Jeffrey D. Serrill, Daphne R. Mattos, Ian R. Humphreys and Karina N. Destine assisted with laboratory work. Dr. Kerry McPhail contributed to the isolation of coibamide A, mandelalide A and related structures and data analysis. Dr. Shay Bracha, Cheri Goodall provided some of reagents and assisted with the design of all canine projects. Dr. Christian Badr developed and kindly provided invaluable experimental advice and tools for our the study of coibamide A and drug screening projects. Dr. Shinya Oishi contributed to the synthesis of coibamide and analogous. Dr. Amos B. Smith III contributed to the synthesis of mandelalide A.

TABLE OF CONTENTS

TABLE OF CONTENTS (Continued)

TABLE OF CONTENTS (Continued)

LIST OF FIGURES

LIST OF FIGURES (Continued)

LIST OF FIGURES (Continued)

LIST OF FIGURES (Continued)

LIST OF TABLES

GENERAL INTRODUCTION

CHAPTER ONE

Xuemei Wan

Antitumor drugs from natural products

As the 2015 Nobel Prize has been awarded for the discovery of natural products, the greatest pride and optimism have been brought into the community of natural products. Natural products are evolutionarily optimized to be a ready-made drug and are still the best sources of drugs and drug leads [1]. The discovery of new compounds every year not only reveals many unique structures, but also helps to study novel mechanisms of actions through the addition of new molecular probes for biological studies. In addition to terrestrial plants, which historically have dominated as the original source of therapeutic agents, the marine enviroment, bacteria and fungi have also provided remarkable pharmaceutical agents, most notably in the areas of antibiotics and cancer therapies.

Nowadays, cancer is the second leading cause of death in the United States. In 2018, it is estimated that there will be 1,735,350 new cases of cancer of any site and an estimated 609,640 people will die of this disease (National Cancer Institute. http://seer.cancer.gov/statfacts/html/all.html). There is still a great need for the discovering of new anticancer drugs and new targets. Even though in the late 1990s targeted therapies, which were largely identifed from small molecule high throughput screening, drew much attention from pharmaceutical companies, chemotherapeutic agents derived from natural products still provide significant benifits and remain part of standard-of-care in the treatment of many solid tumors. Moreover, although targeted agents can produce significant effects in tumors with specific oncogenic addictions, the vast majority of common tumors were found to be not dependent on a single oncogenic mutation, which revitalized the development of natural products in cancer treatment [2]. Statistical analyses have revealed that natural products tend to have more chiral center, oxygen atoms and varied ring system [3]. This structural complexity gives natural products a tendency to be more selective to their target than fully synthetic drugs, and display less off-target effects [4].

To date, over 60% of the current anticancer drugs were developed from the discovery of natural products [1]. Historically, terrestrial plants have been used by various cultures for the treatment of many diseases, and they are still the primary

source for drug discovery. Taxanes are the most widely used drugs and they are semisynthetic analogues from the leaves of taxus, which has been used for thousands of years in traditional medicine in Asia. Paclitaxel and docetaxel are two of the most clinically effective drugs in chemotherapy and are used in the treatment of non-small cell lung cancer (NSCLC) [5], breast cancer [6] and ovarian cancer [7]. Some analogues have been approved for the treament of prostate, or are in clinical trials for bladder and brain cancers [8].

The marine habitat has also produced a significant number of anti-tumor agents that show high potency for inhibition of cancer cell growth *in vitro*, in preclinical *in vivo* models and in humans [9]. Cytarabine (cytosine arabinoside) as a chemotherapy medication to treat leukemia is the analogue of arabinose containing nuclesides discovered from Caribbean sponge *Tethya crypta* [10]. From 2004 [11], other marine product derivatives like trabectedin (ET473 [12], eribulin mesylate [13] and brentuximab vedotin (SGN-35) [14] have also been approved for cancer treatment. Even though covering 71% of the planet's surface, the deep sea is still the least explored and understood that only 5% of the deep sea has been pharmacologically expored [15].

In 2008, a new N-methylated lariat cyclic depsipeptide natural product structure coibamide A was discovered by Dr. Kerry McPhail. It was isolated from a cyanobacterial assemblage found in the Coiba National Park, Panama. The structure displayed significant selectivity and potent cytotoxicity at nanomolar concentrations against the National Cancer Institution-60 panel which indicated a potentially unique mechanism of action [16]. Recently we revealed that coibamide A induces mTOR-independent autophagy [17]. In addition, coibamide A inhibits the expression of vascular endothelial growth factor receptor 2 (VEGFR2) and the secretion of VEGF A, and suppresses tumor growth in glioblastoma xenografts [18]. In chapter 3, we continued the study of the mechanism of coibamide A-induced cell death and revealed that coibamide A promotes cross-signaling between ATG5-dependent autophagy and caspase-dependent apoptosis [19]. In chapter five we ulitlized a functional assay of cellular secretion to reveal that coibamide A is a secretory inhibitor and interacts directly with the translocon protein Sec61α.

A macrolide series of natural products, the mandelalides, were originally isolated from a South African *Lissoclinum* tunicate by Kerry McPhail's laboratory in small quantities in 2012. The original analogies were named mandelalide A-D [20] [21] [22]. Among them, mandelalide A shows low nanomolar cytotoxicity to cancer cell lines in NCI-60 panel with selectivity. These series of cytotoxic compounds attracted synthetic attention from multiple laboratories all over the world. Now the total synthesis of mandelalide A has been achieved [23, 24]. One other natural congener of 'A-type' mandelalides -- mandelalide L, was purified and revealed to have similar cytotoxic and antiproliferative potency as mandelalide A. In the meantime, we proved that mandelalide A inhibits ATP-linked respiration in living cells and inhibited complex V activity in isolated mitochondria. As a result, mandelalide A triggers caspase-dependent apoptosis in HeLa cells [25]. In view of the fact that mandelalide A shows differential activity in cancer cell lines, in chapter 2 we hypothesized that cells with an oxidative phenotype and/or compromised adaptive survival responses are most likely to exhibit mandelalide-induced changes in proliferation rate and activation of cell death signaling in vitro.

AMP-activated protein kinase in cancer

Just like motorcycles, living cells need inter-convertible chemicals that can provide energy. In cells, ADP and ATP are the pair of chemicals that create fuel by the reaction ATP ↔ ADP + phosphate. A high ratio of ATP to ADP maintained by catabolism is needed to drive energy-requiring processes in cells. For most eukaryotic organisms, cellular energy is generally produced in mitochondria by oxidation of the major products of glucose: pyruvate and NADH. The "molecular machine" – ATP synthase within the inner mitochondrial membrane is the enzyme that creates ATP [26]. Inhibition of ATP synthase is crucial to cells viability. The macrocyclic polypeptide mandelalide A was recently found to be a direct ATP synthase inhibitor, and it displayed nanomolar cytotoxic potency to cancer cell lines [25].

In living cells, ATP consumption and ATP generation need to maintain a balance between each other, which requires regulatory proteins that sense the ratio of ADP/ATP and AMP/ATP. The principal energy sensor in most eukaryotic cells is the AMP-activated protein kinase (AMPK). Once it detects increases in AMP/ATP and ADP/ATP ratios caused by an energetic stress, AMPK is activated to restore energy homeostasis by switching on catabolic pathways that generate ATP, while switching off ATP-consuming processes, including anabolic pathways required for cell growth and proliferation [27].

AMPK is a heterotrimeric protein kinase comprising of a catalytic α-subunit and regulatory β- and Y-subunits. The catalytic α-subunit contains a conventional Ser/Thr residue referred as Thr172 in the activation loop. In basal level two sites in the Y-subunit are occupied by ATP. During moderate stress, where the ratio of ADP/ATP increases, the ATP in Y-subunit are replaced by ADP, which promotes phosphorylation of Thr172, [28] causing a 100-fold increase in kinase activity [29]. During more severe stress, replacement of ATP by AMP at another site in the Y-subunit causes a further 10-fold allosteric activation. In mammals, the two major upstream kinases are the LKB1-STRAD-MO25 complex [30] and the Ca^{2+}/calmodulin-activated protein kinase kinases, especially CaMKKβ [31]. What need to be noticed is that the effects of AMP and /or ADP on Thr172

phosphorylation status are a result of their binding to AMPK, and such effects are independent of the upstream kinases and phosphatases that phosphorylate or dephosphorylate Thr172 [27]. The AMPK system can be activated by a large variety of metabolic and cellular stresses which increase ADP/ATP or AMP/ATP ratio, including glucose deprivation, hypoxia, oxidative stress, and anti-diabetic drugs including metformin and thiazolidinediones [32]. Activation of AMPK triggers phosphorylation of a group of substrates and results in the inhibition of ATP utilizing anabolic processes such as glycogen, protein, and lipid synthesis, as well as the activation of ATP-generating catabolic processes including fatty acid oxidation and glycolysis [27].

According to Warburg, most cancer cells predominantly produce their energy through a high rate of glycolysis followed by lactic acid fermentation even in the presence of oxygen. This aerobic glycolysis, also called Warburg effect [33], represents a fundamental metabolic difference between cancer and normal cells. AMPK as a key metabolic regulator can possibly play an active role in the inhibition of tumorigenesis through regulation of cell growth, cell proliferation, autophagy, stress response and cell polarity [34]. Indeed, several known drugs that are AMPK activators, such as salicylate and phenformin, have been shown to provide protection against development of cancer [35]. It has been revealed that AMPK regulation is associated with cancer at multiple molecular levels. Firstly, AMPK activation will down-regulate the activity of mammalian target of rapamycin complex-1 (mTORC1) by direct phosphorylation of both tuberous sclerosis complex 2 (TSC2) and raptor (mTORC1 binding partner) [36] [37]. As a key regulator of cell growth, activated mTORC1 promotes cell growth and proliferation, and ultimately result in tumor development. AMPK inhibits the mTOR pathway to reduce the tumor growth. Also AMPK-induced apoptosis and cell cycle arrest through activation of p53 [38], which is a most frequently mutated tumor suppressor gene in human cancer.

Given the critical functions of AMPK in cellular energy sensing and signaling, it is not surprising that AMPK plays an important role in normal cell growth regulation and tumorigenesis. Recent progress in the AMPK field implies an exciting potential for the use of AMPK activators in cancer treatment. In chapter 2, we investigate

the effect in AMPK signaling by exposure to the new ATP synthase inhibitor mandelalide A, and also explored the potential of utilizing mandelalides as adjuvant agent in chemotherapy in non-small cell lung cancer treatment.

Autophagy, apoptosis and their crosstalk

Apoptosis is the process of programmed cell death that has morphologically characteristic forms. It is considered a vital component of various processses, including cell development, cell turnover, functionality of the immune system, atrophy and chemical-induced cell death [39]. The mechanims of apoptosis are highly complex and sophosticated, involving an energy-dependent cascade of molecular events. One branch of the apoptotic pathway is the extrinsic death receptor pathway that is triggered by death ligand and activates cysteine-aspartic proteases 8 (caspase 8). Another apoptosis pathway is the intrinsic or mitochondrial pathway and initiates caspase 9 activation. Each pathway will converge on the execution pathway which begins with caspase 3, caspase 6 and caspase 7 activation, following the cleavage of various substrates including poly (ADP-ribose) polymerase 1 (PARP-1), cytokeratins and others. The whole process of apotosis is completed by the formation of apoptotic bodies and finally phagocytosis of the apoptotic bodies by adjacent parenchymal cells, neoplastic cells or macrophages [39].

Macroautophagy (hereafter known as autophagy) is the degradation of dysfunctional cellular components through the fusion of double-membrane vesicles (autophagosomes) with lysosomes [40]. This protective response, activated by cell stress or nutrient deprivation, is essential for cellular adaptation to recycle nutrient resources [41]. The autophagy pathway starts with the formation of an isolation membrane initiated by the ULK1 (UNC-51-like kinase) complex which is negatively regulated by the mTOR complex (mTORC1). The lipid kinase vacuolar protein sorting 34(VPS34)-Beclin 1complex, which is usually inactivated by anti-apoptotic BCL-2 family, activates the nucleation of the isolation membrane. The elongation of autophagasomal membrane then relies on two ubiquitin-like (UBL) protein conjugation systems: ATG12-ATG5 and the protein light chain 3 (LC3)-phosphatidylethanolamine system [42]. Conjugation of phosphatidylethan- olamine to the C terminus of LC3-I produces the LC3-II form that tightly associates with the autophagosomal membrane [43]. In addition, the polyubiquitin-binding protein p62/SQSTM1 is found directly interacting with LC3 during the formation of autophagosome formation, and it will be destroyed in autophagy, hence a

reduction in p62/SQSTM1 abundance can be used as a useful indirect measurement of autophagy [44]. Autophagy is known to play a role in many diverse disease processes including cancer, aging, and autoimmune disease. It can paradoxically have pro-death or pro-survivial functions depending on the context.

Autophagy and apoptosis often occur in the same cell, mostly in a sequence in which autophagy precedes apoptosis [45]. Many stimuli that ultimately cause cell death also trigger autophagy because many signal tranduction pathways that are activated by intrinsic cell stress regulate both autophagy and apoptosis. This applies to transcription factor p53, several BH3 (BCL-2 homology 3)-only proteins, death associated protein kinase (DAPK) and JUN N-terminal kinase (JNK) [46]. Although autophagy generally constitutes a cytoprotective process, autophagosomes or autophagy-related (ATG) proteins may participate in cell death signaling in some context. Autophagosome formation, in which caspase 8 forms a complex with ATG5 and colocalizes with LC3 and P62, rather than the degradative process, has been implicated in the activation of caspase 8 [47]. ATG proteins, such as ATG12 and ATG7, also contribute to lethal signaling independently of the autophagic process[46].

By contrast, there is inhibitory crosstalk between autophagy and apoptosis. For example, autophagy can attenuate cell death by selectively reducing the abundance of pro-apoptotic proteins in the cytosol. The modification of ubiquitylation enable the proteins to interact with autophagy receptors including p62/SQSTM1, that bind both ubiquitylated substrates and LC3 to process autophagy [48]. In the other way, caspases can digest several essential autophagy proteins, resulting in the inactivation of the autophagic programme, perhaps in the purpose to abort its cytoprotective function and accelerate cellular demise [46].

In our study of the marine natural product coibamide A, we found that this depsipeptide induces mTOR-independent autophagy in cultured human cells and mouse fibroblasts within an hour of treatment [17]. Moreover, coibamide A effectively induced caspase-dependent apoptosis in ATG5-null cells, which implies that autophagy serves as an indirect stress response that persists in dying cells.

In the following study (chapter 3) we extended our analysis of wild-type and autophagy-deficient mouse embryonic fibroblast (MEFs) to gain a better understanding of the role of coibamide-induced autophagy in cell fate.

The Secretory Pathway and GRP78 as potential targets for cancer therapy

In mammalian cells, almost one third of proteins reside in or transit through the secretory pathway. Secretory proteins are segregated from the cytosol and translocated across the ER membrane [49]. Nascent peptide chains are co-translationally translocated through the ER membrane at sites termed translocons [50]. The heterotrimeric Sec61 complex forms the structural core of the translocon channel [51]. After entering the ER lumen, most nascent polypeptide chains are rapidly modified by covalent addition of one or more oligosaccharides to nitrogen of asparagine or arginine side-chains, called N-linked glycosylation. Recent studies have revealed the critical contribution of the secretory pathway in cancer development, which raises the possibility of targeting the secretory pathway, such as inhibition of translocation in cancer treatment. One translocation inhibitor with anticancer properties is the natural product apratoxin A [52]. Given the increasing need for discovery of more secretory inhibitors, in chapter 5 we developed a novel screening workflow using the combination of a functional Gluc secretion assay with assessment of cell viability. We performed an initial high-throughput screening from small molecule library and characterized the activity of several known natural products in preparation for future use of these assays to screen new natural product libraries for both general inhibitors of secretory function and/or specific inhibitors of the Sec61 translocon complex.

Glucose regulated protein 78 (GRP78) is a member of heat shock protein 70 (Hsp70) family and mainly stays in the ER as a resident chaperone protein [53]. GRP78 associates with the Sec61 channel complex on the luminal side of the ER and is the only soluble protein necessary and sufficient to control the closure of the translocon channel and engaged in the early stages of translocation [54]. Working with other ER chaperones, GRP78 binds to nascent proteins to prevent aggregation as most of them will be N-linked glycosylated [55].On the other hand, GRP78 also regulates the unfolded protein response (UPR) by association with the major ER stress sensors on the ER membrane [56]. In past decades, genome wide and immunohistochemical analyses of clinical samples from patients has shown that GRP78 is overexpressed in several aggressive tumors refractory to

therapy like prostate cancer [57], breast cancer [58] and glioblastoma [59]. Increased levels of GRP78 seems to be the key survival feature for cancer cells in that they are able to chronically upregulate the UPR without however inducing apoptosis. Even though the role of GRP78 in development of chemoresistance is just revealed, and the mechanism is still under study [60], it has been widely believed that GRP78 inhibition will be a promising direction for chemotherapy development and that GRP78 will emerge as a druggable target. In chapter 4, we sought to characterize GRP78 expression and patterns of cell signaling in cultured canine osteosarcoma cells, relative to a range of human cancer cell types that included those known to display high-level GRP78 expression. We find that canine osteosarcoma and human cancer cells share a similar adaptive survival response to ER stress and that GRP78 may eventually be exploited in canines and humans for therapeutic advantage.

In our collaborative studies of the chemistry and biology of coibamide A we have found that the marine natural product coibamide A is a putative secretory pathway inhibitor. Coibamide A selectively inhibits vascular endothelial growth factor receptor 2 (VEGFR2) expression in human umbilical vein endothelial cells (HUVECs) and behaves like apratoxin A in several basic cellular assays [18]. In chapters 3 and 5 we investigated the effect of coibamide A on the secretory pathway with a particular emphasis on changes in GRP78. As a client of the Sec61 translocon, we find that nascent GRP78 is particularly vulnerable to coibamide A. We found that coibamide A decreases the expression of GRP78 consistent with the hypothesis that GRP78 is an indirect target of coibamide A. This particular aspect of coibamide-induced toxicity, and the potential for indirect targetting of GRP78 biosynthesis to disrupt ER proteostasis, is a particularly exciting consequence of coibamide A action. In general, translocon inhibitors may be attractive as a future class of chemotherapeutic agents especially for aggressive human (and canine) cancers characterized by GRP78 overexpression and poor prognosis.

Reference

1. Newman, D.J. and G.M. Cragg, *Natural products as sources of new drugs over the 30 years from 1981 to 2010.* J Nat Prod, 2012. **75**(3): p. 311-35.
2. Basmadjian, C., et al., *Cancer wars: natural products strike back.* Front Chem, 2014. **2**: p. 20.
3. Reichel, T.H.R.M.B.H.M.F., *Statistical Investigation into the Structural Complementarity of Natural Products and Synthetic Compounds.* Angewandte Chmie

, 1999. **38**(5): p. 643-647.
4. Ganesan, A., *The impact of natural products upon modern drug discovery.* Curr Opin Chem Biol, 2008. **12**(3): p. 306-17.
5. Hanna, N., et al., *Systemic Therapy for Stage IV Non-Small-Cell Lung Cancer: American Society of Clinical Oncology Clinical Practice Guideline Update Summary.* J Oncol Pract, 2017. **13**(12): p. 832-837.
6. M.J.PiccartF.Cardoso, *Progress in systemic therapy for breast cancer: an overview and perspectives.* European Journal of Cancer Supplements, 2003. **1**(2): p. 56-69.
7. Ozols, R.F., et al., *Phase III trial of carboplatin and paclitaxel compared with cisplatin and paclitaxel in patients with optimally resected stage III ovarian cancer: a Gynecologic Oncology Group study.* J Clin Oncol, 2003. **21**(17): p. 3194-200.
8. Villanueva, C., et al., *Cabazitaxel: a novel microtubule inhibitor.* Drugs, 2011. **71**(10): p. 1251-8.
9. Newman, D.J. and G.M. Cragg, *Marine-sourced anti-cancer and cancer pain control agents in clinical and late preclinical development.* Mar Drugs, 2014. **12**(1): p. 255-78.
10. Werner. Bergmann, a.D.C.B., *CONTRIBUTIONS TO THE STUDY OF MARINE PRODUCTS. XXXIX. THE NUCLEOSIDES OF SPONGES. III. SPONGOTHYMIDINE AND SPONGOURIDINE.* The Journal of Organic Chemistry, 1955. **20**(11): p. 1501-1507.
11. Ruiz-Torres, V., et al., *An Updated Review on Marine Anticancer Compounds: The Use of Virtual Screening for the Discovery of Small-Molecule Cancer Drugs.* Molecules, 2017. **22**(7).
12. Rinehart, K.L., *Antitumor compounds from tunicates.* Med Res Rev, 2000. **20**(1): p. 1-27.
13. Schafer, E.S., et al., *A phase 1 study of eribulin mesylate (E7389), a novel microtubule-targeting chemotherapeutic agent, in children with refractory or recurrent solid tumors: A Children's Oncology Group Phase 1 Consortium study (ADVL1314).* Pediatr Blood Cancer, 2018: p. e27066.
14. Newland, A.M., et al., *Brentuximab vedotin: a CD30-directed antibody-cytotoxic drug conjugate.* Pharmacotherapy, 2013. **33**(1): p. 93-104.
15. Ramirez-Llodra, E., et al., *Deep, diverse and definitely different: unique attributes of the world's largest ecosystem.* Biogeosciences, 2010. **7**(9): p. 2851-2899.
16. Medina, R.A., et al., *Coibamide A, a potent antiproliferative cyclic depsipeptide from the Panamanian marine cyanobacterium Leptolyngbya sp.* J Am Chem Soc, 2008. **130**(20): p. 6324-5.

17. Hau, A.M., et al., *Coibamide A induces mTOR-independent autophagy and cell death in human glioblastoma cells.* PLoS One, 2013. **8**(6): p. e65250.

18. Serrill, J.D., et al., *Coibamide A, a natural lariat depsipeptide, inhibits VEGFA/VEGFR2 expression and suppresses tumor growth in glioblastoma xenografts.* Invest New Drugs, 2016. **34**(1): p. 24-40.

19. Wan, X., et al., *ATG5 Promotes Death Signaling in Response to the Cyclic Depsipeptides Coibamide A and Apratoxin A.* Mar Drugs, 2018. **16**(3).

20. Smith, A.B., 3rd and W.M. Wuest, *Evolution of multi-component anion relay chemistry (ARC): construction of architecturally complex natural and unnatural products.* Chem Commun (Camb), 2008(45): p. 5883-95.

21. Smith, A.B., 3rd and C.M. Adams, *Evolution of dithiane-based strategies for the construction of architecturally complex natural products.* Acc Chem Res, 2004. **37**(6): p. 365-77.

22. Sikorska, J., et al., *Mandelalides A-D, cytotoxic macrolides from a new Lissoclinum species of South African tunicate.* J Org Chem, 2012. **77**(14): p. 6066-75.

23. Veerasamy, N., et al., *Enantioselective Total Synthesis of Mandelalide A and Isomandelalide A: Discovery of a Cytotoxic Ring-Expanded Isomer.* J Am Chem Soc, 2016. **138**(3): p. 770-3.

24. Nguyen, M.H., et al., *Synthetic Access to the Mandelalide Family of Macrolides: Development of an Anion Relay Chemistry Strategy.* J Org Chem, 2018.

25. Nazari, M., et al., *New Mandelalides Expand a Macrolide Series of Mitochondrial Inhibitors.* J Med Chem, 2017. **60**(18): p. 7850-7862.

26. Okuno, D., R. Iino, and H. Noji, *Rotation and structure of FoF1-ATP synthase.* J Biochem, 2011. **149**(6): p. 655-64.

27. Hardie, D.G., F.A. Ross, and S.A. Hawley, *AMPK: a nutrient and energy sensor that maintains energy homeostasis.* Nat Rev Mol Cell Biol, 2012. **13**(4): p. 251-62.

28. Hawley, S.A., et al., *Characterization of the AMP-activated protein kinase kinase from rat liver and identification of threonine 172 as the major site at which it phosphorylates AMP-activated protein kinase.* J Biol Chem, 1996. **271**(44): p. 27879-87.

29. Suter, M., et al., *Dissecting the role of 5'-AMP for allosteric stimulation, activation, and deactivation of AMP-activated protein kinase.* J Biol Chem, 2006. **281**(43): p. 32207-16.

30. Shaw, R.J., et al., *The tumor suppressor LKB1 kinase directly activates AMP-activated kinase and regulates apoptosis in response to energy stress.* Proc Natl Acad Sci U S A, 2004. **101**(10): p. 3329-35.

31. Hawley, S.A., et al., *Calmodulin-dependent protein kinase kinase-beta is an alternative upstream kinase for AMP-activated protein kinase.* Cell Metab, 2005. **2**(1): p. 9-19.

32. Fryer, L.G., A. Parbu-Patel, and D. Carling, *The Anti-diabetic drugs rosiglitazone and metformin stimulate AMP-activated protein kinase through distinct signaling pathways.* J Biol Chem, 2002. **277**(28): p. 25226-32.

33. Vander Heiden, M.G., L.C. Cantley, and C.B. Thompson, *Understanding the Warburg effect: the metabolic requirements of cell proliferation.* Science, 2009. **324**(5930): p. 1029-33.

34. Wang, W. and K.L. Guan, *AMP-activated protein kinase and cancer.* Acta Physiol (Oxf), 2009. **196**(1): p. 55-63.

35. Shackelford, D.B., et al., *LKB1 inactivation dictates therapeutic response of non-small cell lung cancer to the metabolism drug phenformin.* Cancer Cell, 2013. **23**(2): p. 143-58.

36. Inoki, K., et al., *Rheb GTPase is a direct target of TSC2 GAP activity and regulates mTOR signaling.* Genes Dev, 2003. **17**(15): p. 1829-34.

37. Gwinn, D.M., et al., *AMPK phosphorylation of raptor mediates a metabolic checkpoint.* Mol Cell, 2008. **30**(2): p. 214-26.

38. Jones, R.G., et al., *AMP-activated protein kinase induces a p53-dependent metabolic checkpoint.* Mol Cell, 2005. **18**(3): p. 283-93.

39. Elmore, S., *Apoptosis: a review of programmed cell death.* Toxicol Pathol, 2007. **35**(4): p. 495-516.

40. Kerr, J.F., *History of the events leading to the formulation of the apoptosis concept.* Toxicology, 2002. **181-182**: p. 471-4.

41. Mizushima, N., et al., *A protein conjugation system essential for autophagy.* Nature, 1998. **395**(6700): p. 395-8.

42. Mehrpour, M., et al., *Overview of macroautophagy regulation in mammalian cells.* Cell Res, 2010. **20**(7): p. 748-62.

43. Kabeya, Y., et al., *LC3, GABARAP and GATE16 localize to autophagosomal membrane depending on form-II formation.* J Cell Sci, 2004. **117**(Pt 13): p. 2805-12.

44. Klionsky, D.J., et al., *Guidelines for the use and interpretation of assays for monitoring autophagy (3rd edition).* Autophagy, 2016. **12**(1): p. 1-222.

45. Maiuri, M.C., et al., *Self-eating and self-killing: crosstalk between autophagy and apoptosis.* Nat Rev Mol Cell Biol, 2007. **8**(9): p. 741-52.

46. Marino, G., et al., *Self-consumption: the interplay of autophagy and apoptosis.* Nat Rev Mol Cell Biol, 2014. **15**(2): p. 81-94.

47. Young, M.M., et al., *Autophagosomal membrane serves as platform for intracellular death-inducing signaling complex (iDISC)-mediated caspase-8 activation and apoptosis.* J Biol Chem, 2012. **287**(15): p. 12455-68.

48. Shaid, S., et al., *Ubiquitination and selective autophagy.* Cell Death Differ, 2013. **20**(1): p. 21-30.

49. Walter, P. and A.E. Johnson, *Signal sequence recognition and protein targeting to the endoplasmic reticulum membrane.* Annu Rev Cell Biol, 1994. **10**: p. 87-119.

50. Johnson, A.E. and M.A. van Waes, *The translocon: a dynamic gateway at the ER membrane.* Annu Rev Cell Dev Biol, 1999. **15**: p. 799-842.

51. Gorlich, D., et al., *A mammalian homolog of SEC61p and SECYp is associated with ribosomes and nascent polypeptides during translocation.* Cell, 1992. **71**(3): p. 489-503.

52. Liu, Y., B.K. Law, and H. Luesch, *Apratoxin a reversibly inhibits the secretory pathway by preventing cotranslational translocation.* Mol Pharmacol, 2009. **76**(1): p. 91-104.

53. LM, H., *The ER function BiP is a master regulator of ER function.* Mt Sinai J Med, 2004. **71**((5)): p. 289-97.

54. Hamman, B.D., L.M. Hendershot, and A.E. Johnson, *BiP maintains the permeability barrier of the ER membrane by sealing the lumenal end of the translocon pore before and early in translocation.* Cell, 1998. **92**(6): p. 747-58.

55. Otero, J.H., B. Lizak, and L.M. Hendershot, *Life and death of a BiP substrate.* Semin Cell Dev Biol, 2010. **21**(5): p. 472-8.
56. Hendershot, L.M., et al., *Localization of the gene encoding human BiP/GRP78, the endoplasmic reticulum cognate of the HSP70 family, to chromosome 9q34.* Genomics, 1994. **20**(2): p. 281-4.
57. Daneshmand, S., et al., *Glucose-regulated protein GRP78 is up-regulated in prostate cancer and correlates with recurrence and survival.* Hum Pathol, 2007. **38**(10): p. 1547-52.
58. Scriven, P., et al., *Activation and clinical significance of the unfolded protein response in breast cancer.* Br J Cancer, 2009. **101**(10): p. 1692-8.
59. Pyrko, P., et al., *The unfolded protein response regulator GRP78/BiP as a novel target for increasing chemosensitivity in malignant gliomas.* Cancer Res, 2007. **67**(20): p. 9809-16.
60. Roller, C. and D. Maddalo, *The Molecular Chaperone GRP78/BiP in the Development of Chemoresistance: Mechanism and Possible Treatment.* Front Pharmacol, 2013. **4**: p. 10.

Mandelalide A activates AMP-activated protein kinase signaling and has the potential to enhance the efficacy of Erlotinib in EGFR mutant Non-Small Cell Lung Cancer cells

CHAPTER 2

Xuemei Wan, Jeffrey D. Serrill, Ian R. Humphreys, Minh H. Nguyen, Amos B. Smith III, Kerry L. McPhail, and Jane E. Ishmael

Abstract

Microbial secondary metabolites have historically been an important source of inspiration for new drugs. Mandelalide A, originally isolated from *Lissoclinum* tunicate, was found to have selective cancer cell cytotoxicity and was recently revealed to be a direct inhibitor of mitochondrial ATP synthase. We investigated the action of mandelalide A in representative human glioblastoma cells, lung cancer cells and mouse embryonic fibroblast (MEFs) to better understand it's mechanism. Mandelalide A showed anti-proliferative and cytotoxic effects in human HeLa cervical and U87-MG glioblastoma cells. Type A mandelalide (A and L) induced transient AMPK activation in a liver kinase B1(LKB1) – dependent way. AMPKα deficient MEFs lacked AMPK activation by mandelalide A and were more vulnerable to mandelalide-induced toxcity than AMPKα wild-type MEFs. The dominant upstream kinase of AMPK, LKB1, is frequently mutated in human Non-Small Cell Lung Cancer cells (NSCLC). We found AMPK activation by mandelalide A in NSCLCs to be dependent on LKB1 status but is not predictive of the anti-proliferative action of mandelalide A. However, when mandelalide was tested in combination with clinically relevant compounds, we found the combination of erlotinib or paclitaxel with mandelalide A has a synergistic effect on EGFR mutant NSCLC 11-18 and pC-9 cell lines. The selective cytotoxicity of mandelalide A, and the potential for a synergistic action when used in combination with first-line anti-cancer drugs, raises the biological significance of mandelalide and warrants further pre-clinical evaluation of this compound as an anti-cancer agent.

Introduction

Marine secondary metabolites from invertebrates such as tunicates and sponges are important sources of novel drugs with diverse structures and biological mechanisms [1, 2]. In past decades, several marine natural products have been advanced for consideration as anticancer drugs [3, 4]. Macrolide natural products mandelalides were originally isolated from a South African *Lissoclinum* tunicate by Kerry McPhail's laboratory in small quantities in 2012. These compounds were named mandelalide A-D [5] [6] [7]. Among them, mandelalide A, B and L showed low nanomolar cytotoxicity to mouse Neuro-2A neuroblastoma (A and B), human HeLa cervical cancer and NCI-H460 lung cancer cell lines [8]. Mandelalide B also showed low nanomolar cytotoxicity to human U87-MG glioblastoma and HCT116 colon cancer cells [7] [9]. This series of cytotoxic compounds attracted synthetic attention from multiple laboratories all over the world [10] [11] [12] [13] [14], leading to the total synthesis of mandelalide A [13, 15]. In the meantime, we determined that mandelalide A inhibits ATP-linked respiration in living cells and through inhibition of mitochondrial complex V activity. As a mitochindrial toxin, mandelalide A eventually triggers caspase-dependent apoptosis in sensitive cell types [8]. In view of the fact that mandelalide A shows selective and differential activity in cancer cell lines, we hypothesized that cells with an oxidative phenotype and/or compromised adaptive survival responses are most likely to exhibit mandelalide-induced changes in proliferation rate and activation of cell death signaling.

AMP-activated protein kinase (AMPK) is the principal energy sensor in most eukaryotic cells. In mammalian cells, AMPK is activated by metabolic stresses that induce increases in cellular AMP/ATP ratio, ADP/ATP ratio or cytosolic Ca^{2+} concentration. AMPK is a heterotrimeric protein complex comprised of a catalytic α subunit and regulatory β and γ subunits. Competitive Binding of AMP and ADP to the γ subunit allosterically activates the complex, improving the ability of AMPK α subunit to serve as a substrate for phosphorylation on in the activation loop of the α subunit by the primary upstream kinase Liver Kinase B1 (LKB1) [16].

Activation of AMPK switches on catabolic pathways that generate ATP while switching off biosynthetic pathways that consume ATP. For example, AMPK

phosphorylation leads to the inactivation of acetyl CoA carboxylase (ACC2), and ultimately activates fatty acid oxidation. On the other hand, AMPK phosphorylates ACC1 to inhibit fatty acid synthesis. [17]. In our previous studies of mandelalide A, we found that the cytotoxic potential of this structure is based primarily on the basal metabolic phenotype of cell rather than histological selectivity or genetic background [8]. We hypothesized that cells switch metabolic phenotype and also utilize the AMPK signaling pathway to adapt to changes such as energy stress caused by mandelalide exposure.

LKB1 is known as a tumor suppressor, is the crucial upstream kinase for activation of the AMPK pathway [18, 19]. It has been shown that biguanide structures are more effective in the treatment of mouse tumors that lack a functional LKB1-AMPK pathway [20]. Moreover, LKB1 is one of the most commonly mutated genes in sporadic human lung cancers [21], particularly in non-small cell lung carcinoma (NSCLC) with a least 15-35% of cases have this lesion [22]. In addition, 20% of cervical carcinomas were found to be somatically mutated in LKB1 [23]. Therefore, LKB1 and AMPK responses could identify new targets and drugs for cancer therapy.

In the present study we utilized human HeLa cervical cancer cells, glioblastoma cells, non-small cell lung carcinoma (NSCLC) cells and mouse embryonic fibroblasts (MEFs) to study the status of AMPK signaling in response to mandelalides A and L.

About one quarter of NSCLC had muations in the epidermal growth factor receptor (EGFR) tyrosine kinase domain and these were associated with increased receptor expression in 75% of cases [24]. EGFR receptor tyrosine kinase inhibitors (TKIs), such as erlotinib have been used in EGFR mutated cases to improve the effectiveness of treatment. We also tested the effect of combining mandelalide A with two clinically relevant chemotherapeutic agents: erlotinib and paclitaxel in EGFR mutated NSCLCs.

Materials and Methods

Mammalian Cell culture

All cell lines were maintained as adherent cultures under standard laboratory conditions at 37°C with 5% CO_2. U87-MG and HeLa were cultured in Minimum Essential Media (Corning Cellgro, Manassas VA) with 10% fetal bovine serum (FBS; VWR, Radnor PA), L-glutamine (2mM), and 1% penicillin and streptomycin. MEFs wildtype and AMPK dKO cells were cultured in Dulbecco's modified Eagle's medium (Corning Cellgro) with 10% FBS, 1% penicillin and streptomycin. NCI-H460, H292, H3122, 11-18 and PC-9 cells were cultured in RPMI-1640 (Sigma Aldrich, St. Louis US) supplemented with 10% FBS; and 1% penicillin and streptomycin. A549 cells were cultured in F-12K medium (Thermo Fisher Scientific Inc., Waltham CA) with 10% FBS, 1% penicillin and streptomycin.

Chemicals and reagents

The synthesis of mandelalides A and L has been described previously [15]. Oligomycin A was purchased from Santa Cruz Biotech (cat# sc-201551, Dallas TX). Dorsomorphin was from Abcam (cat# ab120843, Cambridge UK). Paclitaxel was from Sigma Aldrich (cat #T7402, Darmstadt, Germany). Erlotinib was from Enzo Life Sciences (Farmingdale, NY USA).

All of the reagents were reconstituted in 100% DMSO, aliquot and stored in amber borosilicate glass vials at -20°C for use in biological studies. Cell culture-grade DMSO was used as the vehicle for all treatments and final concentrations of DMSO for *in vitro* experiments never exceeded 0.1%.

Primary and secondary antibodies were from Cell Signaling Technology, Inc. (Danvers, MA, USA). Specific codes were as follows: AMPK (#5831), pAMPKα T172 (#50081), ACC (#3676), pACC S79 (#11818), GAPDH (#5174). General laboratory reagents were from VWR International (Radnor, PA, USA). General laboratory reagents for biological studies were obtained from VWR.

Cell lysis and immunublot analysis

Cell lysates were prepared using freshly made ice-cold Lysis Buffer containing 50nM Tris-HCl (PH 7.5), 1mM EDTA, 1mM EGTA, 1% Triton X-100, 0.27 M Sucrose, 50mM sodium fluoride, 1mM sodium orthovanadate, 5mM sodium pyrophosphate, 1mM PMSF and 1mM benzamidine. All cell lysates were cleared by centrifugation at 16,000x*g* for 20min at 4°C and the protein concentration was determined by bicinchoninic acid (BCA) method indicated by the manufacturer's recommendations (Thermo Fisher Scientific)

For immunoblot analysis, cell lysates were adjusted by protein concentration and equal amounts (50μg) separated by SDS-PAGE gel. Then proteins were transferred onto PVDF membrane (Thermo Fisher Scientific) in transfer buffer contains 25nM Tris, 192mM glycine, 10%methanol. Membranes were then blocked in 5%(w/v) non-fat milk in 50mM Tris-HCl, pH7.4, 150mM NaCl (TBS) with 0.05% Tween-20 (TBS-T), and incubated at 4°C for 16hrs with appropriate primary antibody in 5%(w/v) bovine serum albumin (BSA) in TBS-T. On the following day, membranes were washed with TBS-T for 2 x 5min, then incubated in appropriate HRP-conjugated secondary antibody for 1hr at room temperature. Membranes were then washed in TBS-T for 3 x 5min, and target proteins were detected by chemiluminescence (Amersham™ ECL™ Chemiluminescent Labeling and detection Reagents for Proteins, GE Healthcare), using myECL™ Imager system (Thermo Scientific).

Cell viability assay

Cells were seeded at a density of 3000 cells/well in 100μL of complete medium in 96-well plates. After 18 hr, cells were treated with mandelalide A or vehicle (0.1%DMSO). Cell viability was assessed using a CellTiter-Glo® Luminescent Cell Viability Assay kit (Promega Corp., Madison, WI) or standard 3-(4,5-dimethylthiazol-2-yl)-2,5-diphenyltetrazolium bromide (MTT) assays, with the viability of vehicle-treated cells defined as 100%.

To determine 50% of Growth inhibition, the cell viability at the time of treatment was determined as T_0. After 72hr, Cell viability was measured as C. Then the percentage of growth was decided by the formula as follows [25] [26] :

$$\text{Percentage of Growth (\% Growth)} = \frac{(T_1 - T_0)}{(C - T_0)} \times 100\%$$

T_0 --- the cell viability at time starting the treatment.

T_1 – the cell viability of drug treated group.

C-- the cell viability in vehicle treatment

Non-linear regression analysis was done using Graphpad Prism Software (La Jolla, CA). 50% reduction in cell growth (GI_{50}), total growth inhibition (TGI) and 50% cytotoxcity (LC_{50}) were determined at the concentrations of % Growth = 50%, 0, -50%, respectively.

Drug combination assay

Human 11-18 or PC-9 lung cancer cells were seeded at density of 1,000/well in 384 well white-wall solid flat bottom plates (Greiner Bio-One) with 50µL of complete medium. After 18hr, cells were treated with vehicle (0.1% DMSO) or titration of mandelalide A (0.6 nM-1 µM) in combination with paclitaxel (0.2 – 100 nM) or erlotinib (1nM-1µM). Treatment was completed by Hewlett-Packard (HP) Tecan D300 Digital dispenser. After 72hr of treatment, cell viability was assessed using a CellTiter-Glo® Luminescent Cell Viability Assay kit (Progema Corp). The heatmap was generated to depict the average percentage cell viability normalized to vehicle (0.1%DMSO) at different concentrations and combinations.

To evaluate the effect of drug combination, the method of Chou and Talalay [27, 28] was used with the help of CompuSyn program (ComboSyn, Inc,. Paramus, NJ. USA). The percentages of cell viability of cells treated with mandelalide A , erlotinib and paclitaxel alone, or combination of constant ratio of mandelalide A with erlotinib (1:1), or mandelalide A with paclitaxol (30:1) were used for the analysis.

Median-effect relationships were determined by generating dose-response curves for mandelalide A, erlotinib, paclitaxel, and their combinations. Medium-effect dose

(D_m indicating concentrations that inhibits cell growth by 50%) and slope of the curve (m) from each median-effect relationships were used in the equation as follows to calculate D_x .

$$D_X = D_m[f_a/(1 - f_a)]^{1/m} \quad [27]$$

Where the fa is fraction affected (fa=0.5 mean 50% reduction of cell viability.)

Combination index (CI) value is a quantitative measure of the degree of drug interaction and were then calculated at different combinations of drug concentrations. The Combination Index (CI) was calculated by the CompuSyn software which takes into account both the potency (Dm) and shape of the dose-effect curve (m). CI equation for two drugs

$$CI = \frac{(D)_1}{(D_x)_1} + \frac{(D)_2}{(D_x)_2} [27]$$

where in the denominators, $(D_x)_1$ is the dose of $Drug_1$ alone that inhibits x%, likewise for $(D_x)_2$. In the numerators, $(D)_1$ is the portion of Drug 1 in combination $(D)_1$ + $(D)_2$ also inhibits x%, likewise $(D)_2$.

According to Chou and Talalay, a CI of <1 indicates a synergistic interaction, a CI of 1 indicates an additive interaction, and a CI of >1 indicates an antagonistic interaction[27] [29].

Data Analysis

Dose-response relationships were analyzed using GraphPad Prism Software (Graphpad Software Inc. San Diego, CA). GI_{50}, TGI, LC_{50}, or EC_{50} values were determined by nonlinear regression analysis fit to a logistic equation. For immunoblot analysis, target protein signals were normalized to the intensity of controls (Tubulin or GAPDH) and quantified relative to control using ImageJ software (rsbweb.nih.gov/ij). Statistical significance of data derived from cell viability assays and quantification of immunoblot assay were performed using a one-way analysis of variance(ANOVA) followed by a Student's *t*-test comparing

untreated controls and treatment groups. p-values of 0.05 or less were considered statistically significant.

Results

Analysis of LKB1/AMPK status in representative mandelalide-sensitive cell types.

As the mandelalides represent a series of natural product inhibitors of ATP synthase [8], we reasoned that activation of AMPK signaling could represent one mechanism by which cancer cells may adapt to decreases in intracellular ATP and remain viable. To test this hypothesis we compared the growth characteristics of human HeLa cervical cancer and U87-MG glioblastoma cells in response to mandelalide A (Figure 2.1), and also the status of LKB1/AMPK signaling in response to acute treatment (Figure 2.2). In earlier studies we found human HeLa cervical cancer cells to be a particularly sensitive to mandelalides, to the extent that they were a useful model cell line for comparative analysis of natural and synthetic mandelalides, whereas U87-MG cells tended to be less sensitive [8] [9]. These cell types were seeded at low density and concentration-response relationships were generated to compare the antiproliferative and cytotoxicity activity of mandelalide A against both cell types. By recording the cell density at the time of mandelalide addition (time = zero; black dashed line), as well as the assay end point, it was possible to distinguish the transition from an antiproliferative response (above the dashed line) to a cytotoxic response (below the dashed line) using non-linear regression analysis of the data. These results demonstrated strong antiproliferative activity, and partial cytotoxic efficacy, of mandelalide A against both cell types (Figure 2.2A). HeLa cells remained slightly more sensitive than U87-MG cells under these conditions, with GI_{50} values of 1.0 nM versus 1.5 nM and TGI values of 3.7 nM and 8.2 nM for HeLa and U87-MG, respectively (Table 2.2).

We compared the status of AMPK and liver kinase B1 (LKB1) in both cell types after short exposures to mandelalide A. Liver kinase B1 (LKB1) is the major kinase that phosphorylates the $AMPK\alpha$ at Thr172 in conditions of energy stress [18, 19]. Treatment of cells with, or without, 30nM or 100nM mandelalide A for 30min and 90min produced differential effects on these cell types. Using immunoblot analysis, we detected a statistically significant increase in the phosphorylation of

AMPKα (Thr172), and phosphorylation of ACC (Ser79), a direct downstream target of AMPK, in U87-MG cells that express functional LKB1, but no evidence of activation in HeLa cells (Figure 2.2B-C) which lack LKB1 (Figure 2.2B-C). AMPK activation in U87-MG cells appeared to be transient and influenced by both time and concentration, in that phosphorylation of AMPKα (Thr172) was significantly higher than vehicle-treated control cells at 30min (in response to 100nM mandelalide A) but had declined by 90 min exposure (Figure 2.2C). This result indicated that the lack of LKB1 may render HeLa cells more vulnerable to mandelalide A exposure.

We then tested whether a natural mandelalide analogue, with the same type A macrocycle, known as mandelalide L [8] can also induce the activation of AMPK pathway in U87-MG cells under similar conditions. Similar to mandelalide A, mandelalide L also induced a statistically significant increase in the phosphorylation of AMPKα (Thr172), and ACC (Ser79) that was influenced by time of exposure and/or mandelalide concentration (Figure 2.3A, B). Activation of AMPK by mandelalide L was also transient in that when the concentration was fixed phospho-AMPKα (Thr172), and phospho-ACC (Ser79) immunireactivity declined by 4 hrs (Figure 2.3C, D).

Mandelalide A is an indirect activator of the AMPK signaling pathway

We used immortalized mouse embryonic fibroblasts (MEFs) as a model cell type to extend our analysis of mandelalide-induced signaling to a non-cancer cell type. Wild-type MEFs responded in an identical manner to HeLa and U87-MG cells and showed a statistically significant, but transient, increase in the phosphorylation of AMPKα (Thr172) and ACC (Ser79) (Figure 2.4A,B). Activation of the AMPK pathway in wild-type MEFs by mandelalide A showed an identical pattern to the ATP synthase inhibitor oligomycin A, and both signals were attenuated when cells were treated with mandelalide A in the the presence of the AMPK inhibitor dorsomorphin (also known as compound C.). Immunoblot analysis of MEF cell lysates treated with dorsomorphin alone, revealed no evidence of AMPK activation (Figure 2.4C, D).

AMPK is a heterotrimeric protein complex comprised of a catalytic α subunit and regulatory β and γ subunits [30]. We utilized double knockout MEFs, devoid of $\alpha1$ and $\alpha2$ isoforms of AMPK, to determine if the catalytic subunit of AMPK was required for the observed activity. Wild-type and knockout cells were treated in parallel with, or without, mandelalide A (30nM) or oligomycin A (1µM) for 1hr. Immunoblot analysis revealed statistically signifcant increases in the phosphorylation of AMPKα (Thr172) and ACC (Ser79) in wild type MEFs in response to mandelalide A or oligomycin A (Figure 2.5). In contrast, phosphorylation of ACC (Ser79) was not detected in AMPKα-null MEFs treated with either compound (Figure 2.5A and B). These results indicate that the presence of the AMPKα subunit is required for activation of AMPK by mandelalide A or oligomycin A.

AMPKα deficient MEFs are more vulnerable to mandelalide A than wild-type MEFs.

We next treated wild-type and AMPKα-null MEFs with increasing concentrations of mandelalide A (0.3nM to 1µM) or vehicle (0.1% DMSO) then analyzed cell viability at 24 h, 48 h or 72 h. By using CellTiter Glo assay, which determines the number of viable cells in culture by quantifying ATP, we observed a clear deference in sensitivity of wild-type versus AMPKα-null MEFs (Figure 2.6). When end point were determined at 24 h, mandelalide A displayed limited cytotoxic efficacy against wild-type MEFs with only up to 40% cell viability inhibition and higher efficacy against AMPKα-null MEFs with 60% cell viability inhibition with the concentration of 100nM to 1µM (Figure 2.6A). If exposure times were extended to 48 h or 72 h, the efficacy of mandelalide A was greatly enhanced against both wild-type and AMPKα-null MEFs. In all of the three end points, the dose-response curves of AMPKα-null MEFs constantly fall to the left of wild-type MEFs (Figure 2.6A-C). More importantly, nonlinear regression analysis of these cell viability data revealed that EC_{50} of mandelalide A to AMPKα-null MEFs was statistically significantly lower than wild-type MEFs in both 48 h (13.5 ± 1.4nM versus 37.1 ± 0.1nM) and 72 h (10.6 ± 1.9nM versus 33.0 ± 4.9nM) (Table 2.1). The result shows that MEFs with functional AMPK are more resistant to mandelalide A.

Analysis of AMPK activation by Mandelalide A in Non-Small Cell Lung Cancer Cells

Having established that the status of LKB1/AMPK pathway can influence mandelalide sensitivity we investigated a panel of NSCLC cell types. LKB1 is wildly mutant in human NSCLC cells and is considered a clinically significant mutation [22]. We investigated the status of LKB1 in six NSCLCS including NCI-H460, H292, H3122, A549, 11-18 and PC-9 cells. In addition, we analysed lysates derived from NCLCS and HeLa cells treated with, or without, mandelalide A for changes in the AMPK signaling pathway. As anticipated for these well characterized and validated laboratory cell lines, LKB1 was detected in H292, H3122 and PC-9 cells, whereas A549, 11-18 and NCI-H460 cells lacked the LKB1 protein. More importantly, while all of the cell lines in this survey had similar basal expression of AMPKα, they displayed a differential pattern of phospho-AMPKα (Thr172) and phospho-ACC (Ser79). The pattern of responses to mandelalide A across this panel showed statistical significance corresponding to the presence of LKB1. Activation of AMPK was associated with the presence of LKB1 in H292, H3122 and PC-9 cells, whereas cells lack LKB1, including NCI-H460, A549, 11-18 and HeLa, don't have detectable AMPK activation (Figure 2.7A, B).

We've known that type A mandelalides shows different cytotoxic or antiproliferative effect to different cell lines. We then tested if the status of LKB1 and the AMPK pathway is a general determinant of the sensitivity of these cell lines to mandelalide A. Six NSCLCs cell lines were treated with increasing concentrations of mandelalide A (0.1nM to 3 µM) for 72 h. By recording the cell density at the time of mandelalide addition (time = zero; black dashed line), we distinguished antiproliferative response (above the dashed line) to a cytotoxic response (below the dashed line) as before. These studies demonstrated variation in the antiproliferative activity of mandelalide A against the NSCLCs tested (Figure 2.8. In NCLCLs with wild-type LKB1 (H3122, H292, PC-9), mandelalide A showed a consistent antiproliferative effects (Figure 8A). In those cells LKB1 mutated cells, mandelalide A showed wide variations in antiproliferative activity and with especially limited efficacy to A549 (Figure 2.8B). Using nonlinear regression

analysis, we summarized the 50% of growth inhibition, the total growth inhibition and 50% cytotoxicity of all the cell lines (Table 2.2). Unlike to what we expected, the rank order of sensitivity to mandelalide A of the six NSCLC cell lines is not consistent with their status of LKB1 or AMPK pathway activity against mandelalide A. Thus, LKB1 status is likley not the sole determinant of mandelalide A sensitivity.

Analysis of mandelalide in combination with clinically relevant drugs in EGFR mutant NSCLCs

Mutation of endoplasmic growth factor (EGF)-receptor is a major determinant of chemotherapeutic resistance in NSCLCs. We selected 11-18 and PC-9 cells or further analysis as these two cell lines harbor mutations in EGFR: EGFR (L8848R) or EGFR (E746-A750). Tyrosine kinase inhibitor (TKI) erlotinib and the microtubule stabilizer paclitaxel [31] have been used as two of the first-line medicine in NSCLC treatment [32]. We first characterized the effect of inhibition of cell viability for paclitaxel, erlotinib and mandelalide A alone on 11-18 and PC-9 cells. After 72 h treatment, consistent with growth inhibition assay (Figure 2.9), we observed limited anti-proliferative efficacy by mandelalide A to both 11-18 and PC-9 cells (Figure 2.9A). In the meantime, 11-18 cell line displays the similar extent of resistance to erlotinib as it does to mandelalide A as only half of cell viability was inhibited, whereas PC-9 is more sensitive to erlotinib where more than 90% of inhibition of cell viability can be achieved at 30nM concentration (Figure 2.9B). In contrast, paclitaxel displayed similar cytotoxic efficacy to both 11-18 and PC-9 cells (Figure 2.9C).

In order to test whether mandelalide A has a potential synergistic action with erlotinib or paclitaxel, we utilized these two hard-to-treat cell lines 11-18 and PC-9 to examine their viability after exposure to titration of mandelalide A in combination with erlotinib or paclitaxel. The drug matrix heatmap (Figure 2.10, 2.11) indicates that there are slightly argumentations for inhibition of cell viability while combining medium range of mandelalide A and paclitaxel for 11-18 and PC-9 cells, or mandelalide A and erlotinib for PC-9 cells (Figure 2.10, 2.11) compare to these drugs alone. In addition, there is a significant enhancement of sensitivity of 11-18 cells in response to the combination of mandelalide A and erlotinib compared to

both of the drugs alone (Figure 2.10A). The the combination achieved 74% inhibition of cell viability (1-26%) which is much higher than the efficacy of erlotinib or mandelalide A alone.

We then utilized Chou-Talalay Method [29] [28] to determine whether the observed change of cell viability in Figure 9 were additive or synergistic. The Chou-Talalay method for drug combination analysis is derived from the mass-action law principle and based on the median-effect equation. This method determines an interaction as synergistic, additive or antagonistic by calculating the difference between the expected additive effect and the observed combination effect. The method introduced a scientific term "combination index" which quantitatively depicts synergism (CI<1), additive effect (CI=1), and antagonism (CI>1). The CI values and the fraction affected (Fa) from actual experimental result were used to generate the Fa-CI plots with simulated curve (Figure 2.10, 2.11).

For the clinical study of drug combination, CI value of Fa > 0.5 has more therapeutical indication of synergism. When synergies are detected, it is almost always dependent on the dose ratio of the combination that is tested [33]. Therefore, we choose a subset of cell viability data from cells treated with drug combination carried out with constant ratio. Under the combination of mandelalide A with erlotinib at constant ratio of 1:1 treated to 11-18, the CI values from actual experimental result were determined <0.5 (Figure 2.10 A), and the simulated CI values of Fa = 0.5, 0.75, 0.9 are determined between 0-0.2 (Table 2.3), which indicates strong synergism. However the same condition did not display synergic affect on PC-9 cells, which displayed average of CI values near 1. The result might be attribute to the high sensitivity of PC-9 cells to erlotinib alone. We choose to analysis the CI values under the combination of mandelalide A with paclitaxel in a constant ratio of 30:1, due to the high potency of palitaxel alone to both PC-9 and 11-18 cell lines (Figure 2.9). All the CI value were determined nearly 0.5 which indicates moderate synergistic effect, and the simulated CI values of Fa = 0.5, 0.75, 0.9 are determined between 0.3 - 1 (Table 2.3), which indicates a slight to moderate synergism . This data indicates a synergistic interaction between mandelalide A and erlotinib on 11-18 or paclitaxel on both 11-18 and PC-9 cells.

Discussion

The mechanistic basis of mandelalide A selectivity to cancer cell types has been attributed to it's molecular target -- ATP synthase. Given the advanced understanding for the complexity of cancer cells metabolism, our goal in the present study was to evaluate the mechanistic basis for the selectivity profile of the mandelalides and explore their value when used in combination with first-line chemotherapic agents in human lung cancer cell lines. Using wild-type and genetically-modified MEFS as a model system, we demonstrated here that mandelalides induce indirect activation of then AMPK pathway. Mandelalide A and L induced phosphorylation of the $AMPK\alpha$ subunit at Thr172 and triggered phosphorylation of the downstream protein ACC at Ser79 in a time- and concentration-dependent manner. AMP-activated protein kinase is activated in response to a variety of changes that depleting cellular energy, including nutrient starvation or mitochondrial inhibition [34]. Our finding that mandelalides are indirect AMPK activators is consistent with the fact that the primary binding target of the mandelalides is mitochondrial complex V or ATP synthase leading to eventual depletion of intracellualr ATP.

The AMPK activation by mandelalide A is transient, meaning the cells were temporarily triggered to switch on to catabolic status in response to the change of ATP/ADP (or AMP) ratio caused by mitochondrial inhibition by mandelalides. In other words, the AMPK activation helps the cells to survive an energy stress caused by exposure to mandelalide A. The important role of AMPK in this adaptive signaling response was demonstrated when generically-manipulated MEFs with deficient $AMPK\alpha$ showed no increase in the phosphorylation state of ACC (Ser79) after exposure to mandelalide A. Further, mandelalide A-induced activation of AMPK could be a pharmacologically inhibited by the AMPK inhibitor dorsomorphin. More interestingly, we found that within the same conditions, $AMPK\alpha$-null MEFs which do not have a functional AMPK pathway are more vulnerable than wild-type MEFs with a statistic significant smaller EC_{50}. These enhanced efficacy and potency to $AMPK\alpha$ deficient MEFs revealed the central role of energy stress caused by mandelalides in their effect of antiproliferation to cancer cells.

As the marine environment has been relatively unexplored, most of the known natural product AMPK activators are found from secondary metabolites produced by plants and bacteria [35] [30]. Like mandelalides, those diverse natural structures activate AMPK indirectly as a result of targeting mitochondrial function to inhibit cellular respiration. These include oligomycins from microbial metabolites of *Streptomyces*, resveratrol extracted from red grapes [36] and epigallocatenchin gallate from green tea [37], berberine from *Coptis chinensis* [38] and curcumin from *Curcuma longa [39]*. The widely used anti-diabetic drug metformin is a synthetic derivative of guanide that is a natural product from the plant *Galega officinalis* [40]. People have found the action of metformin are attributable to AMPK activation [41]. Another compound Salicylate traditionally extracted from willow bark has been reported recently as a direct activator of AMPK [42] . What's more interesting is that both of them have been revealed to reduce the incidence of cancer or reduce tumor growth [43] [44].

In past decades there have been increasing number of studies to uncover the role of AMPK in tumorigenesis. Several reports have indicated AMPK regulated pathways as a potential therapeutic target for the treatment of cancer [45] . For example, AMPK has been shown to inhibit mammalian target of rapamycin (mTOR) by phosphorylation of Tuberous Sclerosis Complex 2 (TSC2) [46] [47]. AMPK also down-regulates rRNA synthesis by phosphorylation of RNA polymerase I (Pol I)-associated transcription factor TIF-IA [48]. Both mTOR and TIF-IA are required for rapidly cell proliferation. In addition, G1 cell cycle arrest has been shown as a downstream effect of AMPK activation, as the result of activation of p53, followed by induction of the cell cycle inhibitor protein p21 [49] [50]. Moreover, metabolic stress induced AMPK activation has been shown to induce the phosphorylation and concomitant stabilization of the cyclin-dependent kinase inhibitor p27(kip1) to mediate the decision to enter autophagy or apoptosis [51]. In other words, cancer cells can utilize AMPK activation to protect them against the action of cytotoxic agents, energy stress. Therefore, AMPK could be a double-sword in the treatment of cancer.

In our study we found that mandelalide A-induced AMPK activation is largely dependent upon LKB1. When two mandelalide-sensitive human cancer cell lines

HeLa cervical and U87-MG glioblastoma were treated with mandelalide A in a short period of time, AMPK activation was induced only in U87-MG which has a functional LKB1, whereas there was no AMPK activation detected in HeLa which lacks LKB1. As a major AMPK upstream kinase, LKB1 was discovered as a tumor suppressor that connecting AMPK to cancer biology [16]. Genetic mutations of LKB1 are responsible for Peutz-Jeghers syndrome (PJS) which predisposes individuals to cancer [52]. LKB1 is one of the most commonly mutated genes in sporadic human lung cancer, particularly in NSCLC [21]. Recent studies have revealed that LKB1-deficient NSCLC cells showed selective response to the mitochondrial inhibitor phenformin, resulting in apoptosis in cancer cells and prolonged survival in mouse models [20]. From our present study, in growth inhibition assay with six NSCLC cell lines, the difference in status of LKB1 failed to predict the rank order of 50% growth inhibition (GI_{50}) against mandelalide A, raising the possibility that LKB1 status isn't the only factors that determine the cells sensitivity to mandelalide A. Even though our studies indicated that AMPK activation in NSCLC is LKB1-dependent, there might be other factors that affect the sensitivity to mandelalide A, such as the KRAS mutation status, or the metabolic features of cells.

Drug combinations are widely used in the treatment of cancer and viral infections such as AIDS. The basic goals are to improve the probability and magnitude of therapeutic responses by reducing the dose of the drug, and in turn, the potential for toxicity and development of drug resistance [53]. EGFR mutations account for 10-17% of all NSCLC cases in North American and Europe, and 30-50% of NSCLCs in Asian countries [54, 55]. Recently tyrosine kinase inhibitors (TKIs) targeted against the human EGFR have become standard treatment in the clinic for patients with advanced EGFR-mutant NSCLC. The first generation of TKIs - Erlotinib - is approved by the U.S. Food and Drug Administration (FDA) as a first-line treatment of metastatic NSCLC in patients with tumors that have EGFR exon 19 deletion or exon 21(L858R) substitution mutations [56]. One of the most intriguing findings here is that the combination of mandelalide A with the tyrosine kinase inhibitor erlotinib has a synergy effect on EGFR mutant (L858R) lung cancer cells 11-18. Even though both erlotinib and mandelalide A only have limited efficacy in 11-18 cells with 50% and 40% of cell viability inhibition, respectively, the

combination of both compounds achieved almost 80% reduction of cell viability. The microtubule stabilizer paclitaxel is also widely used for treatment of NSCLC in combination with platinum compoundsthe . In our study, paclitaxel displays potent cytotoxicity against 11-18 and PC-9 cells. According to CI values of Fa = 0.5, 0.7, 0.9 (Table 2.3) which were computationally simulated from the actual experimental result, the combination with constant concentration ratio (30:1) of mandelalide A with paclitaxel has a moderate synergism in 11-18 cells. Clinically, at high does or high effect levels (Fa >0.5), the synergistic interaction is more relevant to therapy than at low effect levels (e.g. Fa <0.2) [28]. The synergism of mandelalide A in combination with erlotinib or paclitaxel is a powerful indication that it can be developed as a pre-clinical drug in cancer treatment.

Acknowledgments

Author Contributions: J.E.I. conceived and designed the experiments; K.L.M. and A.B.S contributed materials and edited the manuscript; X.W., J.D.S., I.R.H. performed the experiments; X.W.and J.E.I. analyzed the data and wrote the manuscript.

Reference

1.   Newman, D.J. and G.M. Cragg, *Marine-sourced anti-cancer and cancer pain control agents in clinical and late preclinical development.* Mar Drugs, 2014. **12**(1): p. 255-78.
2.   Ruiz-Torres, V., et al., *An Updated Review on Marine Anticancer Compounds: The Use of Virtual Screening for the Discovery of Small-Molecule Cancer Drugs.* Molecules, 2017. **22**(7).
3.   Nuijen, B., et al., *Pharmaceutical development of anticancer agents derived from marine sources.* Anticancer Drugs, 2000. **11**(10): p. 793-811.
4.   Newman, D.J. and G.M. Cragg, *Natural products as sources of new drugs over the 30 years from 1981 to 2010.* J Nat Prod, 2012. **75**(3): p. 311-35.
5.   Smith, A.B., 3rd and W.M. Wuest, *Evolution of multi-component anion relay chemistry (ARC): construction of architecturally complex natural and unnatural products.* Chem Commun (Camb), 2008(45): p. 5883-95.
6.   Smith, A.B., 3rd and C.M. Adams, *Evolution of dithiane-based strategies for the construction of architecturally complex natural products.* Acc Chem Res, 2004. **37**(6): p. 365-77.
7.   Sikorska, J., et al., *Mandelalides A-D, cytotoxic macrolides from a new Lissoclinum species of South African tunicate.* J Org Chem, 2012. **77**(14): p. 6066-75.
8.   Nazari, M., et al., *New Mandelalides Expand a Macrolide Series of Mitochondrial Inhibitors.* J Med Chem, 2017. **60**(18): p. 7850-7862.
9.   Nazari, M., et al., *Discovery of Mandelalide E and Determinants of Cytotoxicity for the Mandelalide Series.* Org Lett, 2016. **18**(6): p. 1374-7.
10.   Lei, H., et al., *Total synthesis and stereochemical reassignment of mandelalide A.* Angew Chem Int Ed Engl, 2014. **53**(25): p. 6533-7.
11.   Brutsch, T.M., P. Bucher, and K.H. Altmann, *Total Synthesis and Biological Assessment of Mandelalide A.* Chemistry, 2016. **22**(4): p. 1292-300.
12.   Reddy, K.M., et al., *Synthesis of proposed aglycone of mandelalide A.* Org Lett, 2014. **16**(10): p. 2658-60.
13.   Veerasamy, N., et al., *Enantioselective Total Synthesis of Mandelalide A and Isomandelalide A: Discovery of a Cytotoxic Ring-Expanded Isomer.* J Am Chem Soc, 2016. **138**(3): p. 770-3.
14.   Nguyen, M.H., et al., *Total Synthesis of (-)-Mandelalide A Exploiting Anion Relay Chemistry (ARC): Identification of a Type II ARC/CuCN Cross-Coupling Protocol.* J Am Chem Soc, 2016. **138**(11): p. 3675-8.
15.   Nguyen, M.H., et al., *Synthetic Access to the Mandelalide Family of Macrolides: Development of an Anion Relay Chemistry Strategy.* J Org Chem, 2018.
16.   Alessi, D.R., K. Sakamoto, and J.R. Bayascas, *LKB1-dependent signaling pathways.* Annu Rev Biochem, 2006. **75**: p. 137-63.
17.   Hardie, D.G., F.A. Ross, and S.A. Hawley, *AMPK: a nutrient and energy sensor that maintains energy homeostasis.* Nat Rev Mol Cell Biol, 2012. **13**(4): p. 251-62.
18.   Shackelford, D.B. and R.J. Shaw, *The LKB1-AMPK pathway: metabolism and growth control in tumour suppression.* Nat Rev Cancer, 2009. **9**(8): p. 563-75.

19.   Hardie, D.G., *The LKB1-AMPK pathway-friend or foe in cancer?* Cancer Cell, 2013. **23**(2): p. 131-2.

20.   Shackelford, D.B., et al., *LKB1 inactivation dictates therapeutic response of non-small cell lung cancer to the metabolism drug phenformin.* Cancer Cell, 2013. **23**(2): p. 143-58.

21.   Sanchez-Cespedes, M., et al., *Inactivation of LKB1/STK11 is a common event in adenocarcinomas of the lung.* Cancer Res, 2002. **62**(13): p. 3659-62.

22.   Ji, H., et al., *LKB1 modulates lung cancer differentiation and metastasis.* Nature, 2007. **448**(7155): p. 807-10.

23.   Wingo, S.N., et al., *Somatic LKB1 mutations promote cervical cancer progression.* PLoS One, 2009. **4**(4): p. e5137.

24.   Shigematsu, H. and A.F. Gazdar, *Somatic mutations of epidermal growth factor receptor signaling pathway in lung cancers.* Int J Cancer, 2006. **118**(2): p. 257-62.

25.   Paull, M.R.B.K.D., *Some Practical Considerations and Applications of the National Cancer Institute In Vitro Anticancer Drug Discovery Screen.* Drug development research, 1995. **34**: p. 91-109.

26.   Rubinstein, M.R.B.D.P.R., *Data Display and Analysis Strategies for the NCI Disease-Oriented in Vitro Antitumor Drug Screen.* Cytotoxic Anticancer Drugs: Models and Concepts for Drug Discovery and Development, 1992. **68**: p. 11-34.

27.   Chou, T.C., *Drug combination studies and their synergy quantification using the Chou-Talalay method.* Cancer Res, 2010. **70**(2): p. 440-6.

28.   Chou, T.C., *Theoretical basis, experimental design, and computerized simulation of synergism and antagonism in drug combination studies.* Pharmacol Rev, 2006. **58**(3): p. 621-81.

29.   Chou, T.C. and P. Talalay, *Quantitative analysis of dose-effect relationships: the combined effects of multiple drugs or enzyme inhibitors.* Adv Enzyme Regul, 1984. **22**: p. 27-55.

30.   Hardie, D.G., F.A. Ross, and S.A. Hawley, *AMP-activated protein kinase: a target for drugs both ancient and modern.* Chem Biol, 2012. **19**(10): p. 1222-36.

31.   Horwitz, S.B., *Taxol (paclitaxel): mechanisms of action.* Ann Oncol, 1994. **5 Suppl 6**: p. S3-6.

32.   David S. Ettinger, M.D.E.W., MD, FRCSEd; Dara L. Aisner, MD, PhD; Wallace Akerley, MD;, et al., *Non–Small Cell Lung Cancer, Version 5.2017 Clinical Practice Guidelines in Oncology.* National Comprehensive Cancer Network 2017. **15(4):504-535**.

33.   Tallarida, R.J., *Quantitative methods for assessing drug synergism.* Genes Cancer, 2011. **2**(11): p. 1003-8.

34.   Mihaylova, M.M. and R.J. Shaw, *The AMPK signalling pathway coordinates cell growth, autophagy and metabolism.* Nat Cell Biol, 2011. **13**(9): p. 1016-23.

35.   Kim, J., et al., *AMPK activators: mechanisms of action and physiological activities.* Exp Mol Med, 2016. **48**: p. e224.

36.   Park, C.E., et al., *Resveratrol stimulates glucose transport in C2C12 myotubes by activating AMP-activated protein kinase.* Exp Mol Med, 2007. **39**(2): p. 222-9.

37. Hwang, J.T., et al., *Genistein, EGCG, and capsaicin inhibit adipocyte differentiation process via activating AMP-activated protein kinase.* Biochem Biophys Res Commun, 2005. **338**(2): p. 694-9.

38. Lee, Y.S., et al., *Berberine, a natural plant product, activates AMP-activated protein kinase with beneficial metabolic effects in diabetic and insulin-resistant states.* Diabetes, 2006. **55**(8): p. 2256-64.

39. Kim, T., et al., *Curcumin activates AMPK and suppresses gluconeogenic gene expression in hepatoma cells.* Biochem Biophys Res Commun, 2009. **388**(2): p. 377-82.

40. Foretz, M., et al., *Metformin: from mechanisms of action to therapies.* Cell Metab, 2014. **20**(6): p. 953-66.

41. Zhou, G., et al., *Role of AMP-activated protein kinase in mechanism of metformin action.* J Clin Invest, 2001. **108**(8): p. 1167-74.

42. Hawley, S.A., et al., *The ancient drug salicylate directly activates AMP-activated protein kinase.* Science, 2012. **336**(6083): p. 918-22.

43. Huang, X., et al., *Important role of the LKB1-AMPK pathway in suppressing tumorigenesis in PTEN-deficient mice.* Biochem J, 2008. **412**(2): p. 211-21.

44. Rothwell, P.M., et al., *Short-term effects of daily aspirin on cancer incidence, mortality, and non-vascular death: analysis of the time course of risks and benefits in 51 randomised controlled trials.* Lancet, 2012. **379**(9826): p. 1602-12.

45. Rehman, G., et al., *Role of AMP-activated protein kinase in cancer therapy.* Arch Pharm (Weinheim), 2014. **347**(7): p. 457-68.

46. Gwinn, D.M., et al., *AMPK phosphorylation of raptor mediates a metabolic checkpoint.* Mol Cell, 2008. **30**(2): p. 214-26.

47. Inoki, K., T. Zhu, and K.L. Guan, *TSC2 mediates cellular energy response to control cell growth and survival.* Cell, 2003. **115**(5): p. 577-90.

48. Hoppe, S., et al., *AMP-activated protein kinase adapts rRNA synthesis to cellular energy supply.* Proc Natl Acad Sci U S A, 2009. **106**(42): p. 17781-6.

49. Jones, R.G., et al., *AMP-activated protein kinase induces a p53-dependent metabolic checkpoint.* Mol Cell, 2005. **18**(3): p. 283-93.

50. Imamura, K., et al., *Cell cycle regulation via p53 phosphorylation by a 5'-AMP activated protein kinase activator, 5-aminoimidazole- 4-carboxamide-1-beta-D-ribofuranoside, in a human hepatocellular carcinoma cell line.* Biochem Biophys Res Commun, 2001. **287**(2): p. 562-7.

51. Liang, J., et al., *The energy sensing LKB1-AMPK pathway regulates p27(kip1) phosphorylation mediating the decision to enter autophagy or apoptosis.* Nat Cell Biol, 2007. **9**(2): p. 218-24.

52. Hemminki, A., *The molecular basis and clinical aspects of Peutz-Jeghers syndrome.* Cell Mol Life Sci, 1999. **55**(5): p. 735-50.

53. Lehar, J., et al., *Synergistic drug combinations tend to improve therapeutically relevant selectivity.* Nat Biotechnol, 2009. **27**(7): p. 659-66.

54. Kris, M.G., et al., *Using multiplexed assays of oncogenic drivers in lung cancers to select targeted drugs.* JAMA, 2014. **311**(19): p. 1998-2006.

55. Barlesi, F., et al., *Routine molecular profiling of patients with advanced non-small-cell lung cancer: results of a 1-year nationwide programme of the French Cooperative Thoracic Intergroup (IFCT).* Lancet, 2016. **387**(10026): p. 1415-1426.

56.   Ettinger, D.S., et al., *Non-Small Cell Lung Cancer, Version 5.2017, NCCN Clinical Practice Guidelines in Oncology.* J Natl Compr Canc Netw, 2017. **15**(4): p. 504-535.

Mandelalide A   Mandelalide L
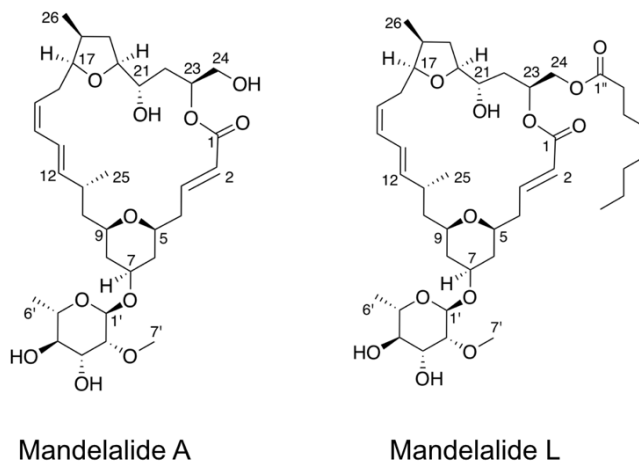
Figure 2.1 Structure of mandelalide A and mandelalide L
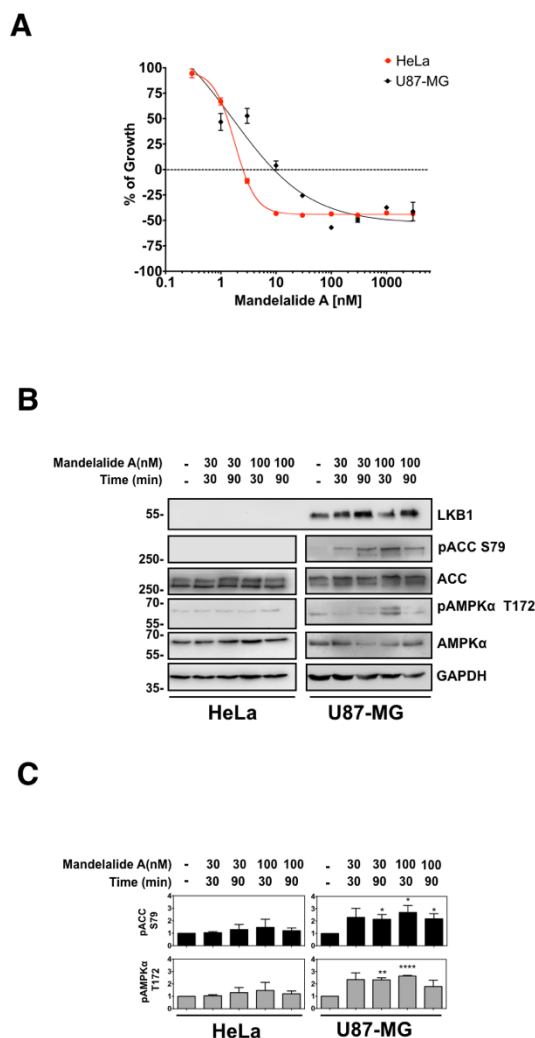
Figure 2.2. Mandelalide A shows anti-proliferative and cytotoxic effects against human cervical and glioblastoma cells and mandelalide A-induced AMPKα activation requires liver kinase B1 (LKB1).

(A) Percentage of Growth of human Hela cervical and U87-MG glioblastoma cells against increasing concentration of mandelalide A (0.3nM to 3μM). The MTT assay was used to calculate the effect of on the growth (positive values) and cytotoxicity (negative values) of cell line. The cell density at the time of drug addition is indicated by the dashed black line at 0% growth. Graphs represent from at least three independent comparisons. (B) Immunoblots of HeLa or U87-MG treated with 30nM or 100nM of mandelalide A for 30min or 90min. Whole cell lysates were probed with antibodies as indicated. Graphs represent from at least three independent comparisons. (C) Histograms show quantification of immunoblot data from (B) from three independent experiments, normalized to GAPDH and relative to vehicle lysates (* P< 0.05, ** P < 0.01, *** P < .001, compared to vehicle, N = 3).

A

Mandelalide L (h)   -   -   0.5   1   4

250-   pACC S79

250-   ACC

70-
55-   pAMPKα T172

70-
55-   AMPKα

35-   GAPDH

U87-MG

B

Mandelalide L (h)   -   -   0.5   1   4

U87-MG

C

Mandelalide L (nM)   -   0.1   1   10   100   1000

250-   pACC S79

250-   ACC

70-
55-   pAMPKα T172

70-
55-   AMPKα

35-   GAPDH

U87-MG

D

Mandelalide L (nM)   -   0.1   1   10   100   1000

U87-MG

Figure 2.3. Mandelalide L induces activation of AMPK pathway in time and concentration-dependent manner to U87-MG cells.

(A)Immunoblots of U87-MG treated with 1 μM of mandelalide L for 30 min, 1 h or 4 h. (B) Immunoblots of U87-MG treated with 0.1nM to 1 μM of mandelalide L for 30 min. Whole cell lysates were probed with antibodies as indicated. (C)(D) Histograms show quantification of immunoblot data of (A) and (B) from three independent experiments, normalized to GAPDH and relative to vehicle lysates (* P< 0.05, ** P < 0.01, *** P < .001, compared to vehicle, N = 3).
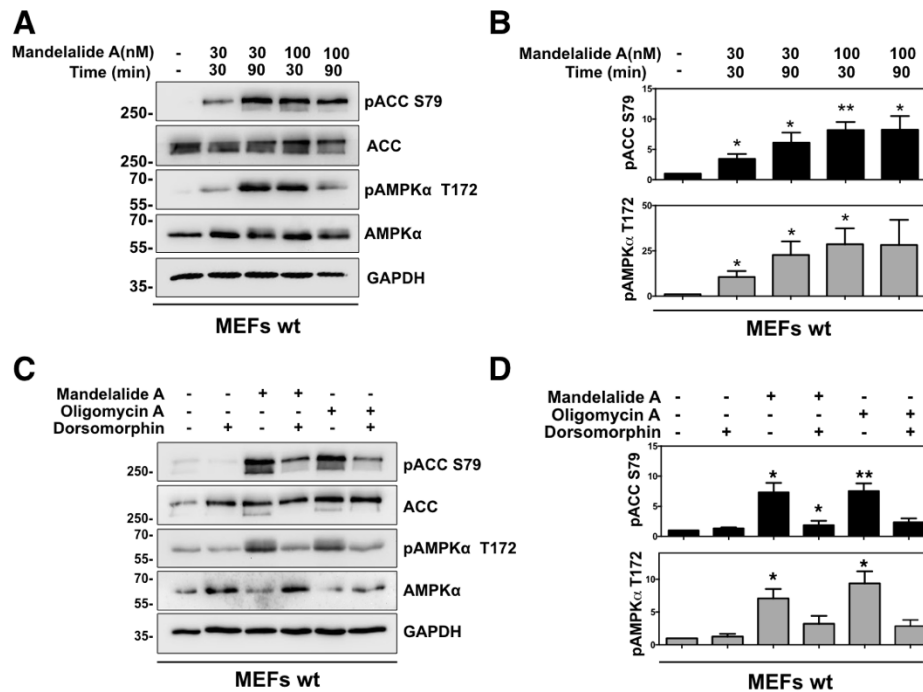
Figure 2.4. Wild-type MEFs showed time and concentration-dependent activation of AMPK pathway in response to mandelalide A.

(A) Immunoblots of wild-type mouse embryonic fibroblasts (MEFs) treated with 30nM or 100nM of mandelalide A for 30min or 90min. Whole cell lysates were probed with antibodies as indicated. (B) Histograms show quantification of immunoblot data of (A) from three independent experiments, normalized to GAPDH and relative to vehicle lysates (* P< 0.05, ** P < 0.01, *** P < .001, compared to vehicle, N = 3). (C)Mandelalide A-induced phosphorylation of ACC is attenuated by the AMPK inhibitor dorsomorphin. Immunoblots of MEFs treated with, or without, mandelalide A (30nM) and dorsomorphin (10 mM) in standard medium for 1 h. Whole cell lysates were probed with antibodies as indicated. Graphs represent from at least three independent comparisons. (D) Histograms show quantification of immunoblot data of (C) from three independent experiments, normalized to GAPDH and relative to vehicle lysates (* P< 0.05, ** P < 0.01, *** P < .001, compared to vehicle, N = 3).
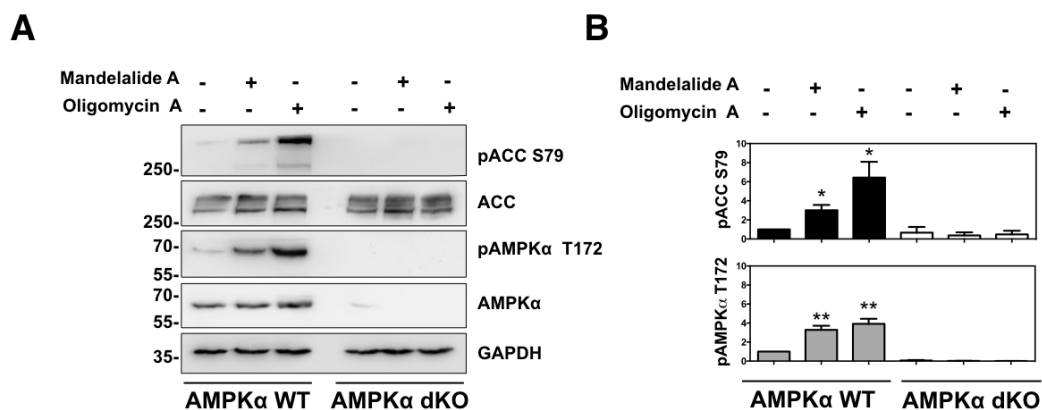
Figure 2.5. Mandelalide A - induced AMPK activation is blocked in AMPKα-null MEFs.

(A) Immunoblots of wildtype and AMPKα dKO mouse embryonic fibroblasts (MEFs) treated with 30nM of mandelalide A or oligomycin A for 90min. Whole cell lysates were probed with antibodies as indicated. (B) Histograms show quantification of immunoblot data from three independent experiments, normalized to GAPDH and relative to vehicle lysates (* P< 0.05, ** P < 0.01, *** P < .001, compared to vehicle, N = 3).
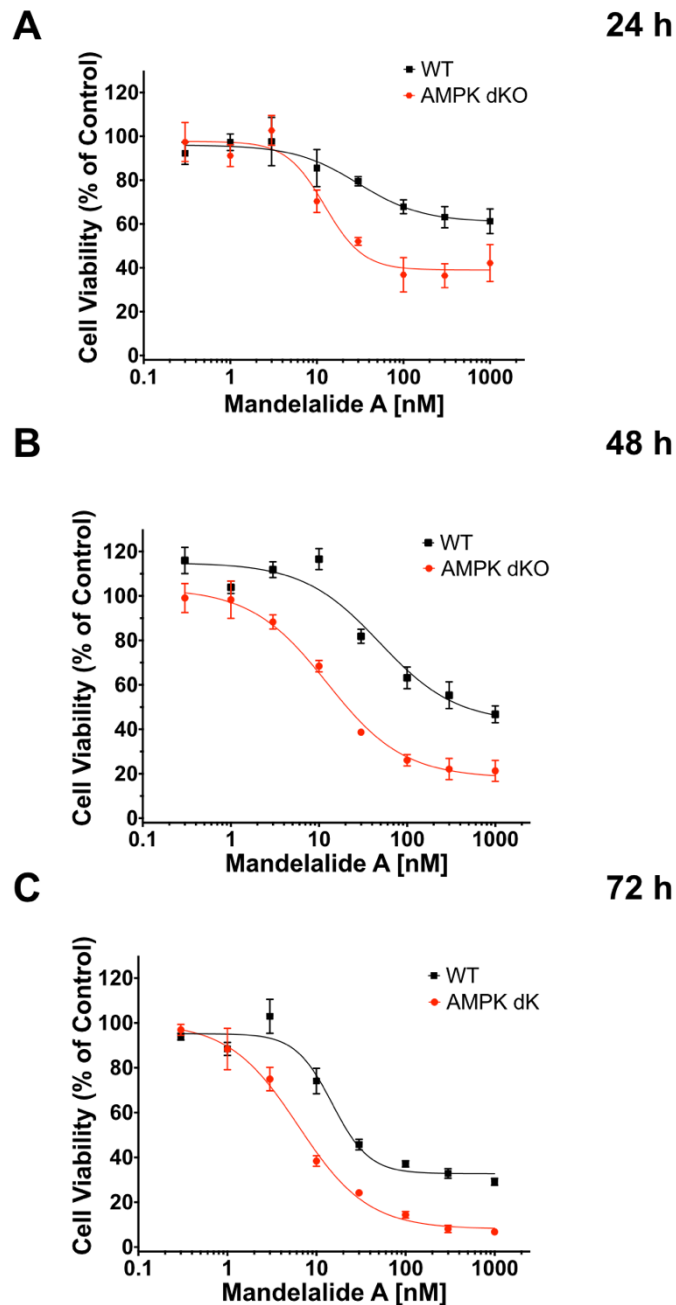
Figure 2.6. AMPKα-null MEFs are more vulnerable to mandelalide A than wild-type MEFs.

The CellTiter Glo assay was used to determine the cell viability of AMPKα-null MEFs and wild-type MEFs after 24hr (A), 48hr (B) and 72hr (C) treatment of increasing mandelalide A concentration. Graphs represent from at least three independent comparisons.
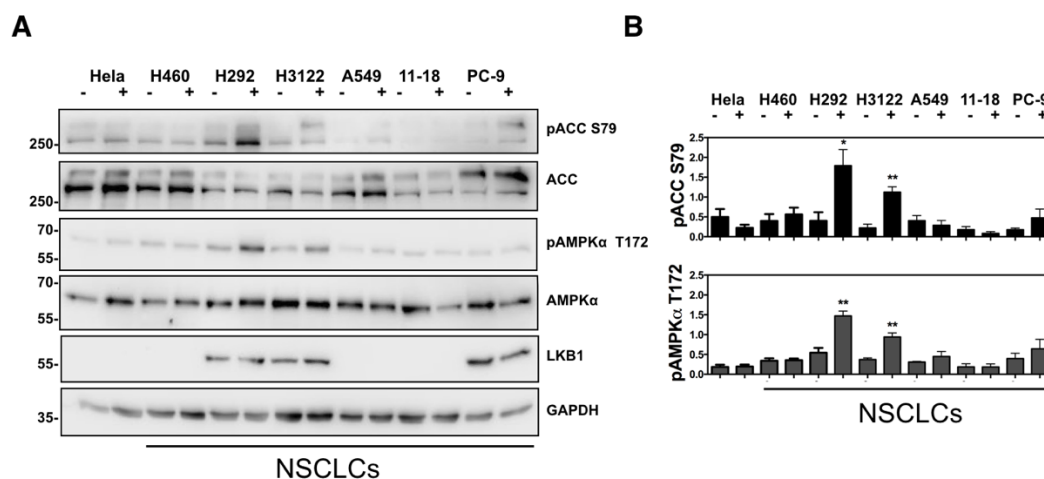
Figure 2.7. Mandelalide A - induced AMPKα activation in non-small cell lung cancer (NSCLC) cells is dependent on the status of LKB1, which is commonly mutated in cancer cells.
(A) Immunoblots of NSCLC cells and HeLa cells treated with 30nM of mandelalide A or vehicle (0.1% DMSO) for 1hr. Whole cell lysates were probed with antibodies as indicated. (B) Histograms show quantification of immunoblot data from three independent experiments, normalized to GAPDH and relative to vehicle lysates (* P< 0.05, ** P < 0.01, *** P < .001, compared to vehicle, N = 3).
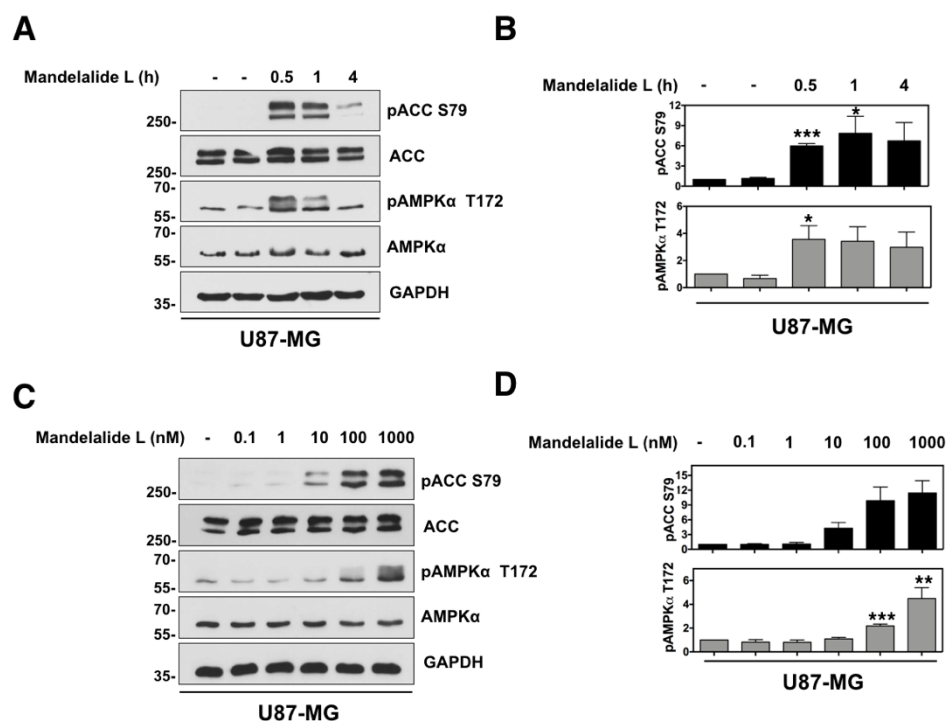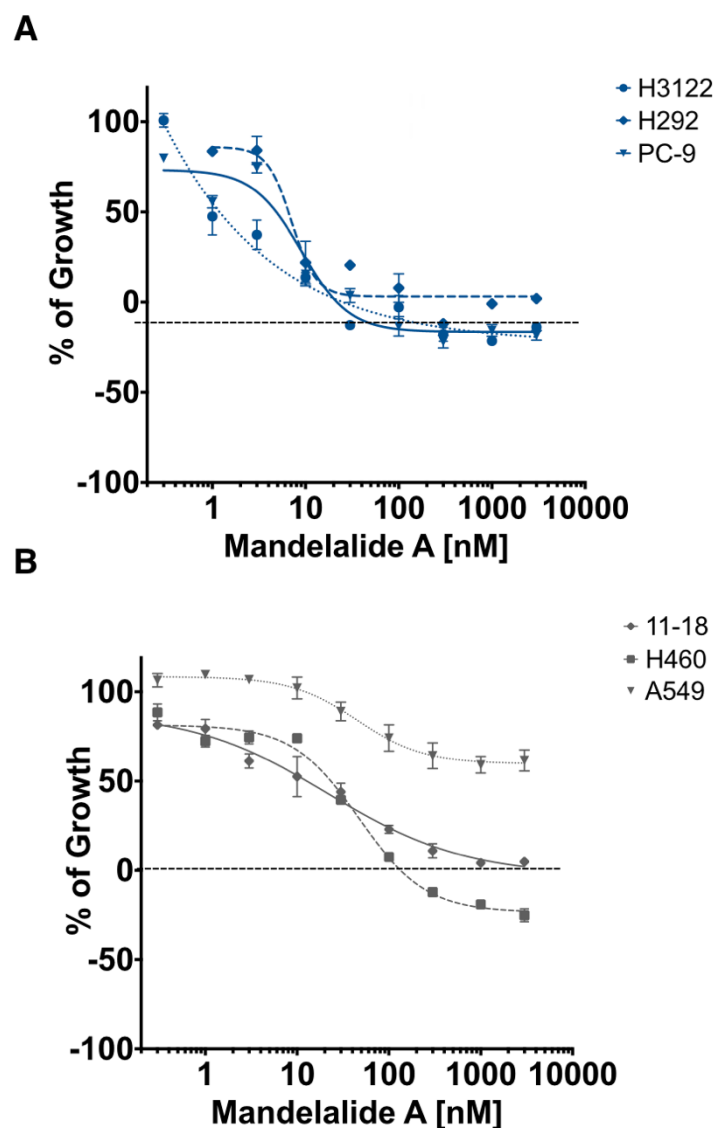
Figure 2.8. Sensitive of molecularly diverse NSCLC cell lines to the anti-proliferative and cytotoxic effects of mandelalide A.

The MTT assay was used to calculate the effect of increasing mandelalide A concentration on the growth (positive values) and cytotoxicity (negative values) of cell line. The cell density at the time of drug addition is indicated by the solid black line at 0% growth. (A) sensitivity of LKB1 wild-type NSCLS cell lines to mandelalide A in 72hr. (B) sensitivity of LKB1 mutant NSCLS cell lines to mandelalide A in 72hr. (C) Histogram of 50% Growth inhibition (GI_{50}) (mean viability ±SEM, N = 3 wells per treatment) of human cervical cancer HeLa and NSCLS cell lines.
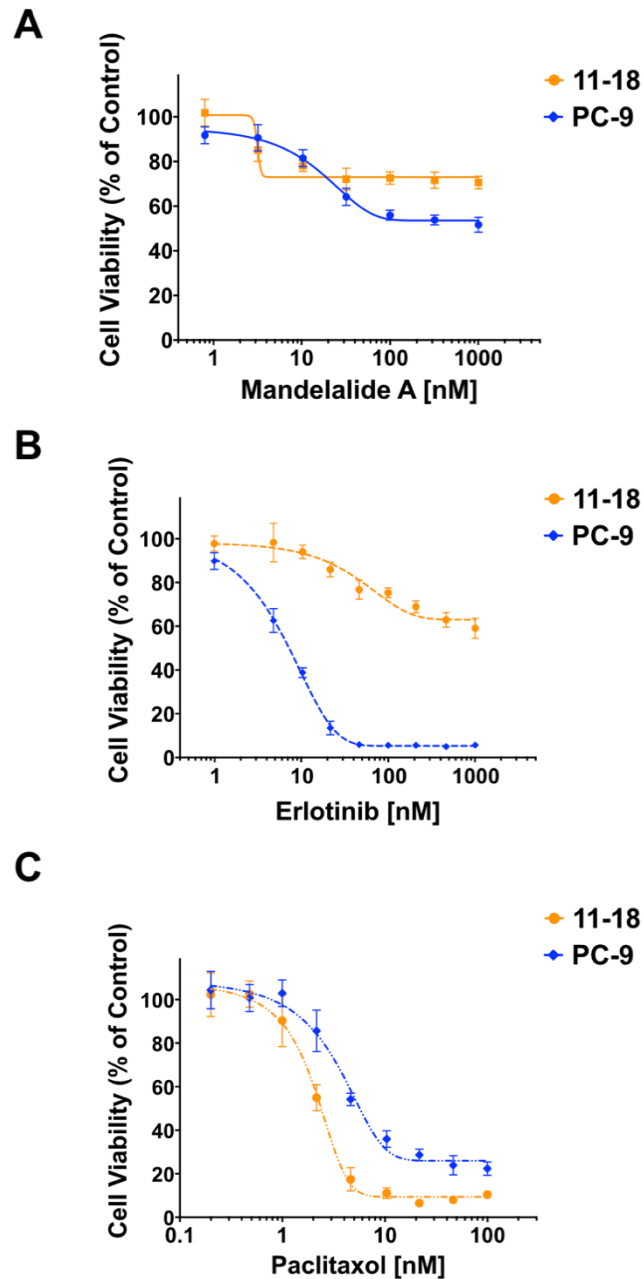
Figure 2.9. Cell viability of NSCLC cell lines 11-18 and PC-9 to mandelalide A and first-line clinical chemotherapeutic agents.

The cell viability of 11-18 and PC-9 were determined by CellTiter Glo assay after 72hr treatment of increasing concentration of mandelalide A(A), erlotinib (B) or paclitaxel (C). Graphs represent from at least three independent comparisons.

A

Mandelalide A

Cell viability %

100
90
80
60
50
30
20
0

Erlotinib

1nM   1µM

98	93	96	91	81	80	75	77	74
98	93	91	88	76	72	74	71	73
94	91	84	86	71	72	71	72	70
86	86	81	76	68	66	61	65	62
77	77	73	65	59	55	51	50	51
75	69	58	53	47	41	39	38	37
69	74	65	51	44	40	37	34	32
63	62	56	48	37	32	28	30	29
59	61	54	42	31	31	27	26	26

11-18

B

Mandelalide A + Erlotinib

C

Mandelalide A

Cell viability %

100
90
80
60
50
30
20
0

Erlotinib

1nM   1µM

101	94	92	81	66	58	58	56	50
63	65	63	61	55	51	46	41	47
39	41	41	43	34	31	25	25	24
13	15	15	13	9	7	7	5	6
6	7	8	7	4	3	3	3	3
6	6	6	6	4	2	3	3	2
6	6	6	5	4	4	3	3	2
5	6	6	5	4	4	3	3	2
6	6	7	6	5	4	3	4	3

PC-9

D

Mandelalide A + Erlotinib

Figure 2.10. Effects of combination of mandelalide A and erlotinib on the cell viability of 11-18 and PC-9 and combination index (CI) *vs* Fraction affected (Fa) plots for evaluation of combination.

(A)(C) Drug matrix heatmap grid illustrating percentage cell viability for NSCLC 11-18 cells and PC-9 for mandelalide A in combination with erlotinib (up to 1 µM). Drug matrix heatmap grids represent from at least three independent experiments. (B) (D) The Chou and Talalay CI method was used by running CompuSyn program. (B) Fa-CI plot of erlotinib in combination with mandelalide A for 11-18. (D) Fa-CI plot of erlotinib in combination with mandelalide A for PC-9.
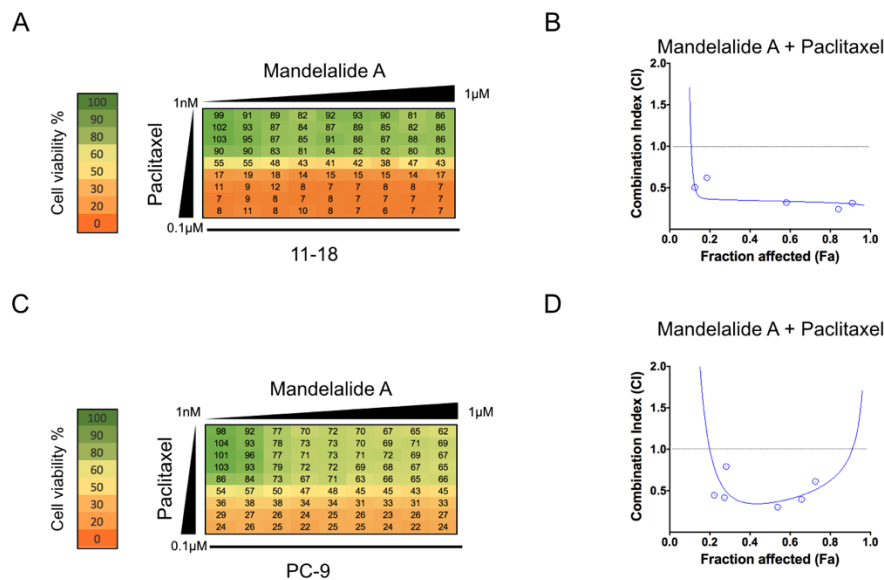
Figure 2.11. Effects of combination of mandelalide A and paclitaxel on the cell viability of 11-18 and PC-9 and combination index (CI) *vs* Fraction affected (Fa) plots for evaluation of combination..

(A)(C) Drug matrix heatmap grid illustrating percentage cell viability for NSCLC 11-18 cells and PC-9 for mandelalide A in combination with paclitaxel (up to 100nM). Drug matrix heatmap grids represent from at least three independent experiments. (B) (D) The Chou and Talalay CI method was used by running CompuSyn program. (B) Fa-CI plot of paclitaxel in combination with mandelalide A for 11-18. (D) Fa-CI plot of paclitaxel in combination with mandelalide A for PC-9.

Mouse Embryonic Fibroblasts	Relative EC_{50} (nM) ± SEM		
	24 h	48 h	72 h
WT	28.2 ± 6.3	37.1 ± 0.1	33.0 ± 4.9
AMPK dKO	9.3 ± 1.3	13.5 ± 1.4 **	10.6 ± 1.9*

Table 2.1 Average EC_{50} ± SEM of AMPKα-null MEFs and WT MEFs after 24hr - 72hr treatment of mandelalide A.

Experiments are replicated three times. The average EC_{50} of AMPK dKO was compared to WT in each time points using unpaired t-test. (* $p < 0.05$, ** $p < 0.005$)

Cell line	Cancer type	EGFR Status	LKB1 Status	GI_{50} (nM) ± SEM	TGI (nM) ± SEM	LC_{50} (nM) ± SEM
HeLa	Cervical	WT	loss	1.0 ± 0.2	3.7 ± 1.3	6.9 ± 1.6
U87-MG	Glioblastoma	WT	WT	1.5 ± 0.1	8.2 ± 0.7	1180 ± 115.5
A549	Lung	WT	loss	>3000	>3000	>3000
11-18	Lung	L848R	loss	2.9 ± 0.9	31.1 ± 4.3	>3000
H460	Lung	WT	loss	3.1 ± 0.7	11.0 ± 0.8	>3000
H3122	Lung	WT	WT	3.7 ± 0.8	24.2 ± 2.6	>3000
H292	Lung	WT	WT	4.5 ± 1.9	29.9 ± 0.6	>3000
PC-9	Lung	Delta E746-A750	WT	4.9 ± 1.7	33.3 ± 5.2	>3000

Table 2.2. Average anti-proliferative and cytotoxic potencies (Mean viability ± SEM) of mandelalide A in cancer cell lines with different EFGR and LKB1 status.

GI_{50} stands for 50% reduction in cell growth. TGI stards for total growth inhibition. LC_{50} stands for 50% cytotoxicity.

Drug combinations	Cell Lines	Parameters			Combination Index (CI)		
		D_m (nM)	m	r	Fa=0.5	Fa=0.75	Fa=0.9
Erlotinib + Mandelalide A	11-18	236.1	0.68	0.97	0.16	0.12	0.09
	PC-9	12.8	1.39	0.95	0.96	0.85	0.73
Paclitaxel + Mandelalide A	11-18	53.6	1.38	0.98	0.35	0.34	0.32
	PC-9	136.3	0.74	0.98	0.35	0.52	0.86

Table 2.3. Calculated Combination Index (CI) by Chou and Talalay's equation.

11-18 cells and PC-9 cells were treated with combination of mandelalide A and erlotinib or paclitaxel at different concentrations for 72 h. CI was calculated by Chou and Talalay's CI equation. D_m is median-effect dose (concentration in nM that inhibits cell viability by 50%), m is shape of the dose-effect curve (where m=1, m>1, m<1 indicate hyperbolic, sigmoidal, and negative sigmoidal curves, respectively), r linear correlation coefficient of the simulation Fa-CI plot indicating conformity of data. Fa = 0.5, Fa = 0.75, Fa = 0.9 mean fraction affected by drug combination for 50%, 75%, 90% cell viability inhibition, respectively.

ATG5 Promotes Death Signaling in Response to the Cyclic Depsipeptides Coibamide A and Apratoxin A

CHAPTER 3

Xuemei Wan, Jeffrey D. Serrill, Ian R. Humphreys, Michelle Tan, Kerry L. McPhail, Ian G. Ganley and Jane E. Ishmael

Abstract

Our understanding of autophagy and lysosomal function has been greatly enhanced by the discovery of natural product structures that can serve as chemical probes to reveal new patterns of signal transduction in cells. Coibamide A is a cytotoxic marine natural product that induces mTOR-independent autophagy as an adaptive stress response that precedes cell death. Autophagy-related (ATG) protein 5 (ATG5) is required for coibamide-induced autophagy but not required for coibamide-induced apoptosis. Using wild-type and autophagy-deficient mouse embryonic fibroblasts (MEFs) we demonstrate that coibamide-induced toxicity is delayed in ATG5$^{-/-}$ cells relative to ATG5$^{+/+}$ cells. Time-dependent changes in annexin V staining, membrane integrity, metabolic capacity and caspase activation indicated that MEFs with a functional autophagy pathway are more sensitive to coibamide A. This pattern could be distinguished from autophagy modulators that induce acute ER stress (thapsigargin, tunicamycin), ATP depletion (oligomycin A) or mTORC1 inhibition (rapamycin), but was shared with the Sec61 inhibitor apratoxin A. Coibamide- or apratoxin-induced cell stress was further distinguished from the action of thapsigargin by a pattern of early LC3-II accumulation in the absence of CHOP or BiP expression. Time-dependent changes in ATG5-ATG12, PARP1 and caspase-3 expression patterns were consistent with the conversion of ATG5 to a pro-death signal in response to both compounds.

Introduction

Although macroautophagy (hereafter abbreviated to autophagy) and apoptosis are most conveniently studied as two distinct signal transduction pathways, the capacity for cross-talk between these processes has been appreciated for many years [1–4]. Autophagy can be induced beyond normal physiological levels as an early adaptive response to internal or external stress as cells attempt to maintain homeostasis through the "self-eating" of proteins and organelles [2]. In this survival mode, such as that triggered by starvation or exposure to an exogenous chemical, autophagy is favored and apoptosis signaling is inhibited [5]. However, if internal or environmental stress is sustained or cells fail to adapt, autophagy signaling can be suppressed or actively used by the cell to favor death signaling. These cell fate decisions can proceed efficiently through the use of intracellular signals that serve dual functions, in that autophagy-related (ATG) protein complexes regulate apoptosis and apoptotic proteins regulate autophagy [1,4]. The dynamic and context-specific nature of autophagy represents a current challenge to the development of autophagy modulators as therapeutic agents for the treatment or prevention of human disease and thus a better understanding of pro-survival versus pro-death roles of autophagy in cell fate is needed [6]. This is especially important in cancer where the function of autophagy changes over time at different stages of the disease [7].

With respect to pharmacological manipulation of autophagy, natural macrocyclic peptides and polyketides represent an important source of molecular structures with the potential to bind complex intracellular targets and reveal new aspects of cell signaling [8,9]. The utility of these molecules is demonstrated by the fact that some well-characterized macrocycles are already widely used as chemical probes for autophagy research [10]. For example, bafilomycin A1 was one of several bafilomycin structures originally isolated from *Streptomyces griseus* strains, that is now routinely used as a tool compound to assess autophagic flux [10,11]. The binding target of bafilomycin A1 is vacuolar (H^+) ATPase (V-ATPase), a hetero-oligomeric proton pump that is critical for autophagosome-lysosomal fusion [12–16]. Bafilomycin A1 can be used as a pharmacological inhibitor to block autophagosome-lysosomal fusion, and therefore autophagosomal degradation, in

cultured cells [10]. Many more natural products are known to reliably modulate autophagy signaling by indirect mechanisms through binding to a specific regulatory target that lies outside the main autophagy pathway [17]. The macrocyclic polyketide rapamycin (sirolimus), originally from *Streptomyces hygroscopicus*, is perhaps the most famous natural product inducer of autophagy [10,18]. Through direct binding to FK506 binding protein 12, the rapamycin-FK506 complex can subsequently bind, and inhibit the function of, the serine/threonine kinase mechanistic Target of Rapamycin (mTOR) to induce autophagy [19,20]. The utility of natural products to probe very specific aspects of cell signaling is demonstrated by the fact that mTOR forms two distinct protein complexes in mammalian cells but these complexes display differential sensitivity to rapamycin (20). Acute rapamycin treatment inhibits the activity of mTOR complex 1 (mTORC1), whereas mTOR complex 2 (mTORC2) is generally considered rapamycin-insensitive or inhibited only after long exposures in some cell types [20–22].

In our studies of the chemistry and biology of the marine natural product coibamide A (Figure 1), we previously noted that this highly *N*-methylated lariat depsipeptide induces autophagy in cultured human cells and mouse fibroblasts within an hour of exposure [23]. This autophagy response displayed specificity, in that it was not due to a global block in the endocytic capacity of the cell, and occurred via a mechanism that is independent of mTOR kinase inhibition [23]. Autophagosome accumulation in response to coibamide A exposure was dependent on the presence of ATG protein 5 (ATG5), a highly conserved protein that is an essential component of the ubiquitin-like conjugation system, which sequentially drives formation of autophagosomes [24]. However, the presence of ATG5 was not required for cell death; coibamide A effectively induced caspase-dependent apoptosis in ATG5-null cells leading us to conclude that autophagy serves as an indirect stress response that persists in dying cells [23]. Given that coibamide A is capable of triggering apoptosis in the presence or absence of autophagy, we extended our analysis of wild-type and autophagy-deficient mouse embryonic fibroblasts (MEFs) to gain a better understanding of the role of coibamide-induced autophagy in cell fate. Genetically-modified and wild-type MEFs represented a convenient, non-cancer cell system for these studies as coibamide-induced cell

death in human cancer cells is context dependent, and can proceed via apoptosis or alternate death pathways [23]. In the present study, the pharmacological action of coibamide A in MEFs was compared to that of other compounds for which the mechanism of action is known. We find evidence of a functional relationship between autophagy and apoptosis following coibamide A exposure, and show that the marine cyanobacterial natural product apratoxin A (Figure 1) produces the same pattern of responses in cells.

Materials and Methods

Chemicals, Reagents and Antibodies

Coibamide A was re-isolated from material collected by hand using SCUBA from Coiba National Park, Panama, and apratoxin A was isolated from a laboratory culture of a Red Sea strain of Moorea producens [33,60]. Rapamycin, thapsigargin, and tunicamycin were purchased from Sigma-Aldrich Corp. (St. Louis, MO, USA). Oligomycin A was from Santa Cruz Biotechnology Inc. (Santa Cruz, CA, USA) and Z-VAD-fmk from ApexBio (Houston, TX, USA). All compounds were reconstituted in 100% cell culture grade DMSO and stored at −20 °C until the day of treatment. The final concentration of DMSO was 0.1% for all studies. General laboratory reagents were from Sigma-Aldrich Corp. or VWR International (Radnor, PA, USA). Primary and secondary antibodies were commercial sources and used according to recommended protocols. Codes for primary antibodies from Cell Signaling Technology, Inc. (Danvers, MA, USA) were as follows: LC3A/B (#4108), ATG5 (D5F5U; #12994) as conjugated ATG5-ATG12, CHOP (#5554), BiP/GRP78 (#3177), acetyl-CoA carboxylase (#3676), GAPDH (#5174), alpha-tubulin (#2125), beta-actin (#4970S), caspase-3 (#9662S), and PARP-1 (#9532). Anti-SQSTM1/p62 (#ab91526) was from Abcam (Cambridge, MA, USA) and a second anti-ATG5 (N-term; # AP1812a) antibody was from Abgent, San Diego, CA, USA.

Mammalian Cell Culture

Wild-type and ATG5$^{-/-}$ embryonic fibroblasts prepared from 13.5 day mouse embryos were a kind gift from Dr. Noboru Mizushima, Tokyo Medical and Dental University [46]. ATG5-null MEFs transduced to re-express ATG5 in the null background have been described and tested previously [32]. All MEFs were cultured in Dulbecco's Modified Eagle's Medium (DMEM; Mediatech Inc., Manassas, VA, USA), supplemented with 10% fetal bovine serum (FBS; HyClone, Logan, UT, USA), L-glutamine (2 mM), 100 I.U./mL penicillin, and 100 µg/mL streptomycin (1% penicillin/streptomycin; Mediatech Inc.).

Analysis of Cell Morphology, Viability and Caspase Activity

Cell morphology was examined and recorded using a Leica DM IL LED microscope fitted with a Leica DFC400 digital camera. Cell viability was assessed using a WST-8 proliferation/cytotoxicity assay (Cayman Chemical Company, Ann Arbor, MI, USA; #10010199) or a Trypan blue exclusion test, with the viability of vehicle-treated cells defined as 100% in all analyses. For WST-8 assays, MEFs were seeded into 96-well plates at a density of 2000 cells/well in 50 µL of medium. After 18 h, cells were treated with a range of concentrations of coibamide A (0.3 nM–1 µM), apratoxin A (0.3 nM–1 µM) or vehicle (0.1% DMSO) delivered in 50 µL of medium. In separate studies, cells were treated with or without coibamide A in the presence of Z-VAD-fmk (50 µM). For Trypan blue exclusion assays, MEFs were seeded at a density of 3000 cells/well prior to treatment with coibamide A (3 nM and 10 nM) or vehicle (0.1% DMSO). Cells were collected up to 48 h after treatment using Trypsin/EDTA (0.25%) and re-suspended in serum-free medium. Trypan blue reagent (Mediatech Inc., 25-900-CI) was added to the cell suspension at a ratio of 1:1, and cells counted and scored (stained and unstained) by microscopy using a hemocytometer. For caspase activation assays, cells were seeded at a density of 2000cells/well into clear bottom white-walled plates (Greiner CellStar®, Kremsmünster, Austria) and caspase 3/7 activation assessed using a Caspase-Glo® 3/7 luminescent assay (Promega, Fitchburg, WI, USA) according to the protocol for multi-well plate formats.

Detection of Annexin V-FITC and Propidium Iodide by FACS

Wild-type and ATG5-null MEFs were exposed to coibamide A (10 nM) or vehicle (0.1% DMSO) for up to 12 h under standard culture conditions, washed in cold phosphate-buffered saline (PBS), and resuspended in annexin binding buffer (50 mM HEPES, 700 mM NaCl, 12.5 mM $CaCl_2$, pH 7.4) before the addition of Annexin V-FITC (2.5 µL per 100 µL cells) and propidium iodide (0.02 µg/µL) (Invitrogen). Cells were incubated at room temperature for 15 min, washed in binding buffer and analyzed immediately by FACS using a CytoFLEX Flow Cytometer (Beckman Coulter Life Sciences, Brea, CA, USA). A number of 50,000 events were recorded and represented as density plots. MEFs treated with 1 µM of Staurosporine (Enzo

Life Sciences Inc., Farmingdale, NY, USA) for 6 h was used as positive control for apoptosis.

Immunoblot Analysis

At the end of treatment, plates were placed on ice and the cell monolayers rinsed with PBS, lysed and processed as described previously [23]. Briefly, cells were collected by gentle centrifugation, the cell pellet rinsed in PBS and then re-suspended in lysis buffer. Cell lysates were cleared by centrifugation at 16,000× g for 20 min at 4 °C and the protein concentration determined using the bicinchoninic acid (BCA) (Thermo Fisher Scientific Inc., Waltham, MA, USA). Cell lysates were adjusted for protein content and equal amounts of total protein were separated by SDS-PAGE and immobilized onto PVDF membranes. Membranes were then blocked in 5% (w/v) non-fat dry milk in 50 mM Tris-HCl, pH 7.4, 150 mM NaCl (TBS) plus 0.1% Tween-20 (TBS-Tween), and subsequently incubated for 16 h at 4 °C with the appropriate primary antibody in 5% (w/v) bovine serum albumin (BSA). The following day, membranes were washed in TBS-Tween (3 × 10 min) and incubated with the appropriate HRP-conjugated secondary antibody for 1 h at room temperature. Finally, membranes were washed in TBS-Tween (4 × 5 min), and proteins revealed using an enhanced chemiluminescence (ECL) reagent.

Data Analysis

Concentration-response relationships were analyzed using Graphpad Prism Software (Graphpad Software Inc., San Diego, CA, USA), and EC_{50} values derived using nonlinear regression analysis fit to a logistic equation. Statistical significance of cell viability was assessed using a one-way analysis of variance (ANOVA) followed by a student's t-test to compare control and treatment groups.

Results

Wild-Type and ATG5-Null MEFs Show Differential Sensitivity to Coibamide A

Using standard end-point viability assays we previously showed that autophagy is not needed for coibamide-induced cell death. Exposure to coibamide A (100 nM) resulted in caspase-dependent apoptosis in both wild-type cells and those lacking a functional autophagy pathway [23]. However, during routine examination of treated wild-type and ATG5-null MEFs by phase-contrast microscopy, morphological changes in the wild-type cultures were consistently detected first. To pursue this observation, we treated wild-type and ATG5-null MEFs with coibamide A or vehicle (0.1% DMSO) and assessed changes in cell morphology and viability over time. By 24 h more wild-type than ATG5-null MEFs showed characteristic signs of cell rounding and detachment from culture plates when exposed to low nanomolar concentrations of coibamide A (Figure 3.2A). This difference in response to coibamide A (3 nM) was more evident at 36 h, with very few wild-type MEFs showing normal morphology relative to ATG5-null MEFs (Figure 3.2A). When cell viability was quantified using a basic Trypan blue exclusion assay, it was apparent that the rate of cell death was accelerated in MEFs with a functional autophagy pathway (Figure 3.2B). Although coibamide A induced time- and concentration-dependent losses in membrane integrity in both wild-type and ATG5-null MEFs, relative to vehicle-treated control cells, wild-type cells were more sensitive to coibamide A than ATG5-null MEFs (Figure 3.2B).

FACS was used to quantify the potential for coibamide A to induce early apoptosis in each cell line as defined by expression of phosphatidylserine (PS) residues on the outer surface of the plasma membrane [25]. Wild-type and ATG5-null MEFs were treated with or without coibamide A (10 nM) for up to 12 h and then incubated with annexin-V conjugated to FITC and propidium iodide (PI) to distinguish early apoptosis versus secondary death signaling in response to treatment. Although the majority of cells were viable (annexin V negative/PI negative) under these conditions, a population of early apoptotic (annexin V positive/PI negative) cells was detected in wild-type cells after exposure times of 6 h and 12 h (Figure 3.3A). In contrast, ATG5-null MEFs remained viable, and indistinguishable from vehicle-

treated control cells, at 6 h but acquired an early apoptotic signature by 12 h exposure to coibamide A (Figure 3.3B,C). To determine if the observed differences in response could be easily explained by inherent differences in cellular proliferation rate, we used real time impedance-based monitoring of cell spreading and growth, and also calculated the average doubling time of each cell line. These studies revealed no clear differences between the untreated wild type and knockout MEFs. Using seeding densities and culture conditions that were comparable to those used in our cell-based assays we found the adhesion and lag phase of both cell types to be similar (Figure 3.S1A). In the period of logarithmic growth, corresponding to the time frame of coibamide A exposure, wild-type MEFs tended to proliferate more slowly than ATG5-null MEFs (Figure 3.S1A) but this did not translate to a statistically significant difference in the average doubling time of each cell type (Figure 3.S1B).

We next treated wild-type and ATG5-null MEFs with increasing concentrations of coibamide A (0.03 nM to 1 µM) or vehicle (0.1% DMSO) and analyzed cell viability at three different end-points (24 h, 40 h, and 48 h). Using a WST-8 assay, which detects a loss in the metabolic capacity of cells as the read-out of cell viability, clear differences were observed in the sensitivity of wild-type versus ATG5-null MEFs. When assays were terminated at 24 h, coibamide A showed limited cytotoxic efficacy against ATG5-null MEFs (Figure 3.4A). If exposure times were extended to 40 h (Figure 3.4B) or 48 h (Figure 3.4C), the efficacy of coibamide A was enhanced against ATG5-null MEFs, however concentration-response curves for wild-type cells consistently fell to the left of ATG5-null MEFs (Figure 3.4A–C). Nonlinear regression analysis of these cell viability data revealed slight increases in the apparent potency of coibamide A against wild-type cells versus ATG5-null MEFs, but differences were not statistically significant by 48 h as anticipated from earlier studies [23].

The viability of both cell types was enhanced, however, when cells were co-treated with coibamide A and the pan caspase inhibitor Z-VAD-fmk (50 µM). For these studies assays were terminated at 24 h to better distinguish responses in wild-type versus ATG5-null cells. This analysis resulted in concentration-response relationships that were shifted in co-treated wild-type and ATG5-null MEFs relative

to cells treated only with coibamide A (Figure 3.5A). Z-VAD-fmk alone produced no change in the viability of either cell line, whereas over 50% of co-treated wild-type cells were still viable at 24 h in the presence of high concentrations of coibamide A (1–3 μM) and Z-VAD-fmk (Figure 3.5A). Immunoblot analysis of whole-cell lysates harvested from adherent wild-type MEFs treated with coibamide A (3–30 nM), showed concentration-dependent accumulation of the lipidated form of ATG8/LC3, LC3-II, a marker of the autophagosomal membrane [10], and the proteolytic processed forms of PARP1 and caspase-3 [26] (Figure 3.5B). This biochemical evidence of apoptosis signaling in coibamide-stressed cells coupled with the cytoprotective effect of Z-VAD-fmk, regardless of ATG5 status, is consistent with caspase-dependent apoptosis as a primary death mechanism in MEFs in response to coibamide A.

To understand if the absence of ATG5 confers the same pattern of differential sensitivity to other compounds, the activity of coibamide A was tested relative to several reference compounds that are known to influence autophagy via indirect mechanisms. When the viability of wild-type and ATG5-null MEFs was tested in response to increasing concentrations of pharmacological inducers of ER stress (thapsigargin and tunicamycin), an inhibitor of ATP synthase (oligomycin A) or rapamycin, none of the compounds gave a pattern that matched that of coibamide A (Figure 3.6A–D). The viability and/or growth characteristics of wild-type and knockout cells was changed in response to increasing concentrations of all four reference compounds, however, in each case the ATG5-null MEFs were either more sensitive, or as sensitive, as the wild-type cells in this assay (Figure 3.6). Taken together, these results demonstrate that autophagy-competent cells are more vulnerable to coibamide A-induced apoptosis than autophagy-deficient MEFs in a pattern that does not generalize to several other well characterized modulators of autophagy.

Coibamide A-Induced Autophagy Is Not Triggered by Acute ER Stress

As ATG5-null and wild-type MEFs showed contrasting patterns of sensitivity to thapsigargin (Figure 3.6A) and coibamide A (Figure 3.4) we tested the ability of coibamide A to induce a typical ER stress response. For these studies, wild-type

MEFs were treated for 4 and 8 h with fixed concentrations of coibamide A (30 nM), thapsigargin (10 µM), tunicamycin (20 µg/mL), or vehicle (0.1% DMSO) and whole cell lysates collected for immunoblot analysis. All three compounds induced accumulation of LC3-II relative to control, however, coibamide A failed to induce expression of common ER-stress biomarkers: binding immunoglobulin protein (BiP), also known as glucose-regulated protein of 78 kDa (GRP78), or CAAT-enhancer-binding homologous *protein (CHOP) [27,28]* (Figure 3.5A). This lack of BiP and CHOP immunoreactivity was in contrast to thapsigargin- and tunicamycin-treated cells, which showed characteristic increases in both BiP and CHOP expression in this time frame (Figure 3.7A). We next compared the action of coibamide A to the marine natural product apratoxin A. Apratoxin A is the first of a series of macrocyclic depsipeptides originally isolated by Luesch and co-workers from cyanobacteria growing in Apra Harbor, Guam [29]. In previous testing against normal human vascular endothelial cells (HUVECs), apratoxin A induced morphological and biochemical changes that, to date, most closely match the action of coibamide A [30]. For these studies, wild-type and ATG5-null MEFs were treated for 4 h with a single concentration of coibamide A (30 nM), apratoxin A (30 nM), thapsigargin (10 µM), or vehicle (0.1% DMSO). Immunoblot analysis revealed accumulation of LC3-II in wild-type cells treated with all three compounds, in a pattern consistent with the requirement of ATG5 protein for LC3 conversion, however, expression of *CHOP was observed only in response to thapsigargi*n and was induced in both wild-type and ATG5-null cells (Figure 3.7B).

Comparison of Coibamide- and Apratoxin-Induced Cell Death

To investigate the possibility that autophagy-competent cells are more sensitive to apratoxin A, the ability of both compounds to induce apoptosis was compared. Cells were treated in parallel over a range of coibamide A or apratoxin A concentrations (1–30 nM) and tested for activity of the major downstream effector caspases-3 and -7. Although apratoxin A was the more potent activator of caspase-3,7, the two compounds displayed similar patterns of activity in both cell lines (Figure 3.8). Apratoxin A and coibamide A induced concentration-dependent activation of caspases-3,7 with higher activity in wild-type MEFs relative to ATG5-null cells at 24 h (Figure 3.8). These results suggest that apratoxin A and

coibamide A share a common pattern of cell death signaling, at least in fibroblasts. Both compounds: (1) induce autophagy in the absence of acute ER stress and, (2) induce caspase-dependent apoptosis in the absence of autophagy. Moreover, the absence of a functional autophagy pathway confers the same survival advantage in response to both compounds.

The concentration-response relationship for caspase-3,7 activation by both natural products (Figure 3.8) was used to inform an assessment of the stability of the ATG5-ATG12 protein complex relative to biomarkers of autophagy and caspase-dependent apoptosis. Although essential for autophagosome formation, ATG5 can undergo proteolytic cleavage to liberate an N-terminal, unconjugated ATG5 fragment that functions as a pro-apoptotic signal [31]. For these studies, cells were treated with coibamide A (30 nM), apratoxin A (30 nM), or vehicle (0.1% DMSO) and cell lysates were collected for up to 30 h for immunoblot analysis of ATG5, SQSTM1/p62, LC3, PARP1, and caspase-3. SQSTM1/p62 is an LC3 binding protein that is destroyed during autophagy and can be used as an indirect measure of autophagy in combination with other biomarkers [2,10]. As we had previously noted that coibamide A induces a concentration- and time-dependent detachment of MEFs and human glioblastoma cells from cell culture dishes [23], we also collected any detaching cells (24–30 h) and analyzed this population separately. A statistically significant decrease in ATG5 expression (detected as loss of ATG5-ATG12) was observed after exposure to either coibamide A (30 h) or apratoxin A (18 to 30 h) relative to control cells treated with vehicle (0.1% DMSO) for 30 h (Figure 3.7A,B). Unfortunately, efforts to detect the specific N-terminal cleavage fragment of ATG5 were not successful due to high non-specific binding of the antibody in coibamide- or apratoxin-treated cell lysates (data not shown).

These lysates did, however, reveal a steady decrease in expression of SQSTM1/p62 that was statistically significant for apratoxin-treated cells, and a general increase in LC3-II levels over time (Figure 3.9A,B). With respect to apoptosis, proteolytic processed forms of PARP1 and caspase-3 were detected by 18 h of exposure to either coibamide A or apratoxin A, consistent with the timing of caspase-3,7 activation (Figure 3.8), whereas lysates harvested at earlier time

points (0 and 4 h) or after 30 h of vehicle treatment expressed only the unprocessed forms of PARP1 and caspase-3 (Figure 3.7A). Particularly strong immunoreactivity corresponding to the cleaved form of caspase-3 was observed in detached populations of both coibamide- and apratoxin-treated cells, accompanied by a loss of the inactive 32 kDa form of this enzyme relative to all adherent cells. Similarly, unprocessed PARP1 was barely detectable in the detached cell lysates that also showed low levels of ATG5, low SQSTM1/p62, and increased LC3-II relative to the adherent vehicle-treated cells (Figure 3.9A).

Partial Rescue of the Wild-Type Phenotype by Expression of ATG5 in ATG5-Null MEFs.

The role of ATG5 in coibamide A- and apratoxin A-induced cell death was investigated further using a stable cell line, where ATG5-null MEFs had been transduced to re-express ATG5 in the null background [32], and then purified by clonal selection (Figure 3.S2). All three cell lines (wild-type, ATG5-null and ATG5$^{-/-}$ (GFP-ATG5)) were treated with vehicle (0.1% DMSO) or increasing concentrations of either coibamide A or apratoxin A for 24 h to better distinguish responses in wild-type versus ATG5-null cells (Figure 3.4A). In these assays, we observed the same shift in the sensitivity of ATG5$^{-/-}$ cells expressing ATG5 to both coibamide A (Figure 3.10A) and apratoxin A (Figure 3.10B). These cells responded with intermediate sensitivity to both coibamide A and apratoxin A, relative to wild-type and ATG5-null MEFs, suggesting that re-expression of ATG5 resulted in a partial rescue of the wild-type phenotype. Taken together, these results indicate that ATG5 has a functional influence on coibamide A- and apratoxin A-induced cell death.

Discussion

The cyanobacterial secondary metabolites coibamide A (The stereochemistry of natural coibamide A was subsequently revised by Yao and coauthors. Yao, G., Pan, Z., Wu, C., Wang, W., Fang, L., Su, W. (2015) Efficient Synthesis and Stereochemical Revision of Coibamide A. J. Am. Chem. Soc. 137, 13,488–13,491) and apratoxin A were discovered independently as new, structurally-unrelated cyclic depsipeptides with striking anti-proliferative and cytotoxic activity against human cancer cells [29,33]. We previously determined that both compounds induce macroautophagy within hours of exposure as part of a protective response to cytotoxic stress [23,30]. In an analysis of LC3-II turnover we observed enhanced autophagic flux in the early stages of exposure to coibamide A and, with longer exposures, a tendency for dying cells to accumulate LC3-II [10,23]. In the present study, we provide insight into the functional role of autophagy in mammalian cells after exposure to these complex natural products. Coibamide A and apratoxin A induced autophagy before the onset of caspase-dependent apoptosis, consistent with a well-recognized pattern in which cells undergo autophagy and apoptosis in sequence [2]. Moreover, evidence of caspase-dependent apoptosis was temporally correlated with a decline in ATG5 expression, suggesting that ATG5 plays an active role in the switch from survival to pro-death signaling in response to a lethal concentration of either compound. Although coibamide A and apratoxin A also induced cell death in ATG5-null cells, side-by-side comparisons in multiple assays revealed a delayed response relative to cells with a functional autophagy pathway. The pattern of responses evoked by coibamide A and apratoxin A in wild-type and autophagy-deficient fibroblasts could be distinguished from autophagy modulation as a result of mTORC1 inhibition (rapamycin), ER stress (thapsigargin and tunicamycin) or ATP depletion (oligomycin A). As the primary mechanism of action of coibamide A and apratoxin A becomes clearer, these data demonstrate the potential utility of these cyclic depsipeptide structures as future molecular probes to study the relationship between a distinct type of stress-induced autophagy and the conversion of ATG5 to a pro-apoptosis signal.

Although the binding target of coibamide A has not yet been determined, preliminary studies suggest that coibamide A may be an inhibitor of the ER

secretory pathway with some similarity to apratoxin A [30]. Apratoxin A, which has been studied more extensively, is known to act by inhibiting cotranslational translocation of a subset of proteins that are sorted to the secretory compartment of mammalian cells, including receptor tyrosine kinases, growth factors and cytokines [34,35]. This action occurs as a result of direct binding of apratoxin A to the alpha, or channel-forming, subunit of the Sec61 protein translocation channel located at the entrance to the ER secretory pathway [36,37]. Inhibition of Sec61 client proteins by apratoxin A leads to a pattern of cellular consequences, some of which appear to be shared with coibamide A, including induction of mTOR-independent autophagy and a cell cycle phase-specific block in G_1 that precedes cell death [23,30,33,34]. In the present study, loss of viability in response to coibamide A and apratoxin A was delayed in ATG5-null MEFs, whereas cells treated with pharmacologic inducers of ER or mitochondrial stress showed the opposite response. ATG5-null, rather than wild-type, cells were generally more sensitive to tunicamycin, thapsigargin, and oligomycin A. The enhanced sensitivity of ATG5-null cells to tunicamycin and thapsigargin is consistent with previous analyses of ER-stress-dependent cell death in these cells. Ogata and coworkers originally showed that ATG5-null cells have increased vulnerability to ER stress, in keeping with a well-established protective role for autophagy in response to ER stress [38,39]. A second feature that distinguished the action of coibamide A and apratoxin A from that of pharmacologic inducers of ER stress, was a lack of CHOP and BiP expression in response to either cyclic depsipeptide despite evidence of LC3-II accumulation and apoptosis signaling. In contrast, we found tunicamycin and thapsigargin to be strong inducers of CHOP and BiP, as anticipated from early characterization of these compounds [40–42]. Early studies by the Luesch laboratory also distinguished the action of apratoxin A from tunicamycin on the basis of their ability to produce opposing effects on BiP expression [35]. This lack of BiP and CHOP induction in response to coibamide A or apratoxin A, is instead more consistent with the lack of conventional ER stress biomarkers noted after exposure to the Sec61 inhibitor mycolactone [43]. Mycolactone, is a natural product macrolide, produced as a virulence factor by *Mycobacterium ulcerans*, which binds Sec61 alpha, but does not induce BiP expression, phosphorylation of

PERK or cause IRE-dependent splicing of XBP-1 in RAW264.7 macrophage cells [43,44].

ATG5 functions in the context of a cytosolic ATG5-ATG12 protein complex that is essential for autophagosome formation [45]. The total knockout of ATG5 in mice results in animals that die hours after birth due to a failure to adapt to the normal state of nutrient depletion that occurs in the early phase of postnatal life [46]. ATG5 is also an example of a protein that has functions outside the autophagy pathway and is recognized as a central node for conversion of a cytoprotective autophagy response to pro-death signaling via multiple mechanisms [2]. Cleavage of ATG5 by calpain inactivates autophagy signaling and produces a truncated [31,47]. Although we were unable to detect this transient N-terminal fragment in lysates harvested from dying cells, immunoreactivity corresponding to the full length ATG5 protein complex declined in response to coibamide A or apratoxin A. The importance of ATG5 was also demonstrated by the fact that re-expression of ATG5, in the ATG5-null background, partially restored the sensitivity of fibroblasts to either coibamide A or apratoxin A. Similar pro-death roles for ATG5 have been described in a number of other experimental settings when ATG5 levels were either enhanced or suppressed and compared to wild-type cells. In earlier studies by Yousefi and co-workers, silencing of ATG5 in cultured human HeLa cervical or MDA-MA-231 triple negative breast cancer cells, with short interfering RNA (siRNA), rendered these cells more resistant to staurosporine or doxorubicin for several days and delayed cell death [31]. ATG5 has also been shown to be strongly induced by the DNA-damaging agents etopside and cisplatin, and under these conditions is translocated to the nucleus to cause ATG5-dependent mitotic catastrophe and early cell death by apoptosis [48]. Furthermore, after tissue-specific knockout of ATG5 in the acinar cells of the salivary gland, ATG5-null acinar cells showed delayed apoptosis and were more resistant to H_2O_2-induced stress relative to cells with a functional autophagy pathway, which showed early apoptosis and senescent phenotypes [49].

In side-by-side comparisons of untreated, non-synchronized cells, ATG-null cells showed no significant difference in average doubling time. As there is potential for cross talk between autophagy signaling and cell cycle progression [50], it is

possible, however, that wild-type and ATG5-null cells responded to the anti-proliferative stress of coibamide A or apratoxin A exposure differently. Studies in non-synchronized cancer cells indicate that the potent anti-proliferative action of both natural products is due to induction of a phase-specific block in G_1 of the cell cycle [30,33,34]. It is still unclear, however, if activation of autophagy is correlated with a specific phase of the cell cycle [47]. A previous analysis of different pharmacologic inducers of autophagy found autophagy activation to be associated with G_1 and S phases [50], whereas other studies have shown no specific link [51]. A clear role for autophagy, and for ATG5 specifically, has been demonstrated for the mechanism by which cells exit the cell cycle and become senescent [52], and thus it is assumed that other phases of the cell cycle were not impacted by the absence of ATG5 in our experiments although we did not test this directly.

Previous studies have shown that a distinct form of autophagy-dependent, non-apoptotic cell death, termed autosis, can be induced by small synthetic peptides, which trigger death with morphological and biochemical characteristics that can be distinguished from apoptosis and other modes of cell death, such as necroptosis [53,54]. Given that wild-type and ATG5-null cells showed clear caspase-dependent apoptosis after exposure to coibamide A or apratoxin A it is unlikely that either of these cyclic depsipeptides are selective inducers of autosis. Further, cell death by autosis is characterized by several unique features including increased cell-substrate adhesion [54,55], whereas coibamide A and apratoxin A tend to show decreased cell-substrate adhesion leading to cell detachment (Figure 3.7 and [23]). The fungal heptadepsipeptide HUN-7293 was originally identified in a screen for potent inhibitors of cell adhesion before later characterization of natural and synthetic analogues revealed an ability of these molecules to target the Sec61 translocation channel [56–58]. Mycolactone has recently been reported to induce anoikis [59], a specific mode of cell death classified as detachment-induced apoptosis [26]. This finding raises the possibility that cytotoxic Sec61 inhibitors will induce cell detachment as a function of their ability to block biosynthesis of cell adhesion molecules. Further studies will be required to define the precise relationship between cell death and loss of cell-substrate adhesion in response to coibamide A as our previous studies indicate that coibamide-induced cell death can proceed via apoptosis or non-apoptotic pathways depending on the

cell type. For example, U87-MG glioblastoma cells and Apaf-1-null MEFs could be induced to detach from culture dishes without any evidence of caspase-3 activation [23], and thus fail to meet the criteria for anoikis.

In summary, coibamide A and apratoxin A appear to be examples of cytotoxic natural products that promote cross-signaling between ATG5-dependent autophagy and caspase-dependent apoptosis. These relatively new cytotoxins may also prove to be valuable tools for the study of alternate modes of regulated cell death in mammalian cells. These results indicate that mTOR-independent autophagy, without activation of common ER stress markers, may represent an early adaptation to changes in proteostasis after pharmacological inhibition of Sec61 function. Significantly, the absence of BiP/GRP78 and CHOP as biomarkers of acute cell stress potentially distinguishes autophagy stress triggered by cytotoxic Sec61 inhibitors, such as apratoxin A and mycolactone, from that caused by compounds that rapidly disrupt proteostasis within the ER, such as thapsigargin and tunicamycin.

Acknowledgments

Author Contributions: I.G.G. and J.E.I. conceived and designed the experiments; K.L.M. contributed materials and edited the manuscript; J.D.S., X.W., M.T., and I.R.H. performed the experiments; J.D.S., X.W., M.T., and J.E.I. analyzed the data and wrote the manuscript.

Abbreviations

The following abbreviations are used in this manuscript:

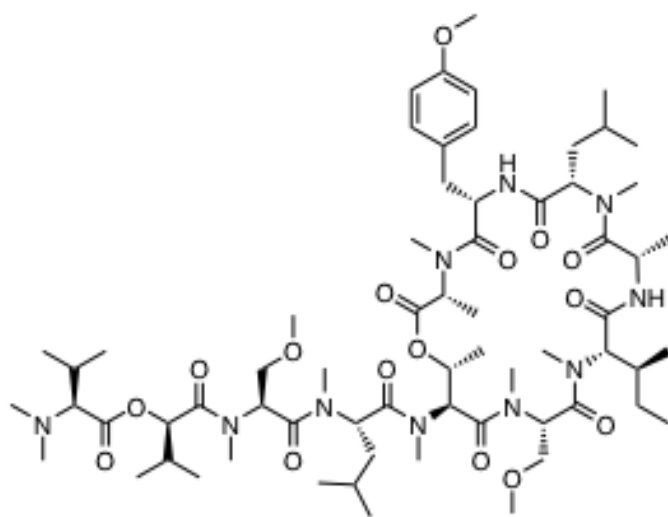|	
PVDF	Polyvinylidene difluoride
SDS-PAGE	sodium dodecyl sulfate-polyacrylamide gel electrophoresis
SCUBA	self-contained underwater breathing apparatus
Z-VAD-fmk	*N*-Benzyloxycarbonyl-Val-Ala-Asp(O-Me) fluoromethyl ketone
FACS	fluorescence-activated cell sorting
DMSO	dimethylsulfoxide

References

1. Rubinstein, A.D.; Kimchi, A. Life in the balance—A mechanistic view of the crosstalk between autophagy and apoptosis. *J. Cell Sci.* **2012**, *125 Pt 22*, 5259–5268, doi:10.1242/jcs.115865.
2. Marino, G.; Niso-Santano, M.; Baehrecke, E.H.; Kroemer, G. Self-consumption: The interplay of autophagy and apoptosis. *Nat. Rev. Mol. Cell Biol.* **2014**, *15*, 81–94, doi:10.1038/nrm3735.
3. Galluzzi, L.; Bravo-San Pedro, J.M.; Vitale, I.; Aaronson, S.A.; Abrams, J.M.; Adam, D.; Alnemri, E.S.; Altucci, L.; Andrews, D.; Annicchiarico-Petruzzelli, M.; et al. Essential versus accessory aspects of cell death: Recommendations of the NCCD 2015. *Cell Death Differ.* **2015**, *22*, 58–73, doi:10.1038/cdd.2014.137.
4. Denton, D.; Xu, T.; Kumar, S. Autophagy as a pro-death pathway. *Immunol. Cell Biol.* **2015**, *93*, 35–42, doi:10.1038/icb.2014.85.
5. Levine, B.; Klionsky, D.J. Development by self-digestion: Molecular mechanisms and biological functions of autophagy. *Dev. Cell.* **2004**, *6*, 463–477.
6. Levine, B.; Packer, M.; Codogno, P. Development of autophagy inducers in clinical medicine. *J. Clin. Investig.* **2015**, *125*, 14–24, doi:10.1172/JCI73938.
7. Mah, L.Y.; Ryan, K.M. Autophagy and cancer. *Cold Spring Harb. Perspect. Biol.* **2012**, *4*, a008821, doi:10.1101/cshperspect.a008821.
8. Driggers, E.M.; Hale, S.P.; Lee, J.; Terrett, N.K. The exploration of macrocycles for drug discovery—An underexploited structural class. *Nat. Rev. Drug Discov.* **2008**, *7*, 608–624, doi:10.1038/nrd2590.
9. Bockus, A.T.; McEwen, C.M.; Lokey, R.S. Form and function in cyclic peptide natural products: A pharmacokinetic perspective. *Curr. Top. Med. Chem.* **2013**, *13*, 821–836.
10. Klionsky, D.J.; Abdelmohsen, K.; Abe, A.; Abedin, M.J.; Abeliovich, H.; Acevedo Arozena, A.; Adachi, H.; Adams, C.M.; Adams, P.D.; Adeli, K.; et al. Guidelines for the use and interpretation of assays for monitoring autophagy. *Autophagy* **2016**, *12*, 1–222, doi:10.1080/15548627.2015.1100356.
11. Werner, G.; Hagenmaier, H.; Drautz, H.; Baumgartner, A.; Zahner, H. Metabolic products of microorganisms. 224. Bafilomycins, a new group of macrolide antibiotics. Production, isolation, chemical structure and biological activity. *J. Antibiot. (Tokyo)* **1984**, *37*, 110–117.
12. Bowman, E.J.; Siebers, A.; Altendorf, K. Bafilomycins: A class of inhibitors of membrane ATPases from microorganisms, animal cells, and plant cells. *Proc. Natl. Acad. Sci. USA* **1988**, *85*, 7972–7976.
13. Zhang, J.; Feng, Y.; Forgac, M. Proton conduction and bafilomycin binding by the V0 domain of the coated vesicle V-ATPase. *J. Biol. Chem.* **1994**, *269*, 23518–23523.
14. Yoshimori, T.; Yamamoto, A.; Moriyama, Y.; Futai, M.; Tashiro, Y. Bafilomycin A1, a specific inhibitor of vacuolar-type H(+)-ATPase, inhibits acidification and protein degradation in lysosomes of cultured cells. *J. Biol. Chem.* **1991**, *266*, 17707–17712.
15. Yamamoto, A.; Tagawa, Y.; Yoshimori, T.; Moriyama, Y.; Masaki, R.; Tashiro, Y. Bafilomycin A1 prevents maturation of autophagic vacuoles by inhibiting
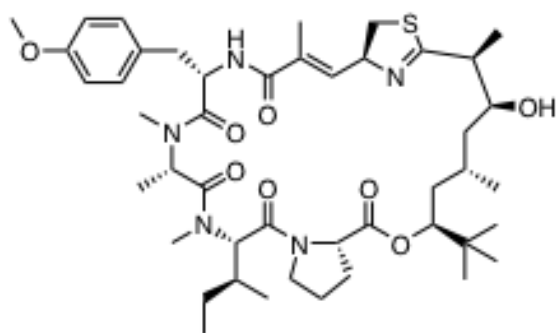
fusion between autophagosomes and lysosomes in rat hepatoma cell line, H-4-II-E cells. *Cell Struct. Funct.* **1998**, *23*, 33–42.

16. Mauvezin, C.; Neufeld, T.P. Bafilomycin A1 disrupts autophagic flux by inhibiting both V-ATPase-dependent acidification and Ca-P60A/SERCA-dependent autophagosome-lysosome fusion. *Autophagy* **2015**, *11*, 1437–1438, doi:10.1080/15548627.2015.1066957.

17. Wang, P.; Zhu, L.; Sun, D.; Gan, F.; Gao, S.; Yin, Y.; Chen, L. Natural products as modulator of autophagy with potential clinical prospects. *Apoptosis* **2017**, *22*, 325–356, doi:10.1007/s10495-016-1335-1.

18. Sehgal, S.N.; Baker, H.; Vezina, C. Rapamycin (AY-22,989), a new antifungal antibiotic. II. Fermentation, isolation and characterization. *J. Antibiot. (Tokyo)* **1975**, *28*, 727–732.

19. Brown, E.J.; Albers, M.W.; Shin, T.B.; Ichikawa, K.; Keith, C.T.; Lane, W.S.; Schreiber, S.L. A mammalian protein targeted by G1-arresting rapamycin-receptor complex. *Nature* **1994**, *369*, 756–758, doi:10.1038/369756a0.

20. Laplante, M.; Sabatini, D.M. mTOR signaling in growth control and disease. *Cell* **2012**, *149*, 274–293, doi:10.1016/j.cell.2012.03.017.

21. Jacinto, E.; Loewith, R.; Schmidt, A.; Lin, S.; Ruegg, M.A.; Hall, A.; Hall, M.N. Mammalian TOR complex 2 controls the actin cytoskeleton and is rapamycin insensitive. *Nat. Cell Biol.* **2004**, *6*, 1122–1128, doi:10.1038/ncb1183.

22. Sarbassov, D.D.; Ali, S.M.; Kim, D.H.; Guertin, D.A.; Latek, R.R.; Erdjument-Bromage, H.; Tempst, P.; Sabatini, D.M. Rictor, a novel binding partner of mTOR, defines a rapamycin-insensitive and raptor-independent pathway that regulates the cytoskeleton. *Curr. Biol.* **2004**, *14*, 1296–1302, doi:10.1016/j.cub.2004.06.054.

23. Hau, A.M.; Greenwood, J.A.; Lohr, C.V.; Serrill, J.D.; Proteau, P.J.; Ganley, I.G.; McPhail, K.L.; Ishmael, J.E. Coibamide A induces mTOR-independent autophagy and cell death in human glioblastoma cells. *PLoS ONE* **2013**, *8*, e65250, doi:10.1371/journal.pone.0065250.

24. Mizushima, N.; Noda, T.; Yoshimori, T.; Tanaka, Y.; Ishii, T.; George, M.D.; Klionsky, D.J.; Ohsumi, M.; Ohsumi, Y. A protein conjugation system essential for autophagy. *Nature* **1998**, *395*, 395–398, doi:10.1038/26506.

25. Kroemer, G.; Galluzzi, L.; Vandenabeele, P.; Abrams, J.; Alnemri, E.S.; Baehrecke, E.H.; Blagosklonny, M.V.; El-Deiry, W.S.; Golstein, P.; Green, D.R.; et al. Nomenclature Committee on Cell, D. Classification of cell death: Recommendations of the Nomenclature Committee on Cell Death 2009. *Cell Death Differ.* **2009**, *16*, 3–11, doi:10.1038/cdd.2008.150.

26. Galluzzi, L.; Vitale, I.; Abrams, J.M.; Alnemri, E.S.; Baehrecke, E.H.; Blagosklonny, M.V.; Dawson, T.M.; Dawson, V.L.; El-Deiry, W.S.; Fulda, S.; et al. Molecular definitions of cell death subroutines: Recommendations of the Nomenclature Committee on Cell Death 2012. *Cell Death Differ.* **2012**, *19*, 107–120, doi:10.1038/cdd.2011.96.

27. Oyadomari, S.; Mori, M. Roles of CHOP/GADD153 in endoplasmic reticulum stress. *Cell Death Differ.* **2004**, *11*, 381–389, doi:10.1038/sj.cdd.4401373.

28. Pyrko, P.; Schonthal, A.H.; Hofman, F.M.; Chen, T.C.; Lee, A.S. The unfolded protein response regulator GRP78/BiP as a novel target for increasing chemosensitivity in malignant gliomas. *Cancer Res.* **2007**, *67*, 9809–9816, doi:10.1158/0008-5472.CAN-07-0625.

29. Luesch, H.; Yoshida, W.Y.; Moore, R.E.; Paul, V.J.; Corbett, T.H. Total structure determination of apratoxin, A.; a potent novel cytotoxin from the marine cyanobacterium Lyngbya majuscula. *J. Am. Chem. Soc.* **2001**, *123*, 5418–5423.

30. Serrill, J.D.; Wan, X.; Hau, A.M.; Jang, H.S.; Coleman, D.J.; Indra, A.K.; Alani, A.W.; McPhail, K.L.; Ishmael, J.E. Coibamide A, a natural lariat depsipeptide, inhibits VEGFA/VEGFR2 expression and suppresses tumor growth in glioblastoma xenografts. *Investig. New Drugs* **2016**, *34*, 24–40, doi:10.1007/s10637-015-0303-x.

31. Yousefi, S.; Perozzo, R.; Schmid, I.; Ziemiecki, A.; Schaffner, T.; Scapozza, L.; Brunner, T.; Simon, H.U. Calpain-mediated cleavage of Atg5 switches autophagy to apoptosis. *Nat. Cell Biol.* **2006**, *8*, 1124–1132, doi:10.1038/ncb1482.

32. Ganley, I.G.; Wong, P.M.; Gammoh, N.; Jiang, X. Distinct autophagosomal-lysosomal fusion mechanism revealed by thapsigargin-induced autophagy arrest. *Mol. Cell.* **2011**, *42*, 731–743, doi:10.1016/j.molcel.2011.04.024.

33. Medina, R.A.; Goeger, D.E.; Hills, P.; Mooberry, S.L.; Huang, N.; Romero, L.; Ortega-Barria, E.; Gerwick, W.H.; McPhail, K.L. Coibamide, A, a Potent Antiproliferative Cyclic Depsipeptide from the Panamanian Marine Cyanobacterium Leptolyngbya sp. *J. Am. Chem. Soc.* **2008**, *130*, 6324–6325.

34. Luesch, H.; Chanda, S.K.; Raya, R.M.; DeJesus, P.D.; Orth, A.P.; Walker, J.R.; Izpisua Belmonte, J.C.; Schultz, P.G. A functional genomics approach to the mode of action of apratoxin, A. *Nat. Chem. Biol.* **2006**, *2*, 158–167, doi:10.1038/nchembio769.

35. Liu, Y.; Law, B.K.; Luesch, H. Apratoxin a reversibly inhibits the secretory pathway by preventing cotranslational translocation. *Mol. Pharmacol.* **2009**, *76*, 91–104, doi:10.1124/mol.109.056085.

36. Paatero, A.O.; Kellosalo, J.; Dunyak, B.M.; Almaliti, J.; Gestwicki, J.E.; Gerwick, W.H.; Taunton, J.; Paavilainen, V.O. Apratoxin Kills Cells by Direct Blockade of the Sec61 Protein Translocation Channel. *Cell chem. Boil.* **2016**, *23*, 561–566, doi:10.1016/j.chembiol.2016.04.008.

37. Huang, K.C.; Chen, Z.; Jiang, Y.; Akare, S.; Kolber-Simonds, D.; Condon, K.; Agoulnik, S.; Tendyke, K.; Shen, Y.; Wu, K.M.; et al. Apratoxin A Shows Novel Pancreas-Targeting Activity through the Binding of Sec 61. *Mol. Cancer Ther.* **2016**, *15*, 1208–1216, doi:10.1158/1535-7163.MCT-15-0648.

38. Ogata, M.; Hino, S.; Saito, A.; Morikawa, K.; Kondo, S.; Kanemoto, S.; Murakami, T.; Taniguchi, M.; Tanii, I.; Yoshinaga, K.; et al. Autophagy is activated for cell survival after endoplasmic reticulum stress. *Mol. Cell. Biol.* **2006**, *26*, 9220–9231, doi:10.1128/MCB.01453-06.

39. Yorimitsu, T.; Nair, U.; Yang, Z.; Klionsky, D.J. Endoplasmic reticulum stress triggers autophagy. *J. Biol. Chem.* **2006**, *281*, 30299–30304, doi:10.1074/jbc.M607007200.

40. Li, W.W.; Alexandre, S.; Cao, X.; Lee, A.S. Transactivation of the grp78 promoter by Ca2+ depletion. A comparative analysis with A23187 and the endoplasmic reticulum Ca(2+)-ATPase inhibitor thapsigargin. *J. Biol. Chem.* **1993**, *268*, 12003–12009.

41. Wang, X.Z.; Lawson, B.; Brewer, J.W.; Zinszner, H.; Sanjay, A.; Mi, L.J.; Boorstein, R.; Kreibich, G.; Hendershot, L.M.; Ron, D. Signals from the

stressed endoplasmic reticulum induce C/EBP-homologous protein (CHOP/GADD153). *Mol. Cell. Biol.* **1996**, *16*, 4273–4280.

42. Zinszner, H.; Kuroda, M.; Wang, X.; Batchvarova, N.; Lightfoot, R.T.; Remotti, H.; Stevens, J.L.; Ron, D. CHOP is implicated in programmed cell death in response to impaired function of the endoplasmic reticulum. *Genes Dev.* **1998**, *12*, 982–995.

43. Hall, B.S.; Hill, K.; McKenna, M.; Ogbechi, J.; High, S.; Willis, A.E.; Simmonds, R.E. The pathogenic mechanism of the Mycobacterium ulcerans virulence factor, mycolactone, depends on blockade of protein translocation into the, E.R. *PLoS Pathog.* **2014**, *10*, e1004061, doi:10.1371/journal.ppat.1004061.

44. Baron, L.; Paatero, A.O.; Morel, J.D.; Impens, F.; Guenin-Mace, L.; Saint-Auret, S.; Blanchard, N.; Dillmann, R.; Niang, F.; Pellegrini, S.; et al. Mycolactone subverts immunity by selectively blocking the Sec61 translocon. *J. Exp. Med.* **2016**, *213*, 2885–2896, doi:10.1084/jem.20160662.

45. Mizushima, N.; Sugita, H.; Yoshimori, T.; Ohsumi, Y. A new protein conjugation system in human. The counterpart of the yeast Apg12p conjugation system essential for autophagy. *J. Biol. Chem.* **1998**, *273*, 33889–33892.

46. Kuma, A.; Hatano, M.; Matsui, M.; Yamamoto, A.; Nakaya, H.; Yoshimori, T.; Ohsumi, Y.; Tokuhisa, T.; Mizushima, N. The role of autophagy during the early neonatal starvation period. *Nature* **2004**, *432*, 1032–1036, doi:10.1038/nature03029.

47. Mathiassen, S.G.; De Zio, D.; Cecconi, F. Autophagy and the Cell Cycle: A Complex Landscape. *Front. Oncol.* **2017**, *7*, 51, doi:10.3389/fonc.2017.00051.

48. Maskey, D.; Yousefi, S.; Schmid, I.; Zlobec, I.; Perren, A.; Friis, R.; Simon, H.U. ATG5 is induced by DNA-damaging agents and promotes mitotic catastrophe independent of autophagy. *Nat. Commun.* **2013**, *4*, 2130, doi:10.1038/ncomms3130.

49. Lin, H.H.; Lin, S.M.; Chung, Y.; Vonderfecht, S.; Camden, J.M.; Flodby, P.; Borok, Z.; Limesand, K.H.; Mizushima, N.; Ann, D.K. Dynamic involvement of ATG5 in cellular stress responses. *Cell Death Dis.* **2014**, *5*, e1478, doi:10.1038/cddis.2014.428.

50. Tasdemir, E.; Maiuri, M.C.; Tajeddine, N.; Vitale, I.; Criollo, A.; Vicencio, J.M.; Hickman, J.A.; Geneste, O.; Kroemer, G. Cell cycle-dependent induction of autophagy, mitophagy and reticulophagy. *Cell Cycle* **2007**, *6*, 2263–2267, doi:10.4161/cc.6.18.4681.

51. Kaminskyy, V.; Abdi, A.; Zhivotovsky, B. A quantitative assay for the monitoring of autophagosome accumulation in different phases of the cell cycle. *Autophagy* **2011**, *7*, 83–90.

52. Young, A.R.; Narita, M.; Ferreira, M.; Kirschner, K.; Sadaie, M.; Darot, J.F.; Tavare, S.; Arakawa, S.; Shimizu, S.; Watt, F.M.; et al. Autophagy mediates the mitotic senescence transition. *Genes Dev.* **2009**, *23*, 798–803, doi:10.1101/gad.519709.

53. Shoji-Kawata, S.; Sumpter, R.; Leveno, M.; Campbell, G.R.; Zou, Z.; Kinch, L.; Wilkins, A.D.; Sun, Q.; Pallauf, K.; MacDuff, D.; et al. Identification of a candidate therapeutic autophagy-inducing peptide. *Nature* **2013**, *494*, 201–206, doi:10.1038/nature11866.

54. Liu, Y.; Shoji-Kawata, S.; Sumpter, R.M., Jr., Wei, Y.; Ginet, V.; Zhang, L.; Posner, B.; Tran, K.A.; Green, D.R.; Xavier, R.J.; et al. Autosis is a Na+,K+-ATPase-regulated form of cell death triggered by autophagy-inducing

peptides, starvation, and hypoxia-ischemia. *Proc. Natl. Acad. Sci. USA* **2013**, *110*, 20364–20371, doi:10.1073/pnas.1319661110.

55. Liu, Y.; Levine, B. Autosis and autophagic cell death: The dark side of autophagy. *Cell Death Differ.* **2015**, *22*, 367–376, doi:10.1038/cdd.2014.143.

56. Hommel, U.; Weber, H.P.; Oberer, L.; Naegeli, H.U.; Oberhauser, B.; Foster, C.A. The 3D-structure of a natural inhibitor of cell adhesion molecule expression. *FEBS Lett.* **1996**, *379*, 69–73.

57. Besemer, J.; Harant, H.; Wang, S.; Oberhauser, B.; Marquardt, K.; Foster, C.A.; Schreiner, E.P.; de Vries, J.E.; Dascher-Nadel, C.; Lindley, I.J. Selective inhibition of cotranslational translocation of vascular cell adhesion molecule 1. *Nature* **2005**, *436*, 290–293, doi:10.1038/nature03670.

58. Garrison, J.L.; Kunkel, E.J.; Hegde, R.S.; Taunton, J. A substrate-specific inhibitor of protein translocation into the endoplasmic reticulum. *Nature* **2005**, *436*, 285–289.

59. Sarfo, F.S.; Phillips, R.; Wansbrough-Jones, M.; Simmonds, R.E. Recent advances: Role of mycolactone in the pathogenesis and monitoring of Mycobacterium ulcerans infection/Buruli ulcer disease. *Cell. Microbiol.* **2016**, *18*, 17–29, doi:10.1111/cmi.12547.

60. Thornburg, C.C.; Cowley, E.S.; Sikorska, J.; Shaala, L.A.; Ishmael, J.E.; Youssef, D.T.; McPhail, K.L. Apratoxin H and apratoxin A sulfoxide from the Red Sea cyanobacterium Moorea producens. *J. Nat. Prod.* **2013**, *76*, 1781–1788, doi:10.1021/np4004992.

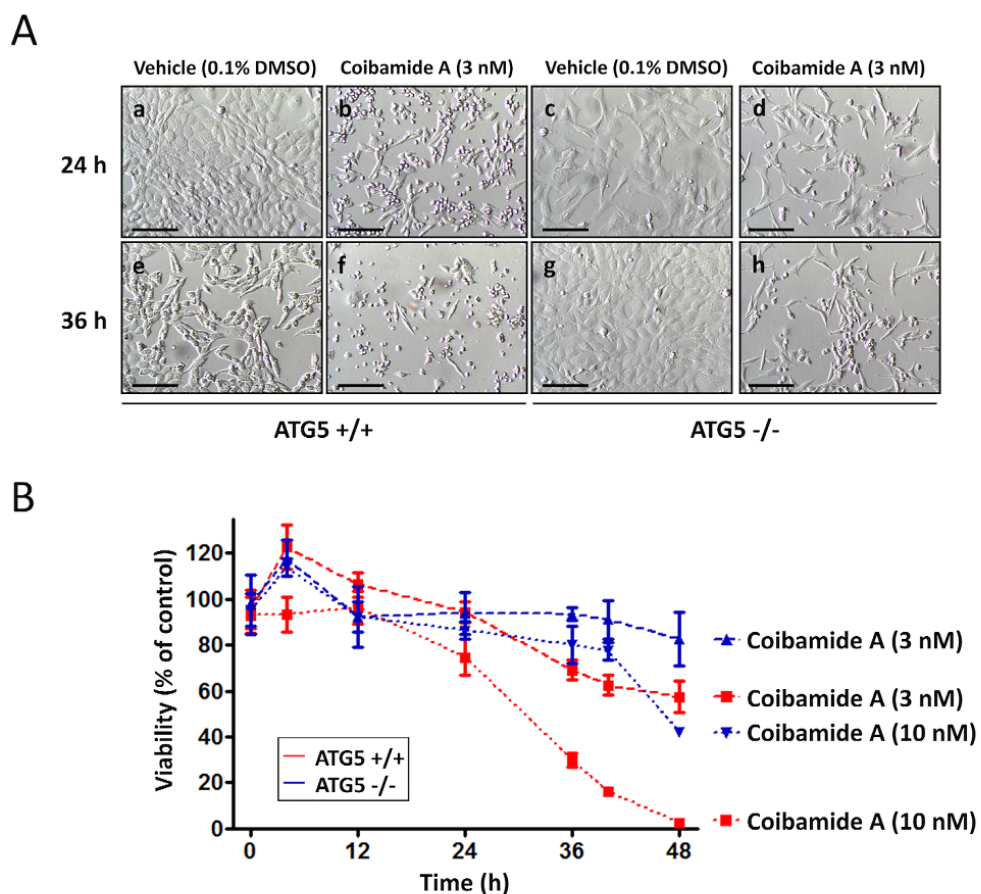**Figure 3.1. Chemical structures of coibamide A and apratoxin A.**

Figure 3.2. ATG5$^{+/+}$ cells are more vulnerable to coibamide A than ATG5$^{-/-}$ cells.

(A) Morphological evaluation of wild-type and ATG5-null mouse embryonic fibroblasts (MEFs) in the presence of coibamide A (3 nM) or vehicle (0.1% DMSO). MEFs were treated as indicated for 24 h (panels a–d) or 36 h (panels e–h) and observed using light microscopy. Scale bar = 500 µm. (B) Trypan blue exclusion test of cell viability in wild-type and ATG5-null MEFs. Cells were seeded at 3000 cells/well and collected up to 48 h after treatment. Trypan Blue exclusion profiles represent mean cell counts ± SE of a time course performed in triplicate with the viability of vehicle-treated cells defined as 100%.
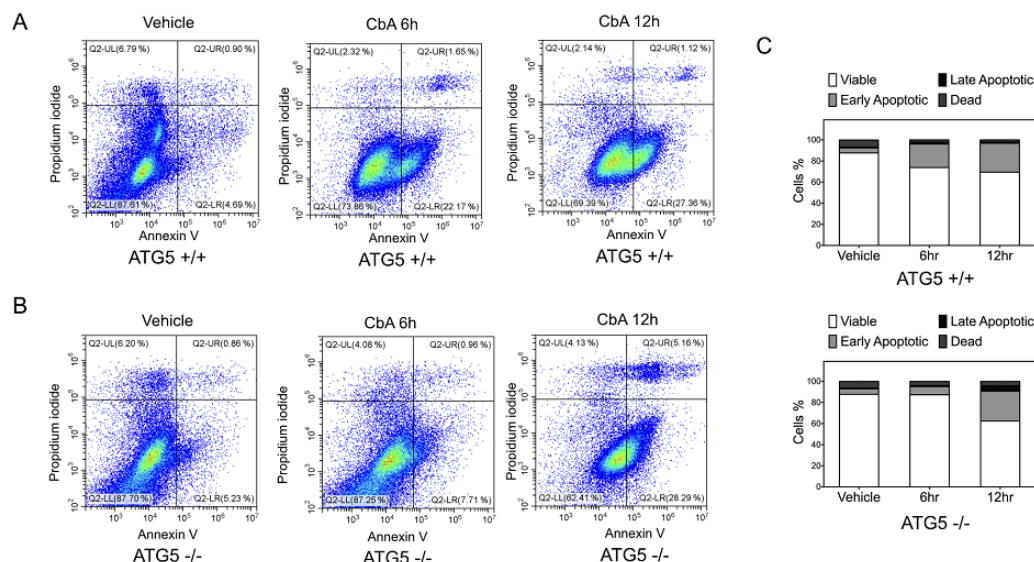
Figure 3.3. Analysis of Annexin V and propidium iodide (PI) staining of ATG5$^{+/+}$ and ATG5$^{-/-}$ cells following coibamide A treatment.

(**A**) Wild-type and (**B**) ATG5-null mouse embryonic fibroblasts (MEFs) were labelled with annexin-V-FITC and PI to separate populations of viable (Lower Left quadrant: annexin V negative/PI negative), early apoptotic (Lower Right: annexin V positive/PI negative), late apoptotic (Upper Right: annexin V positive/PI positive) and dead/necrotic (Upper Left: annexin V negative/PI positive) cells using flow cytometry. Cells were treated with coibamide A (10 nM) or vehicle (0.1% DMSO) for up to 12 h before processing for FACS. Data was collected on a CytoFLEX Flow Cytometer using 1 µM staurosporine-treated cells as a positive control for induction of apoptosis. (**C**) Bar graph represents the percentage of viable, early-stage apoptotic, late-stage apoptotic and dead cells according to treatment. Figure is representative of comparisons made over 2–4 independent experiments.
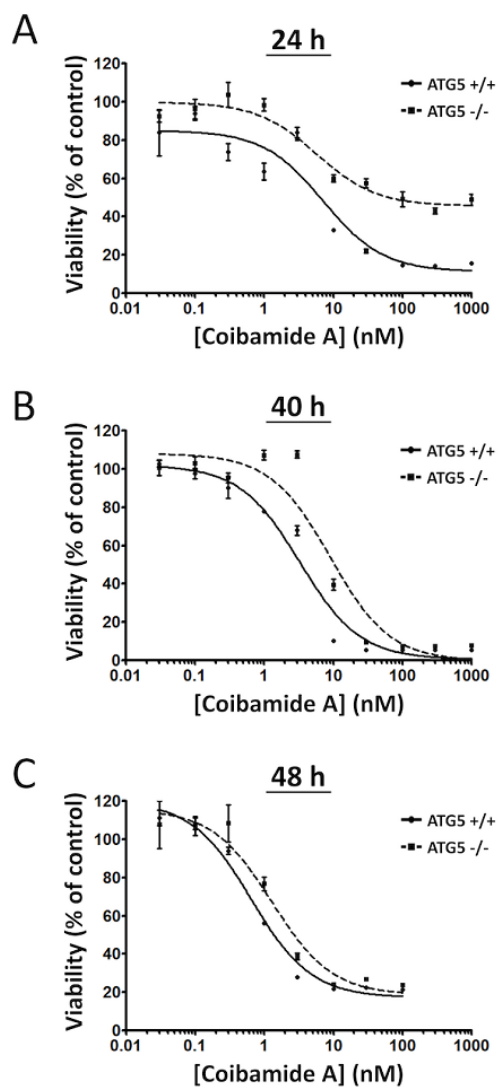
Figure 3.4. Coibamide-induced toxicity is delayed in ATG5$^{-/-}$ cells.

Time- and concentration-dependent changes in the viability of wild-type and ATG5-null mouse embryonic fibroblasts (MEFs) after exposure to coibamide A. Cells were exposed to increasing concentrations of coibamide A (0.3 nM to 1 μM) for (**A**) 24 h, (**B**) 40 h, or (**C**) 48 h. Cell viability was determined at each end-point with a WST-8 proliferation/cytotoxicity assay with the viability of vehicle-treated cells defined as 100%. Data points show mean viability ± SE (*n* = 3 wells per treatment) from a representative comparison that was repeated in three independent experiments.
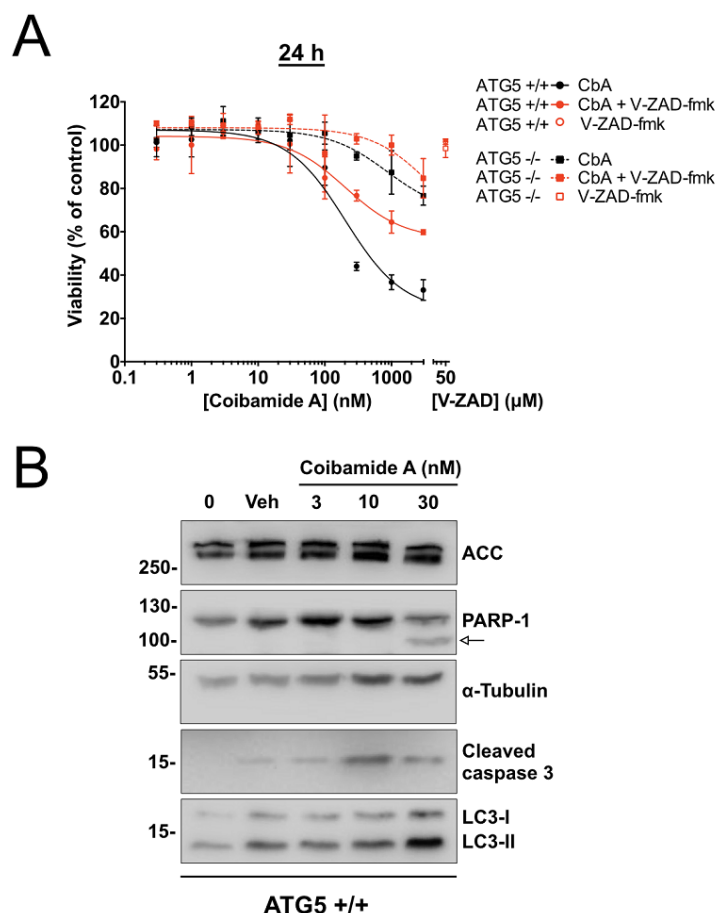
Figure 3.5. The pan caspase inhibitor V-ZAD-fmk inhibits coibamide-induced cytotoxicity in MEFs.

(**A**) Cytoprotective effect of V-ZAD-fmk on both wild-type and ATG5-null mouse embryonic fibroblasts (MEFs) treated with coibamide A. Cells were exposed to increasing concentrations of coibamide A (0.3 nM to 3 µM), with or without V-ZAD-fmk (50 µM), and the viability was determined with a WST-8 proliferation/cytotoxicity assay at 24 h. The viability of vehicle-treated cells was defined as 100%. Data points show mean viability ± SE (n = 3 wells per treatment) from a representative comparison that was repeated in three independent experiments. (**B**) Expression of endogenous biomarkers of autophagy and caspase-dependent apoptosis in wild-type MEFs at 24 h. Immunoblot analysis of: poly [ADP-ribose] polymerase 1 (PARP-1), cleaved caspase-3 and LC3-I/II relative to alpha-tubulin and acetyl-CoA carboxylase (ACC), in cells treated with, or without (0), vehicle (0.1% DMSO) or coibamide A (3–30 nM) for 24 h. Whole cell lysates were probed with appropriate primary antibodies as indicated. Cleavage product of PARP-1 is denoted by an arrow. Each series of blots is representative of patterns that were observed in at least three independent experiments.
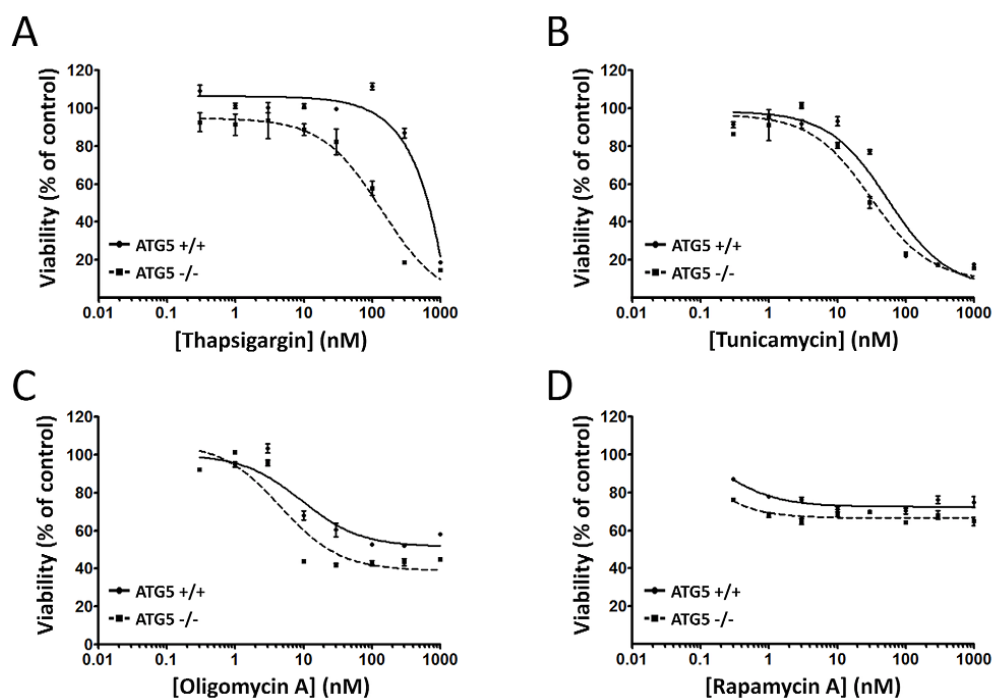
Figure 3.6. Comparison of ATG5$^{+/+}$ and ATG5$^{-/-}$ cell viability in response to known modulators of autophagy.

Concentration-dependent changes in the viability of wild-type and ATG5-null mouse embryonic fibroblasts (MEFs) after exposure to (**A**) thapsigargin, (**B**) tunicamycin, (**C**) oligomycin A, and (**D**) rapamycin A. ATG5$^{+/+}$ and ATG5$^{-/-}$ cells were exposed, in parallel, to increasing concentrations of each compound (0.3 nM to 1 µM) for 48 h. Cell viability was determined by a WST-8 proliferation/cytotoxicity assay, with the viability of vehicle-treated cells defined as 100%. Data points show mean viability ± SE (n = 3 wells per treatment) from a representative comparison that was repeated in three independent experiments.
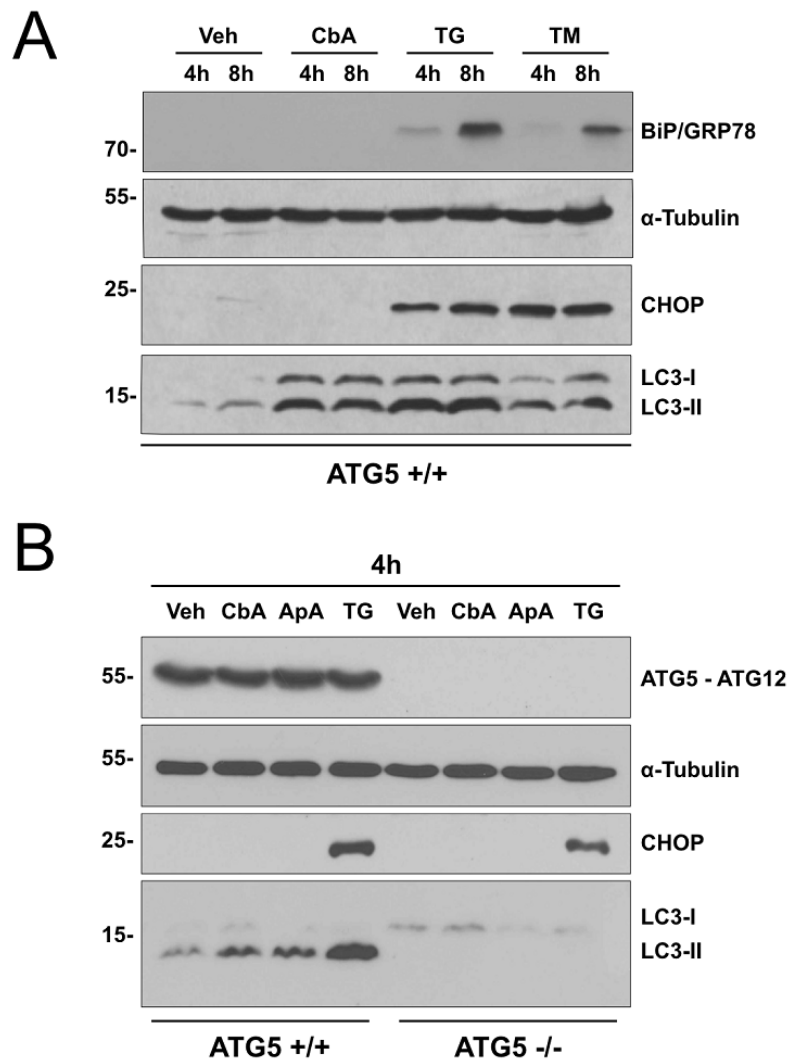
Figure 3.7. Coibamide A-induced autophagy is not triggered by acute ER stress.

Expression analysis of endogenous LC3-II, CHOP, ATG5, and BiP in wild-type and ATG5-null mouse embryonic fibroblasts (MEFs) in response to short-term coibamide A treatment. Immunoblot analysis of: (**A**) LC3-I/II, BiP and CHOP relative to alpha-tubulin after treatment with vehicle (0.1% DMSO), coibamide A (30 nM), thapsigargin (10 µM), and tunicamycin (20 µg/mL) for 4 h and 8 h and, (**B**) LC3 I/II, ATG5, ATG12, and CHOP relative to alpha-tubulin after treatment with vehicle (0.1% DMSO), coibamide A (30 nM), apratoxin A (30 nM), and thapsigargin (10 µM) for 4 h. Whole cell lysates were probed with primary antibodies as indicated; note that ATG5 is detected in the context of the covalent ATG5-ATG12 complex. Each series of blots is representative of patterns that were observed in at least three independent experiments**.**
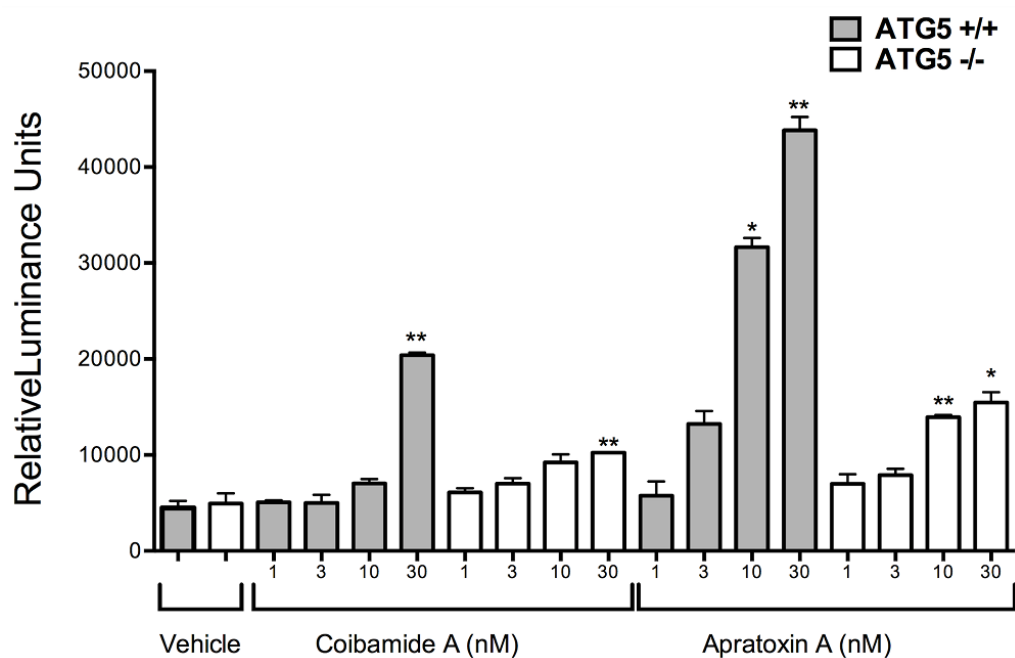
Figure 3.8. Caspase-3,7 activation is delayed in ATG5$^{-/-}$ cells exposed to coibamide A or apratoxin A.

Concentration-dependent analysis of coibamide- or apratoxin-induced caspase activity in wild-type and ATG5-null mouse embryonic fibroblasts (MEFs). Cells were exposed to increasing concentrations of coibamide A (1 nM to 30 nM), apratoxin A (1 nM to 30 nM), or vehicle (0.1% DMSO) for 24 h. Bars represent mean luminescence activity expressed as Relative Light Units ± SE (n = 3 wells per treatment) from three independent comparisons. Statistical significance of activity in treated MEFs relative to control is indicated as * $p < 0.05$, ** $p < 0.01$.
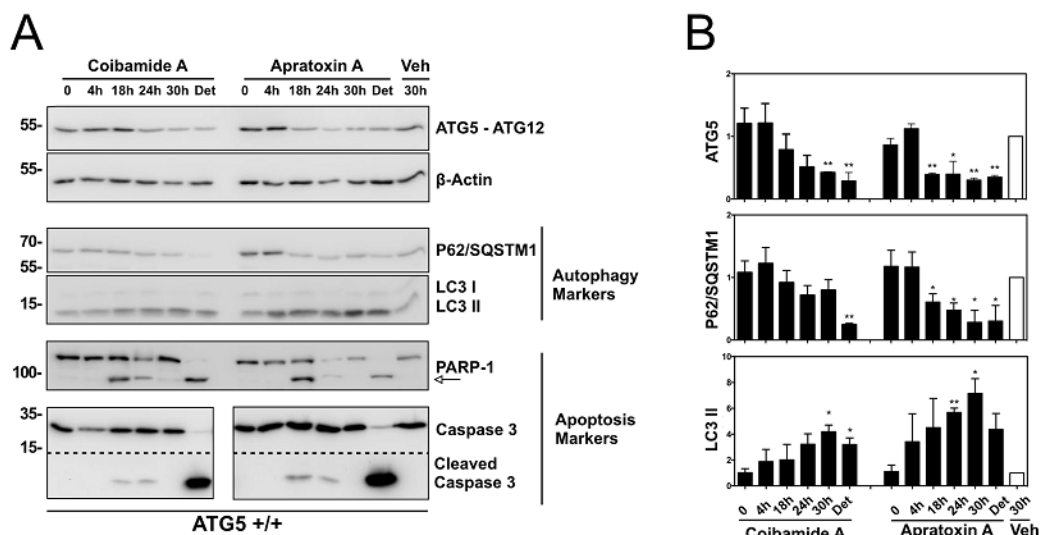
Figure 3.9. Time-dependent analysis of autophagy and apoptosis signals in ATG5$^{+/+}$ cells exposed to coibamide A or apratoxin A.

Wild-type mouse embryonic fibroblasts (MEFs) were treated with, or without (0 unit), coibamide A (30 nM), apratoxin A (30 nM), or vehicle (Veh; 0.1% DMSO) for up to 30 h. Whole cell lysates were collected from adherent and detached (Det) cells (24 and 30 h). (**A**) Immunoblot analysis of ATG5 (detected in the context of the covalent ATG5-ATG12 complex), P62/SQSTM1, LC3, PARP1, caspase 3 expression relative to beta-actin. (**B**) Quantitation of immunoblot data shown in (**A**). Bars represent intensity of bands normalized to beta-actin, relative to vehicle-treated cells (open bars) in three independent experiments. Statistical significance is indicated as * $p < 0.05$ and ** $p < 0.01$.
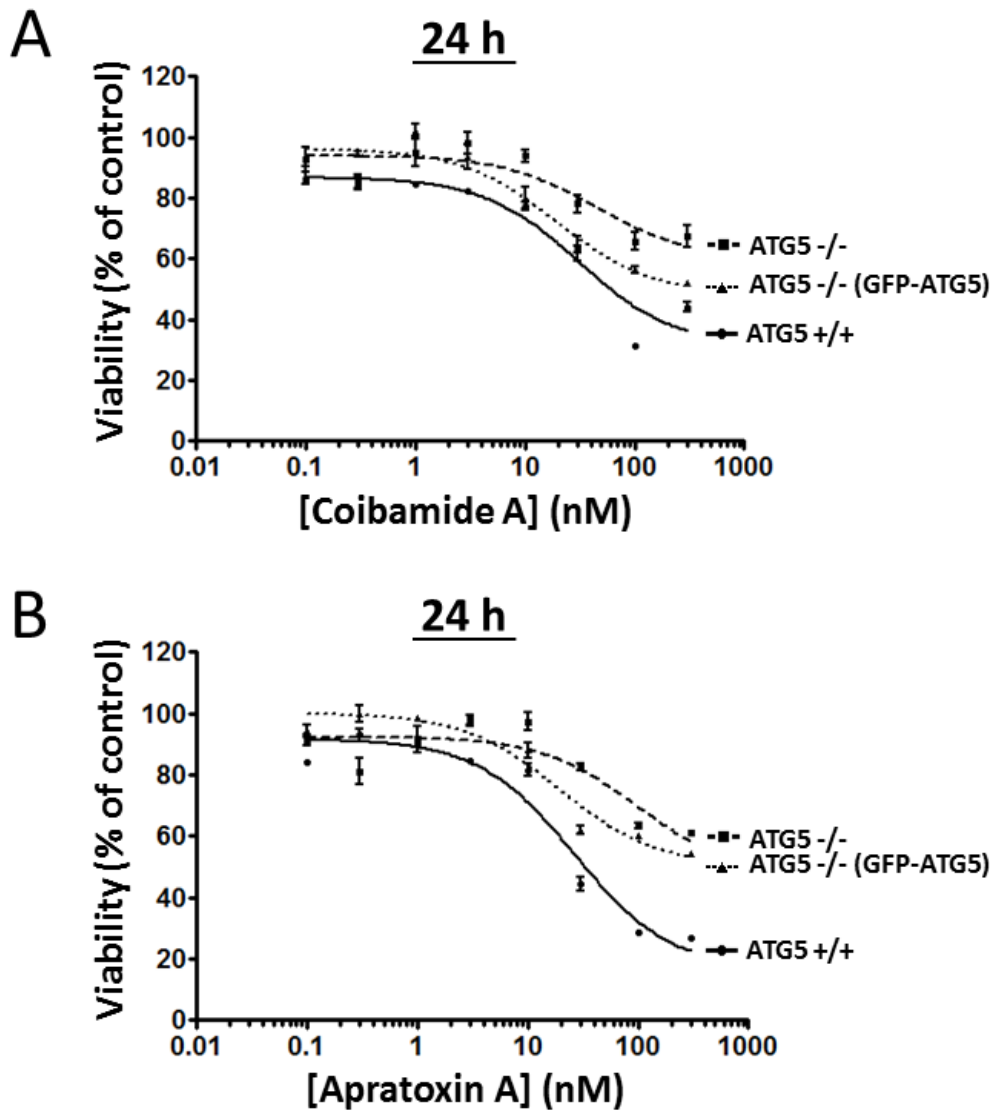
Figure 3.10. Partial rescue of the wild-type phenotype after re-expression of ATG5 in ATG5$^{-/-}$ cells.

Concentration-dependent changes in the viability of wild-type, ATG5-null, and ATG5-null re-expressing ATG5 (ATG5$^{-/-}$ (GFP-ATG5)) in mouse embryonic fibroblasts (MEFs), in response to (**A**) coibamide A or, (**B**) apratoxin A exposure. Cells were exposed to increasing concentrations of coibamide A (0.1 nM to 300 nM), apratoxin A 0.1 nM to 300 nM), or vehicle (0.1 % DMSO) for 24 h. Cell viability was determined in a WST-8 proliferation/cytotoxicity assay, with the viability of vehicle-treated cells defined as 100%. Data points show mean viability ± SE (*n* = 3 wells per treatment) from a representative comparison that was repeated in three independent experiments.
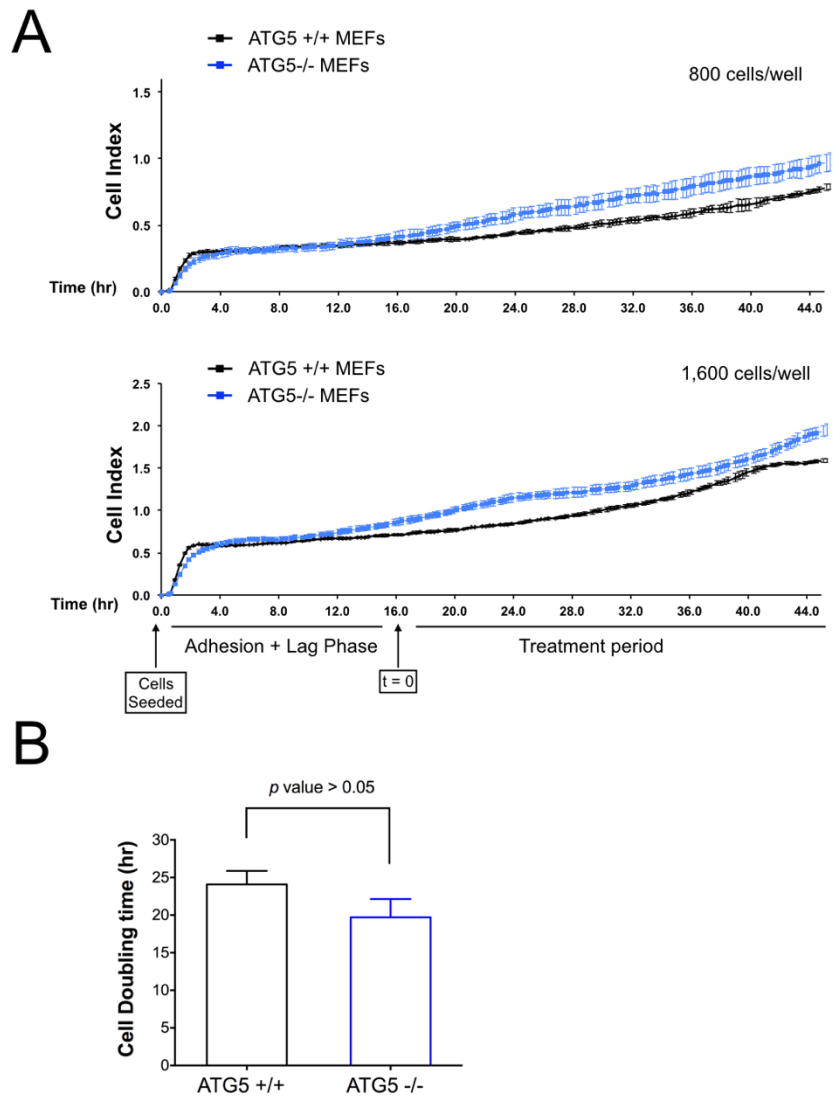
Supplementary S3.1: Comparison of cellular proliferation and doubling time in untreated wild-type, ATG5-nul MEFs.
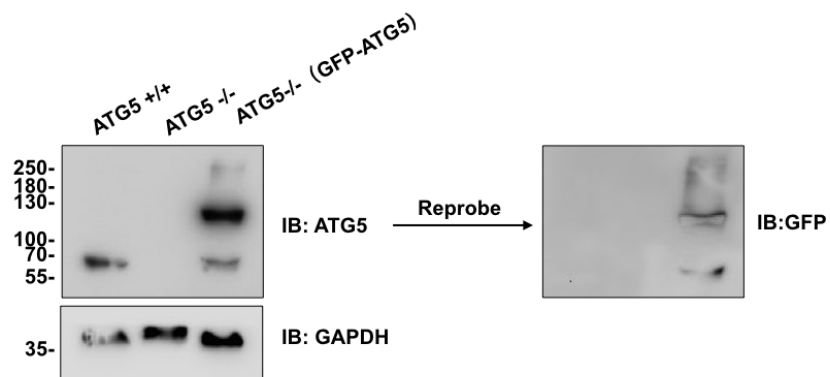
Supplementary S3.2: Analysis of ATG5 expression in wild-type, ATG5-null and ATG5-null mouse embryonic fibroblasts re-expressing GFP-ATG5.

Targeting GRP78 overexpression in canine osteosarcoma cells with the celecoxib derivative OSU-03012 (AR-12)

CHAPTER 4

Xuemei Wan, Daphne R. Mattos, Cheri P. Goodall, Jeffrey D. Serrill, Milan Milovancev, Shay Bracha and Jane E. Ishmael

Abstract

High basal expression of glucose regulated protein 78 (GRP78), and distribution to cellular compartments outside the endoplasmic reticulum (ER), is increasingly associated with several treatment-resistant human cancers. We previously identified peptides corresponding to GRP78 as components of the surface-exposed proteome of cultured canine osteosarcoma cells (*Milovancev et al., BMC Veterinary Research 2013, 9:116*), raising the possibility that GRP78 may also participate in oncogenic signaling in this aggressive spontaneous cancer of the dog. In the present study we characterized GRP78 expression in canine osteosarcoma cells under basal conditions and in response to treatment. GRP78 was upregulated in D17, COS, POS and HMPOS osteosarcoma cells, relative to normal canine osteoblasts, and was further enhanced by pharmacological induction of ER stress by thapsigargin. As canine and human bone cancer showed a conserved ER stress response, we investigated the action of the investigational anti-cancer drug OSU-03012 in canine cells. OSU-03012 induced early inhibition of Akt phosphorylation at Thr308 and Ser473 and decreased expression of GRP78 in POS and HMPOS cells with compensatory increases in the expression of cytosolic heat shock protein (HSP) family members: HSP40 and HSP70. OSU-03012 alone was cytotoxic to canine POS (EC_{50} = 3.8 μM) and HMPOS (EC_{50} = 6.7 μM) cells and, in combination treatment, enhanced the cytotoxic efficacy of carboplatin especially at lower (1-10 μM carboplatin) concentrations. Consistent with the One Health initiative, these results suggest that advances in detection and targeting of GRP78 may eventually benefit a sub-set of canine and human cancer patients.

Introduction

Glucose-regulated protein 78 kDa (GRP78), also known as immunoglobulin heavy chain binding protein (BiP) or heat shock 70 kDa protein 5 (HSPA5), is one of several stress-inducible proteins discovered for their ability to respond to a depletion in intracellular glucose [1-3]. Under normal conditions, GRP78 is located within the lumen of the endoplasmic reticulum (ER) where it functions as the major protein-folding chaperone for new polypeptides entering the secretory pathway [4]. Correct targeting of GRP78 to the ER is mediated by an N-terminal signal peptide that directs nascent GRP78 to the protein translocation machinery at the ER membrane and, after biosynthesis, a classic C-terminal KDEL sorting motif that retains mature GRP78 protein within the ER [3, 4]. In this location, GRP78 has been well-characterized as the major regulator of the unfolded protein response (UPR). In non-stressed cells GRP78 binds to, and inactivates, the function of three independent transmembrane stress receptors: protein kinase RNA-like endoplasmic reticulum kinase (PERK), activating transcription factor 6 (ATF6) and the serine/threonine-protein kinase/endoribonuclease inositol requiring enzyme 1 (IRE1). In the event that the cell has an increased requirement for protein folding, the UPR is triggered to adequately meet this demand, restore homeostasis and avoid a state of stress due to protein overload in the ER [3].

From studies in humans it is now clear that some histological cancer types have a high requirement for protein processing through the secretory pathway in order to meet their high metabolic demands and proliferation rates. These cells have adapted to a state whereby UPR signaling is enhanced and there is high constitutive expression of ER stress proteins [3]. As a major component of this adaptive survival response, GRP78 is increasingly found at high basal levels in many aggressive, chemo-resistant human cancers including glioblastoma, breast cancer, leukemia and castration-resistant prostate cancer (reviewed in [3, 5]). The finding that GRP78 shows atypical expression patterns in cancer cells has also enhanced interest in the potential utility of GRP78 as a biomarker and future druggable target. A sub-population of GRP78 expressed on the plasma membrane of cancer cells, in particular, has inspired the development of monoclonal

antibodies and peptide-mediated targeting strategies as experimental biological therapeutics [6-8].

We previously identified GRP78 and a second ER stress-inducible protein, glucose regulated protein 94 (GRP94), as cell surface-exposed proteins in intact canine osteosarcoma cells (Supplementary Data; [9]). After a sequential biotin-streptavidin labelling and purification technique, multiple unique peptides corresponding to GRP78 and GRP94 were detected using liquid chromatography tandem mass spectrometry (LC-MS/MS). Peptides corresponding to GRP78 and GRP94 were not, however, identified as components of the surface-associated proteome in samples prepared from normal canine osteoblasts [9]. These data raised the possibility that, as in human cancers, resident ER proteins may also be dysregulated in some aggressive canine cancers. In the present study we sought to characterize GRP78 expression and patterns of cell signaling in cultured canine osteosarcoma cells, relative to a range of human cancer cell types that included those known to display high-level GRP78 expression. We find that canine osteosarcoma and human cancer cells share a similar adaptive survival response to ER stress and that GRP78 may eventually be exploited in canines and humans for therapeutic advantage.

Materials and methods

Chemicals, reagents and antibodies

Thapsigargin(#T9033) was purchased from Millipore Sigma(Darmstadt, Germany) and OSU-03012 (AR-12; #A2846-5) was purchased from APExBIO Technology (Houston, TX, USA). Both compounds were reconstituted in 100% cell culture grade dimethyl sulfoxide (DMSO), aliquoted and stored at -20°C. Working concentrations of thapsigargin and OSU-03012 were prepared in DMSO on the day of the experiment; final concentrations of DMSO never exceeded 0.1%. Carboplatin (National Drug Code: 61703-339-50) was purchased as an aqueous solution (10 mg/mL) from Hospira Inc. (Lake Forest, IL, USA). Primary and secondary antibodies were from Cell Signaling Technology, Inc. (Danvers, MA, USA), except anti-HDAC2 (sc-9959) which was from Santa Cruz Biotechnology (Dallas, TX, USA). Specific codes were as follows: GRP78/BiP (#3177), HSP90 (#4877), HSP70 (#4873), HSP40 (#4871), α-Tubulin (#2125), CHOP (#5554) ,GAPDH (#5174) and EGFR (#4267). General laboratory reagents were from VWR International (Radnor, PA, USA).

Mammalian Cell Culture

All cells were maintained as adherent cultures under standard laboratory conditions at 37°C in an atmosphere of 5% CO_2. Human DU145 prostate, U251-MG and U87-MG glioblastoma, MCF-7 breast and canine D17 osteosarcoma cells were cultured in Minimum Essential Media (Corning Cellgro, Corning, NY, USA) supplemented with L-glutamine (2 mM). Human MDA-MB-231 breast cancer cells were cultured in Dulbecco's modified Eagle's medium (Corning Cellgro). Human SAOS-2 osteosarcoma, SK-ES-1 Ewing's sarcoma, HCT116 colon and SKOV-3 ovarian cancer cells were cultured in McCoy's 5A medium (Millipore Sigma). Human SF295 and canine POS, HMPOS and COS osteosarcoma cells were cultured in RPMI 1640 (Corning Cellgro). All medium was supplemented with 10% fetal bovine serum (FBS; VWR International), and 1% penicillin and streptomycin 100 I.U./mL penicillin and 100 μg/mL streptomycin (Mediatech Inc., Manassas, VA). Primary canine osteoblasts (# Cn406K-05) were cultured in canine osteoblast

growth medium (# Cn417K-500) from Cell Applications, Inc. (San Diego, CA, USA).

Cell lysis and fractionation

Whole cell lysates were prepared using fresh ice-cold Lysis Buffer containing Tris-HCl (50 mM; pH 7.5), EDTA (1 mM), EGTA (1 mM), 1% Triton X-100, Sucrose (0.27 M) , sodium fluoride (50 mM), sodium orthovanadate (1 mM), sodium pyrophosphate (5 mM), PMSF (1 mM) and benzamidine (1 mM). All cell lysates were cleared by centrifugation at 16,000 x g for 20 min at 4°C. A subcellular protein fractionatiion kit (Thermo Fisher Scientific Inc. , Walthan, MA) was used to sequentially separate and enrich protein extracts to yield nuclear, cytoplasmic and membrane fractions using the manufacturer's protocol. The protein concentration in all extracts was determined by the bicinchoninic acid (BCA) method (Thermo Fisher Scientific Inc.) and normalized for subsequent analysis.

Western blot analysis

Samples were prepared in 4 x SDS sample loading buffer and subjected to SDS-PAGE. Proteins were then transferred to PVDF membranes (Thermo Fisher Scientific), the membranes blocked in a 5% (w/v) nonfat dry milk in Tris-Buffered saline (TBS): Tris-HCl (50 mM; pH7.4), NaCl (150 mM) containing 0.05% Tween-20 (TBS-T). Membranes were then incubated for 16hrs at 4°C with gentle rotation in the appropriate primary antibody diluted in 5%(w/v) bovine serum albumin (BSA) in TBS-T. On the following day, membranes were washed with TBS-T for 2 x 5 min, then incubated in appropriate horseradish peroxidase (HRP)-conjugated secondary antibody for 1hr at room temperature. Membranes were finally washed in TBS-T for 3 x 5min, and target proteins detected by chemiluminescence using detection reagents (Amersham ECL Chemiluminescent Reagents, GE Healthcare Bio-Sciences, Pitsburg, PA), and visulaized using a myECL™ Imager system (Thermo Fisher Scientific).

Analysis of caspase activity and cell viability

For caspase activity assays, cells were seeded at a density of 3,000 cells/well in 96-well white-walled, clear-bottom plates (Greiner Bio-One, Monroe, NC) and

treated with OSU-03012 (100 nM - 3 µM) or vehicle (0.1% DMSO). At the end of treatment caspase-3,7 activity was measured using a luminescence-based Caspase-Glo 3/7 assay (Promega, WI). The Caspase-Glo reagent, which also serves to lyse the cells, was added directly to each well and the resulting luminescence was measured every 30 min for 2hr using a Synergy HT microplate reader (BioTek Instruments, Vermont, USA). For viability assays, cells were seeded at a density of 3,000 cells/well in 100µL of complete medium in 96-well plates. After 18 hr, cells were treated with OSU-03012, carboplatin or vehicle (0.1%DMSO). Cell viability was assessed using a colormetric 3-(4,5-dimethylthiazol-2-yl)-5-(3-carboxymethoxyphenyl)-2-(4-sulfophenyl)-2H-tetrazolium (MTS) assay (CellTiter 96® Aqueous One, Promega) in which viable cells generate a formazan product detected at 490 nm viable cells using a microplate reader (BioTek Instruments). In all assays, the viability of control, vehicle-treated cells was used to define 100% cell viability.

Data Analysis

Concentration-response relationships were analyzed using GraphPad Prism Software (Graphpad Software Inc. San Diego, CA), and EC_{50} values were determined by nonlinear regression analysis fit to a logistic equation. For immunoblot analysis, signals were normalized to the intensity of control proteins (α-tubulin or GAPDH) and quantified relative to control using ImageJ software (rsbweb.nih.gov/ij). Statistical significance of data derived from cell viability assays and quantification of immunoblot assay were performed using a one-way analysis of variance (ANOVA) followed by a Student's *t*-test comparing untreated controls and treatment groups. *P*-values of 0.05 or less were considered statistically significant.

Results

Canine osteosarcoma cells have high basal expression of GRP78.

In our previous study, peptides matching GRP78 were identified as components of the cell surface proteome of two different canine osteosarcoma cell types (POS, HMPOS) but were not detected as cell surface-associated proteins in normal canine osteoblasts (CnOb) [9]. To understand the potential significance of this finding we compared the basal expression of GRP78 protein, to that of epidermal growth factor receptor (EGFR) in POS, HMPOS and two additional well-characterized canine osteosarcoma cell lines (D17, COS) relative to primary canine osteoblasts. Immunoblot analysis of whole cell lysates prepared from these cells revealed significantly higher basal expression of GRP78 in all four canine osteosarcoma cell types relative to lysates prepared from primary cells (Figure 4.1). GRP78 overexpression was largely consistent across the four canine osteosarcoma cell types and appeared less variable than EGFR expression, which was also elevated in osteosarcoma relative to CnOb but generally showed a more heterogeneous expression pattern (Figure 4.1).

We next compared GRP78 and EGFR expression in canine osteosarcoma cells and several human cancer cell lines representing different histological subtypes. GRP78 expression in canine osteosarcoma cells was comparable, or higher, than that detected in human SK-ES-1 Ewing Sarcoma cells or SAOS-2 osteosarcoma cells, respectively (Figure 4.2). EGFR expression in canine osteosarcoma cell lysates was also higher than EGFR immunoreactivity in human SAOS-2 and SK-ES-1 cells, reflecting a trend whereby the canine osteosarcoma cells tested tended to be clearly positive for both GRP78 and EGFR. Many of the human cell types surveyed showed this similar pattern; lysates harvested from three glioblastoma (U87-MG, SF295, U251-MG), a triple-negative breast cancer (MDA-MB-231), a prostate (DU-145) and colon (HCT116) cancer cell line showed strong co-expression of GRP78 and EGFR (Figure 4.2). In contrast, human breast (MCF-7), ovarian (SKOV-3) and osteosarcoma (SAOS-2) cells with low basal GRP78 expression did not overexpress EGFR.

As GRP78 has been characterized as a biomarker of aggressive, castrate-resistant prostate cancer we selected human DU145 prostate cancer cells as a positive control for analysis of the subcellular distribution of GRP78 in canine POS and HMPOS cells. Membrane fractions of POS and HMPOS cells were strongly immunoreactive for GRP78 relative to the cytoplasmic fraction, whereas the nuclear fractions of canine cells showed weak to no detectable GRP78 immunoreactivity (Figure 4.3, panels A and B). This pattern was consistent with that of EGFR, which was also enriched in the membrane fraction of POS and HMPOS cells, relative to the cytoplasmic fraction. In contrast, heat shock protein 90 (HSP90) was most abundant in the cytoplasmic fraction consistent with the expected subcellular location of this chaperone protein (Figure 4.3). All lysates were probed for histone deacetylase (HDAC-2) and glyceraldehyde 3-phosphate dehydrogenase (GAPDH) which were enriched in nuclear and cytoplasmic fractions, respectively, and thereby served as additional controls to validate the efficiency of the fractionation technique. Together these findings indicate that a significant fraction of the total GRP78 protein in POS and HMPOS cells is associated with endo- or plasma membranes, consistent with our previous study in which GRP78 was identified as a plasma membrane-associated protein. In addition, the expression pattern of GRP78, and other biomarkers, in canine OS cells was generally similar to that seen in human DU145 prostate cancer cells (Figure 4.3, panel C), suggesting that GRP78 may serve a similar function in both cancer cell types.

Pharmacological manipulation of GRP78 expression

To determine if canine osteosarcoma cells respond to pharmacological modulation of GRP78 expression we treated cells with a fixed concentration of thapsigargin (3 µM), a potent inhibitor of the sarcoplasmic or endoplasmic reticulum Ca^{2+} ATPase (SERCA) pump and classic inducer of ER stress [10, 11]. After short-term exposure to thapsigargin all four canine osteosarcoma cells showed large increases in GRP78 expression, relative to vehicle-treated cells, in a pattern that was qualitatively indistinguishable from the response of human SK-ES-1 Ewing Sarcoma cells or SAOS-2 osteosarcoma cells treated under the same conditions (Figure 4.4). Increases in GRP78 were also accompanied by induction of the ER-

stress-associated transcription factor CCAAT-enhancer-binding protein homologous protein (CHOP), detected in all thapsigargin-treated canine and human cells (Figure 4.4). These results indicate that canine osteosarcoma cells undergo a typical UPR, with the ability to upregulate GRP78 beyond basal levels, and likely share common mechanism of ER stress signaling.

We next treated canine osteosarcoma cells with a derivative of the nonsteroidal anti-inflammatory drug celecoxib, known as OSU-03012 (or AR-12). Unlike celecoxib, OSU-03012 does not inhibit COX-2 but was originally developed as an inhibitor of 3-phosphoinositide-dependent kinase-1 (PDK1) with anticancer potential [12, 13]. Although OSU-03012 may affect multiple cellular targets, it has been proposed that the cytotoxic potential of this small molecule is, at least in part, through suppression of GRP78 [14, 15]. As Akt is a major downstream effector of PDK1, and also implicated in oncogenic signaling of cell surface GRP78, we analyzed the phosphorylation status of Akt as a readout of the PDK1/Akt pathway. Immunoblot analysis of whole cell lysates prepared from canine POS and HMPOS cells treated with, or without, OSU-03012 (1 μM to 10 μM) revealed an early, concentration-dependent decrease in phospho-Akt (Thr308 and Ser473) in POS (Figure 4.5 panels A and B) and HMPOS (Figure 4.5, panels C and D) cells, consistent with the known action of OSU-03012 as a PDK1 inhibitor. Expression levels of GRP78 were decreased only in HMPOS cells in this time frame (Figure 4.5, panels C and D), however a statistically significant decrease in GRP78 expression was observed after longer exposures to lower concentrations. After a 24 h exposure to OSU-03012 (300 nM), GRP78 expression was dramatically decreased in both POS (Figure 4.6 panels A and B) and HMPOS (Figure 4.6, panels D and E) cells, relative to vehicle-treated cells (0.1% DMSO). GRP78 immunoreactivity was detected after 36 h treatment, suggesting a potential for desensitization or reversal of this response to OSU-03012, but remained suppressed relative to vehicle-treated cells. In contrast, the cytosolic heat shock proteins (HSPs) 70 and 40 showed clear time-dependent increases in expression in both POS (Figure 4.6, panels A and B) and HMPOS (Figure 4.6, panels D and E) cells in this time frame (24 to 36 h) relative to vehicle-treated cells. These studies confirmed that GRP78 is a downstream target of OSU-03012-induced signaling in POS and HMPOS cells.

OSU-03012 induces cell death in canine osteosarcoma cells

As elevations in HSP70 and HSP40 are typically associated with a pro-survival stress response [16], we tested the ability of OSU-03012 to induce caspase-3,7 activity as a biomarker of apoptosis signaling. When cells were treated with increasing concentrations of OSU-03012 (100 nM to 3 µM), statistically significant increases in caspase-3,7 activity were observed in POS (Figure 4.6, panel C) and HMPOS (Figure 4.6, panel F) at 24h, relative to cells treated with vehicle- (0.1% DMSO) treated cells. Increases in caspase-3,7 activity in response to OSU-03012 were generally higher in POS cells, relative to activity in HMPOS cells (Figure 4.6, panels C and F). Prolonged exposure to OSU-03012 (3 nM to 10 µM), however, induced a concentration-dependent reduction in the viability of both POS (Figure 4.7, panel A) and HMPOS (Figure 4.7, panel B) cells as determined by end point assays at 72 hr. Using an MTS proliferation/cytotoxicity assay, which detects loss of metabolic capacity as the read-out, OSU-03012 induced a sharp decrease in cell viability with EC_{50} values of 3.8 µM and 6.7 µM for POS and HMPOS cells, respectively (Table 1). These results indicate that OSU-03012 is cytotoxic to POS and HMPOS, as a single agent, and provide evidence for apoptosis as a likely cell death mechanism at least in POS cells.

OSU-03012 potentiates the action of carboplatin on canine osteosarcoma cells

Carboplatin is widely used as an adjuvant therapy in canine OS and has been shown to produce a significant increase in median survival time, relative to dogs that receive surgery alone [17]. Using the same experimental conditions to assess cell viability, we tested the potency and efficacy of carboplatin treatment alone and in combination with OSU-03012. Carboplatin alone (1.56 to 200 µM) induced a concentration-dependent reduction in the viability of both POS (Figure 4.7, panel C) and HMPOS (Figure 4.7, panel D) cells with EC_{50} values of 28.4 µM and 10.1 µM for POS and HMPOS cells, respectively (Table 1). When cells were exposed to carboplatin (1.56 to 200 µM) in the presence of a fixed, sub lethal concentration of OSU-03012 (1 µM), the concentration-response curves for combination treatment were shifted for both POS (Figure 4.7, panel C) and HMPOS (Figure 4.7,

panel D) cells. Non-linear regression analysis of these data revealed EC_{50} values of 5.5 µM and 4.6 µM for POS and HMPOS cells, respectively (Table 1). Taken together, these data indicate that OSU-03012 can potentiate the action of carboplatin, leading to enhanced cytotoxic efficacy of carboplatin against cultured POS and HMPOS cells (Figure 4.7).

Discussion

Primary osteosarcoma is one of several spontaneous cancers affecting humans and dogs where a comparative oncology approach has the potential to accelerate our understanding of the disease and the development of new treatments to benefit both species [18, 19]. Current standard of care, for dogs and humans, proceeds with a combination of surgical resection, radiation and chemotherapy, however lung metastases are a significant complication of osteosarcoma leading to extremely low survival rates in patients with progressive disease [20-22]. In the dog, low survival rates are attributed to the fact that most patients have micrometastases that are clinically undetectable at the time of diagnosis [23] [17]. In our search for better tools for the prognosis and treatment of osteosarcoma, we previously identified GRP78 as a surface-exposed protein in canine osteosarcoma cells [9]. In the present study we expanded our analysis of this chaperone protein and find that GRP78 has potential utility as both a biomarker of canine osteosarcoma and a therapeutic target. Comparisons of GRP78 expression in normal canine osteoblasts, and several different human cancer cell types, indicate that the pattern of GRP78 dysregulation in canine osteosarcoma cells is consistent with patterns reported in several aggressive human cancers associated with chemoresistance. Specifically, GRP78 is upregulated in canine osteosarcoma cells under basal conditions and expression can be further enhanced in response to pharmacological induction of ER stress. Canine GRP78 was localized to multiple sub-cellular compartments in osteosarcoma cells and although predominantly associated with membrane fractions was also detected in the cytoplasm. We show that canine osteosarcoma cells are sensitive to micromolar concentrations of the celecoxib derivative OSU-03012 and that the mixed pharmacologic action of this small molecule can be exploited to enhance the cytotoxicity of carboplatin.

Our earlier study identified a sub-set of 113 surface-associated proteins that displayed distinct heterogeneity between samples and provided numerous leads for follow-up analyses [9]. The identification of GRP78 as a surface-exposed protein in intact canine osteosarcoma cells is consistent with the results of similar proteomic analyses of the surface proteome of human cancer cells. Using biotinylation enrichment and mass spectrometric analysis of several different

cancer cell types, Shin and coworkers identified GRP78, other glucose-regulated and heat shock chaperone proteins as cell surface proteins [24]. An increasing body of evidence indicates that cell surface GRP78 serves a distinct function and can promote oncogenic signaling through multiple signal transduction pathways. For example, GRP78 appears to be activated by circulating α_2-macroglobulin to drive Akt/PKB signaling in cancer cells, and can form a distinct complex at the plasma membrane with the GPI-anchored oncoprotein CRIPTO [25-27]. Advanced biochemical studies have concluded that, in the absence of a membrane localization signal, GRP78 is likely translocated to the cell surface of cancer cells through interactions with other client proteins to yield distinct subpopulations [28]. In human cells these independent populations include: (1) extracellular GRP78, that is peripherally associated with the extracellular surface of the plasma membrane, (2) integral forms of GRP78, embedded within the plasma membrane or ER membranes, and (3) soluble, non-membrane associated forms [28]. Taken together, our analyses of intact and fractionated cells indicate that GRP78 may be subject to a similar heterogeneous distribution pattern in canine osteosarcoma cells.

The clinical significance of ER stress signaling has been studied far less in canine cancer, however the same glucose-regulated proteins (GRP78 and GRP94) have been identified by others using global gene expression profiling and proteomics approaches from either patient samples or cultured cells. In an analysis of several spontaneous canine tumors, the gene encoding GRP78 was found to be significantly upregulated in a canine hemangiosarcoma and in an osteosarcoma patient [29]. Moreover, peptides corresponding to GRP78 and GRP94 were previously detected in a proteomic analysis of tissue prepared from canine prostate and bladder and found to be overexpressed in the carcinomas relative to normal tissue [30]. In a recent proteomic analysis of human and canine osteosarcoma cells, GRP78 was identified as a plasma membrane protein in samples prepared from canine POS cells (Supplementary Data; [31]). These authors utilized a different biochemical extraction of plasma membrane proteins, to that used in our studies, followed by peptide mass fingerprinting to focus on proteins with differential expression in metastatic versus non-metastatic cells [31]. In a different study, Asling and co-authors were able to visualize GRP78 in canine D17

osteosarcoma cells using confocal microscopy and found it to be expressed in multiple cellular compartments that changed in response to treatment [32].

In the present study we characterized the action of OSU-03012 against canine POS and HMPOS osteosarcoma cells alone and in combination with carboplatin. Although designed as a PDK1 inhibitor, OSU-03012 has unusual pharmacology and has been tested in phase 1 clinical trials as an oral cancer chemotherapeutic agent (ASCO 2013 meeting http://meetinglibrary.asco.org/content/115148-132). Our results indicate that OSU-03012 alone is relatively toxic to canine POS and HMPOS osteosarcoma cells, in that continuous exposure to low micromolar concentrations resulted in loss of metabolic capacity in both cell types. With respect to the mechanistic basis for the observed cytotoxicity, we detected an early inhibition of phospho-Akt (at Thr308 and Ser473) in POS and HMPOS cells after short exposures to micromolar concentrations of OSU-03012. These results were consistent with the original pre-clinical characterization of this compound in which indirect inhibition of Akt signaling was shown in cultured human PC-3 prostate cancer cells [12]. However, our results are also in agreement with those of other investigators who conclude that PDK1 inhibition alone is unlikely to account for the cytotoxic efficacy of OSU-03012 [14, 15, 33]. After longer exposures to sub-micromolar concentrations of OSU-03012, we observed statistically significant decreases in GRP78 expression that were temporally correlated with elevations in biochemical biomarkers of cell stress (HSP70; HSP40) and death signaling (capspase-3,7), respectively. It has been proposed, from analyses of GRP78 expression after cycloheximide chase experiments, that OSU-03012 induces degradation of GRP78 resulting in a shorter half-life and loss of the mature protein [15]. Recent studies also suggest that OSU-03012 forms a complex with other chaperone proteins and therefore may not be specific to GRP78 [34, 35]. Although the precise mechanism of action of OSU-03012 is still an area of active investigation, the potential for suppression of PDK1/AKt signaling and depletion of the total cellular pool of GRP78 may both be considered attractive properties with the potential to contribute to the overall anti-cancer potential of this unusual compound.

We chose carboplatin as an example of a clinically-relevant chemotherapeutic agent that has been shown to produce a significant improvement in outcomes when used as adjuvant therapy in the treatment of canine osteosarcoma [21]. Carboplatin is a platinum-based drug and one of three older cytostatic agents, along with cisplatin and doxorubicin, that prolong median survival time in osteosarcoma patients relative to dogs that receive only surgery [17]. As OSU-03012 alone was surprisingly cytotoxic to canine POS and HMPOS osteosarcoma cells, we studied the action of carboplatin in the presence of a sub-lethal concentration fixed at 4 to 7 times below the calculated EC_{50} for OSU-03012 against POS and HMPOS cells, respectively. Under these conditions the concentration-response relationship for carboplatin was shifted to the left reflecting superior cytotoxic efficacy of carboplatin, particularly at low range concentrations (1-10 μM), when used with OSU-03012. These results suggest that OSU-03012 has an additive, and for POS cells a possible potentiating, effect on carboplatin when used in combination. This finding is generally consistent with the trend reported by others who have studied OSU-03012 in combination with other clinically approved drugs over a range of different canine and human cancer cell types. For example, OSU-03012 was previously found to suppress PDK1/Akt signaling, inhibit proliferation and induce apoptosis in canine Ace-1 prostate cancer cells and these effects were additive when OSU-03012 was combined with doxorubicin [36]. Oral OSU-03012 also improved the *in vivo* efficacy of tamoxifen, without inducing overt toxicity, in mice bearing human breast cancer xenografts that received treatment each day for five weeks [37]. Several pre-clinical studies in brain tumor, breast and non-small cell lung cancer cells have also reported an enhanced activity of OSU-03012 when used in combination with receptor tyrosine kinase and phosphodiesterase type 5 (PDE5) inhibitors such as lapatinib, gefitinib, and erlotinib or sildenafil, respectively [38-41]. Thus our study of carboplatin serves to expand the range of pharmaceuticals that have been evaluated in combination with OSU-03012 and supports the further investigation of stress-induced proteins as therapeutic targets in canine osteosarcoma. These results also compliment a recent study in which cultured canine osteosarcoma cells were targeted with VER-155008, a small molecule inhibitor of HSP70 function [32]. VER-155008 is a tool compound that was shown to induce apoptosis in canine

osteosarcoma cells, but failed to enhance the efficacy of doxorubicin possibly as a result of compensatory elevations in HSP70 and GRP78 expression [32].

Our comparative analysis of basal GRP78 expression in cultured canine cells, revealed positive immunoreactivity for endogenous EGFR and GRP78 in all four of the lysates tested. This pattern of co-expression is potentially significant as elevated EGFR is an important prognostic biomarker for several human cancers, that in practice leads to the stratification of patients to take advantage of the many targeted medicines that have been developed to inhibit this signaling pathway. With respect to canine osteosarcoma, Selvarajah and co-authors previously reported that a subset of dogs showed high EGFR expression in both primary osteosarcoma and lung metastatic sites in a pattern associated with a significantly shorter survival and disease-free interval [42]. These authors concluded that while EGFR expression alone was not a reliable prognostic biomarker, some dogs may benefit from medicines targeting EGFR signaling [42]. The study of EGFR expression in human osteosarcoma has resulted in similar conclusions in that the receptors are expressed but it is unclear if osteosarcoma patients could benefit from EGFR-targeted monotherapy [43, 44]. Elevated EGFR expression has been linked, however, to stress-induced survival responses in human osteosarcoma although GRP78 was not studied specifically [45]. Our studies raise the possibility that knowledge of GRP78 and EGFR status in canine osteosarcoma may be more informative than EGFR status alone. For example, a recent study of human patients with oropharyngeal carcinoma, found those with co-expression of EGFR and GRP78 had a significantly worse prognosis than patients either biomarker alone [46].

In summary, we have extended our analysis of GRP78 in canine osteosarcoma cells and find evidence for an atypical expression pattern that likely contributes to alternate roles for GRP78 outside the ER in both dogs and humans. Given the intense interest in targeting GRP78 for therapeutic advantage, not only in cancer, but also for the treatment of conditions such as obesity and infectious disease [47-49], it appears that future advances in GRP78 detection and drug development may eventually benefit canine and human cancer patients.
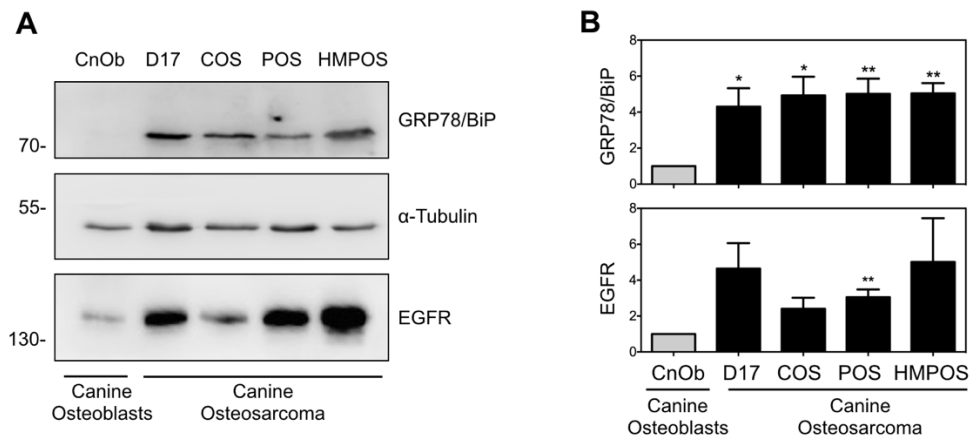
Funding

Figure 4.1 Comparative analysis of GRP78 expression in primary canine osteoblasts versus canine osteosarcoma cells

(**A**) Immunoblot analysis of GRP78/BiP, EGFR and α-tubulin expression in normal canine osteoblasts (CnOb) and four established canine osteosarcoma cancer cell lines (D17, COS, POS, HMPOS). (**B**) Bars represent quantification of immunoblot data from three independent comparisons. Whole cell lysates were prepared at the same time from each adherent culture and processed for Western blot analysis with the antibodies indicated. GRP78/BiP, EGFR signals were normalized to α-tubulin and the statistical significance signals in OS cell compared to those in CnOb is indicated as * p< 0.05, ** p < 0.01).
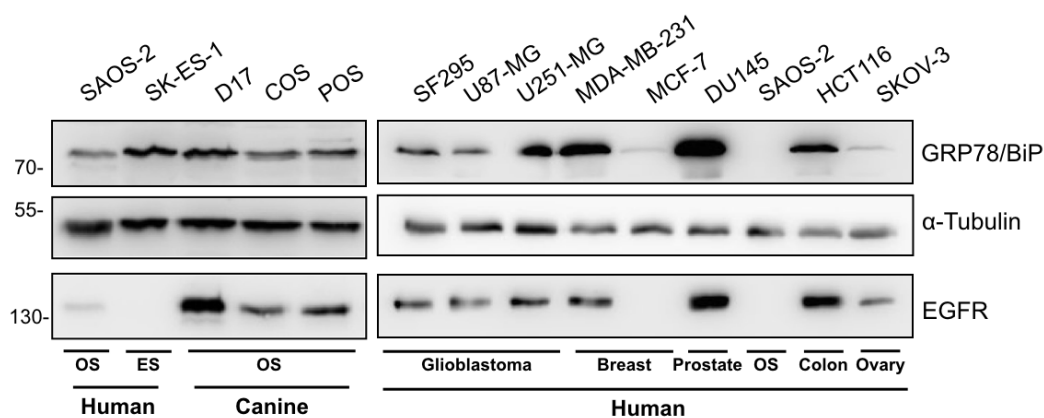
Figure 4.2 Comparative analysis of GRP78 expression in canine and human cells.

Immunoblot analysis of GRP78/BiP, EGFR and α-tubulin expression, from left to right, in human SAOS-2 osteosarcoma, human SK-ES-1 Ewing's sarcoma, canine osteosarcoma (D17, COS, POS), human glioblastoma (SF-295, U87-MG, U251-MG), human breast (MDA-MB-231, MCF-7), human DU145 prostate, human SAOS-2 osteosarcoma, human HCT116 colon and human SKOV-3 ovarian cancer cells. Whole cell lysates, for each panel, were prepared at the same time and processed for Western blot analysis with the antibodies indicated. Human SAOS-2 osteosarcoma cells were common to the 5- and 9-panel comparison; images are representative of three independent comparisons.
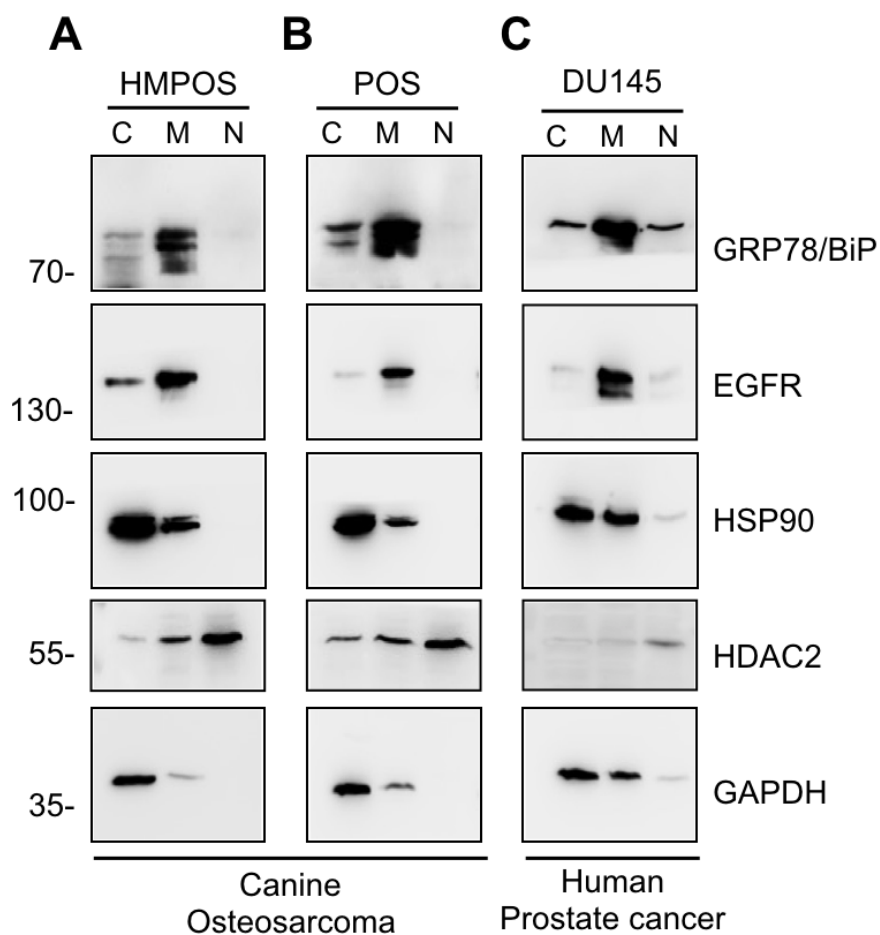
Figure 4.3 Subcellular distribution of GRP78 and representative control proteins in canine and human cells

Immunoblot analysis of fractions prepared from: (A) canine HMPOS osteosarcoma, (B) canine POS osteosarcoma and (C) human DU145 prostate cancer cells. Cells were grown under standard conditions and fractionated to isolate cytoplasmic (C), membrane (M) and nuclear (N) compartments using standard biochemical techniques. Samples were probed with antibodies against GRP78 and proteins of the membrane (EGFR), cytosolic (HSP90, GAPDH), and nuclear (HDAC2) compartments as indicated.
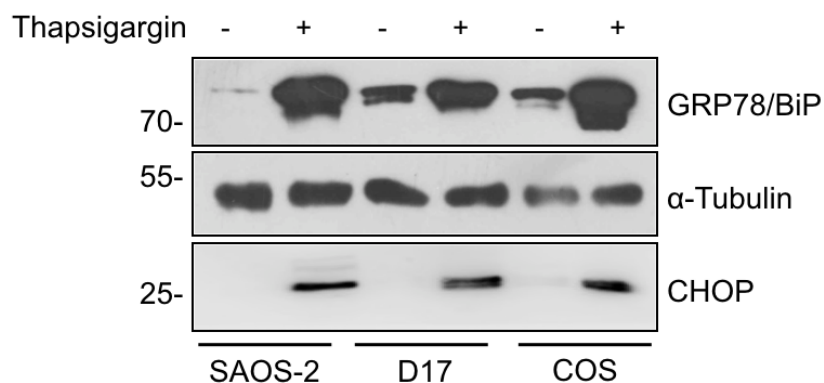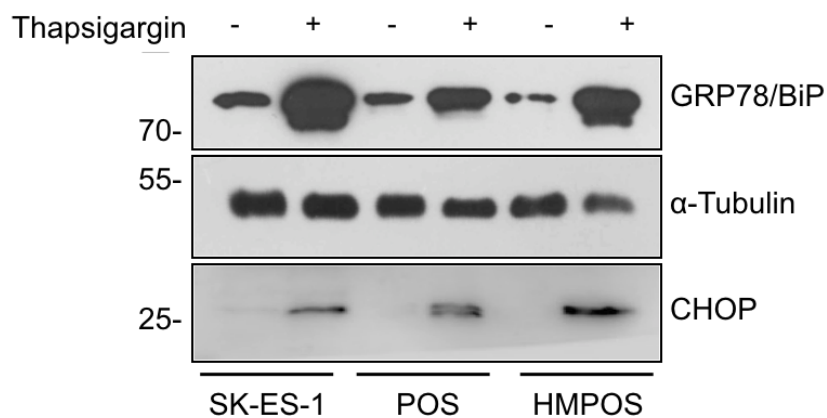
Figure 4.4 Canine osteosarcoma cells show ER stress in response to thapsigargin treatment

Immunoblot analysis of GRP78/BiP, CHOP and α-tubulin expression in the absence (0.1% DMSO) or presence of thapsigargin (3 µM) in: (A) human SAOS-2 osteosarcoma, canine D17 osteosarcoma and canine COS osteosarcoma cells and, (B) and human SK-ES-1 Ewing's sarcoma, canine POS osteosarcoma and canine HMPOS osteosarcoma cells. Cells were grown under standard conditions and treated with, or without, thapsigargin for 24hr. Whole cell lysates were probed with antibodies against GRP78, CHOP and α-Tubulin (loading control) as indicated. Images are representative of a comparison that was repeated three times.
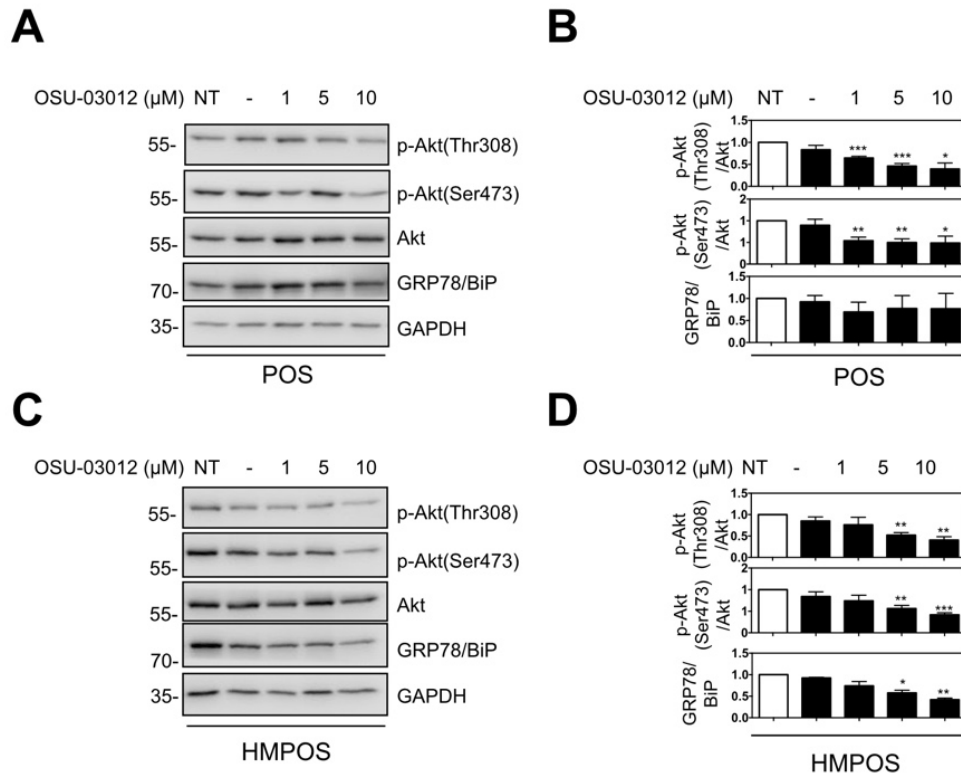
Figure 4.5. Early inhibition of phospho-Akt in canine osteosarcoma cells in response to OSU-03012

Comparative analysis of Akt signaling in canine: (**A** and **B**) POS and (**C** and **D**) HMPOS osteosarcoma cells in the absence ((not treated (NT) and vehicle-treated (0.1% DMSO)) or presence of OSU-03012 (1 to 10 μM) after 1 hr. At the end of treatment whole cell lysates were processed for immunoblot analysis and probed with antibodies against phospho-Akt -Threonine 308, phospho-Akt -Serine 473, total Akt, GRP78, and GAPDH as indicated. (**B** and **D**) Histograms show quantification of expression from three independent experiments. Signals were normalized to GAPDH and phopho-Akt then normalized to total Akt. Statistical significance in treated versus untreated cells indicated as * p< 0.05, ** p< 0.01, ***p< .001.
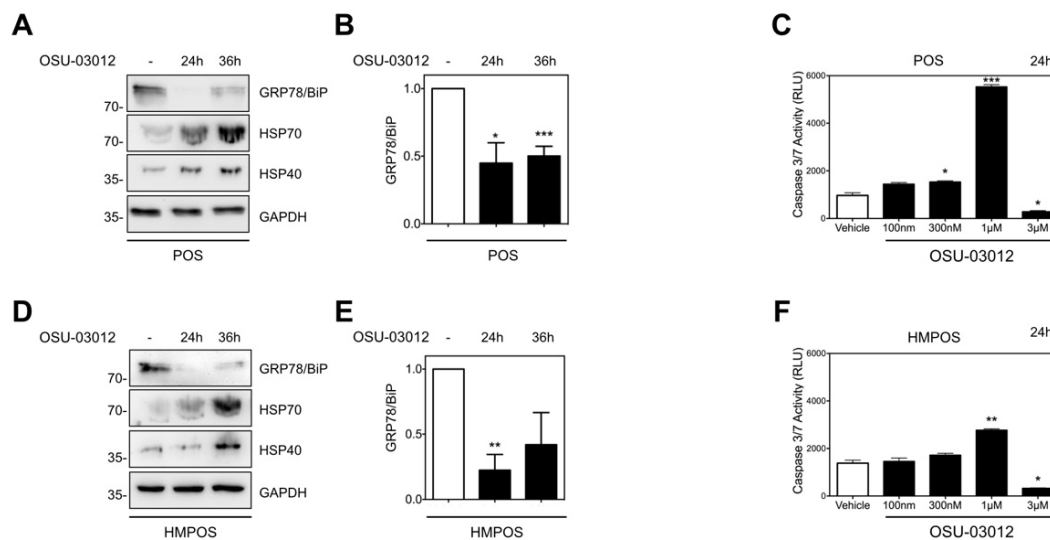
Figure 4.6. OSU-03012 inhibits GRP78 expression and induces caspase-3,7 activity in canine osteosarcoma cells

Comparative analysis of GRP78, HSP70 and HSP40 expression in canine: (A) POS and (D) HMPOS osteosarcoma cells in the absence (0.1% DMSO) or presence of OSU-03012 (300 nM) after 24 hr or 36 hr. At the end of treatment whole cell lysates were processed for immunoblot analysis and probed with antibodies against GRP78, HSP70, HSP40 and GAPDH as indicated. (B and D) Histograms show quantification of GRP78 expression from three independent experiments. Signals were normalized to GAPDH and statistical significance in treated versus untreated cells indicated as * p< 0.05, ** p< 0.01, ***p< .001. (C and F) Concentration–response analysis of 3,7-caspase activity in (C) POS and (F) HMPOS osteosarcoma cells exposed to increasing concentrations of OSU-03012 (100 nM to 3 μM) for 24hr. Bars represent mean luminescence expressed as Relative Light Units ± S.E. (n=3 wells per treatment) from three independent comparisons. Statistical significance of change in treated, relative to vehicle-treated (0.1% DMSO), cells is indicated as * p < 0.05, ** p < 0.01, *** p < .001.
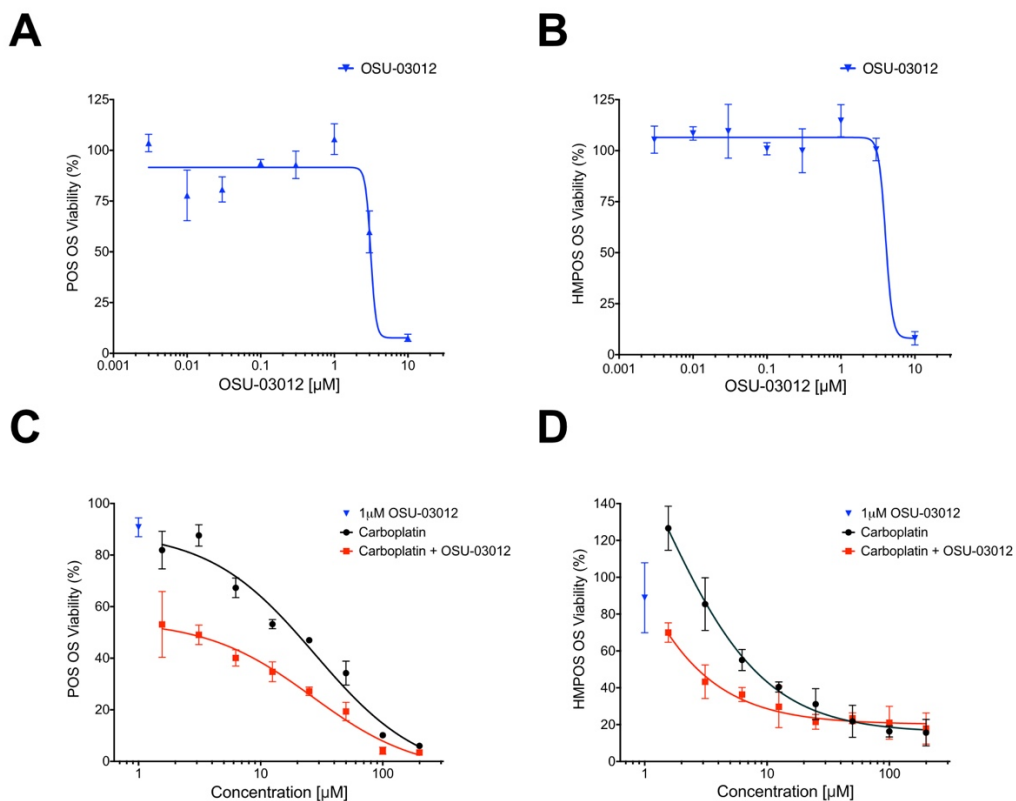
Figure 4.7 OSU-03012 is cytotoxic to canine osteosarcoma cells

Concentration-dependent changes in the viability of canine (A) POS and (B) HMPOS osteosarcoma cells in response to continuous exposure to OSU-03012 (3 nM to 10 µM) for 72 hr. Cell viability was determined using an MTS assay with the viability of vehicle-treated (0.1% DMSO) cells defined as 100 % viability at the end point. Data points represent mean viability ± S.D. (n=3 wells per treatment). Cell viability curves are representative of a comparison that was repeated three times.

EC$_{50}$	OSU-03012 [µM]	Carboplatin [µM]	Carboplatin + OSU-03012 [1µM]
POS	3.8 ± 0.5	28.4 ± 2.8	5.5 ± 2.0
HMPOS	6.7 ± 2.0	10.1 ± 1.7	4.6 ± 1.4

Table 4.1. Cytotoxic potencies of OSU-03012 and carboplatin to canine osteosarcoma cells

Concentration-response relationships for OSU-03012 and carboplatin to reduce canine POS and HMPOS viability were assessed using an MTS cell viability assays. Data were analyzed using GraphPad Prism Software (Graphpad Software Inc. San Diego, CA), and EC$_{50}$ values were determined by nonlinear regression analysis fit to a logistic equation

Reference

1.   Shiu, R.P., J. Pouyssegur, and I. Pastan, *Glucose depletion accounts for the induction of two transformation-sensitive membrane proteinsin Rous sarcoma virus-transformed chick embryo fibroblasts.* Proc Natl Acad Sci U S A, 1977. **74**(9): p. 3840-4.

2.   Pouyssegur, J., R.P. Shiu, and I. Pastan, *Induction of two transformation-sensitive membrane polypeptides in normal fibroblasts by a block in glycoprotein synthesis or glucose deprivation.* Cell, 1977. **11**(4): p. 941-7.

3.   Lee, A.S., *Glucose-regulated proteins in cancer: molecular mechanisms and therapeutic potential.* Nat Rev Cancer, 2014. **14**(4): p. 263-76.

4.   Zimmermann, R., et al., *Protein translocation across the ER membrane.* Biochim Biophys Acta, 2011. **1808**(3): p. 912-24.

5.   Roller, C. and D. Maddalo, *The Molecular Chaperone GRP78/BiP in the Development of Chemoresistance: Mechanism and Possible Treatment.* Front Pharmacol, 2013. **4**: p. 10.

6.   Uckun, F.M., et al., *Inducing apoptosis in chemotherapy-resistant B-lineage acute lymphoblastic leukaemia cells by targeting HSPA5, a master regulator of the anti-apoptotic unfolded protein response signalling network.* Br J Haematol, 2011. **153**(6): p. 741-52.

7.   Liu, R., et al., *Monoclonal antibody against cell surface GRP78 as a novel agent in suppressing PI3K/AKT signaling, tumor growth, and metastasis.* Clin Cancer Res, 2013. **19**(24): p. 6802-11.

8.   Miao, Y.R., et al., *Inhibition of established micrometastases by targeted drug delivery via cell surface-associated GRP78.* Clin Cancer Res, 2013. **19**(8): p. 2107-16.

9.   Milovancev, M., et al., *Comparative analysis of the surface exposed proteome of two canine osteosarcoma cell lines and normal canine osteoblasts.* BMC Vet Res, 2013. **9**: p. 116.

10.   Lytton, J., M. Westlin, and M.R. Hanley, *Thapsigargin inhibits the sarcoplasmic or endoplasmic reticulum Ca-ATPase family of calcium pumps.* J Biol Chem, 1991. **266**(26): p. 17067-71.

11.   Wong, W.L., et al., *Inhibition of protein synthesis and early protein processing by thapsigargin in cultured cells.* Biochem J, 1993. **289 (Pt 1)**: p. 71-9.

12.   Zhu, J., et al., *From the cyclooxygenase-2 inhibitor celecoxib to a novel class of 3-phosphoinositide-dependent protein kinase-1 inhibitors.* Cancer Res, 2004. **64**(12): p. 4309-18.

13.   Johnson, A.J., et al., *A novel celecoxib derivative, OSU03012, induces cytotoxicity in primary CLL cells and transformed B-cell lymphoma cell line via a caspase- and Bcl-2-independent mechanism.* Blood, 2005. **105**(6): p. 2504-9.

14.   Park, M.A., et al., *OSU-03012 stimulates PKR-like endoplasmic reticulum-dependent increases in 70-kDa heat shock protein expression, attenuating its lethal actions in transformed cells.* Mol Pharmacol, 2008. **73**(4): p. 1168-84.

15.   Booth, L., et al., *OSU-03012 suppresses GRP78/BiP expression that causes PERK-dependent increases in tumor cell killing.* Cancer Biol Ther, 2012. **13**(4): p. 224-36.

16.   Jolly, C. and R.I. Morimoto, *Role of the heat shock response and molecular chaperones in oncogenesis and cell death.* J Natl Cancer Inst, 2000. **92**(19): p. 1564-72.

17.   Szewczyk, M., R. Lechowski, and K. Zabielska, *What do we know about canine osteosarcoma treatment? Review.* Vet Res Commun, 2015. **39**(1): p. 61-7.

18.   Thompson, J.P. and M.J. Fugent, *Evaluation of survival times after limb amputation, with and without subsequent administration of cisplatin, for treatment of appendicular osteosarcoma in dogs: 30 cases (1979-1990).* J Am Vet Med Assoc, 1992. **200**(4): p. 531-3.

19.   Schiffman, J.D. and M. Breen, *Comparative oncology: what dogs and other species can teach us about humans with cancer.* Philos Trans R Soc Lond B Biol Sci, 2015. **370**(1673).

20.   Aljubran, A.H., et al., *Osteosarcoma in adolescents and adults: survival analysis with and without lung metastases.* Ann Oncol, 2009. **20**(6): p. 1136-41.

21.   Saam, D.E., et al., *Predictors of outcome in dogs treated with adjuvant carboplatin for appendicular osteosarcoma: 65 cases (1996-2006).* J Am Vet Med Assoc, 2011. **238**(2): p. 195-206.

22.   Saraf, A.J., J.M. Fenger, and R.D. Roberts, *Osteosarcoma: Accelerating Progress Makes for a Hopeful Future.* Front Oncol, 2018. **8**: p. 4.

23.   MacEwen, E.G. and I.D. Kurzman, *Canine osteosarcoma: amputation and chemoimmunotherapy.* Vet Clin North Am Small Anim Pract, 1996. **26**(1): p. 123-33.

24.   Shin, B.K., et al., *Global profiling of the cell surface proteome of cancer cells uncovers an abundance of proteins with chaperone function.* J Biol Chem, 2003. **278**(9): p. 7607-16.

25.   Shani, G., et al., *GRP78 and Cripto form a complex at the cell surface and collaborate to inhibit transforming growth factor beta signaling and enhance cell growth.* Mol Cell Biol, 2008. **28**(2): p. 666-77.

26.   Kelber, J.A., et al., *Blockade of Cripto binding to cell surface GRP78 inhibits oncogenic Cripto signaling via MAPK/PI3K and Smad2/3 pathways.* Oncogene, 2009. **28**(24): p. 2324-36.

27.   Misra, U.K., S. Kaczowka, and S.V. Pizzo, *Inhibition of NF-kappaB1 and NF-kappaB2 activation in prostate cancer cells treated with antibody against the carboxyl terminal domain of GRP78: effect of p53 upregulation.* Biochem Biophys Res Commun, 2010. **392**(4): p. 538-42.

28.   Tsai, Y.L., et al., *Characterization and mechanism of stress-induced translocation of 78-kilodalton glucose-regulated protein (GRP78) to the cell surface.* J Biol Chem, 2015. **290**(13): p. 8049-64.

29.   Elliot, K., et al., *Increase in gene-transcript levels as indicators of up-regulation of the unfolded protein response in spontaneous canine tumors.* Can J Vet Res, 2014. **78**(3): p. 161-7.

30.   LeRoy, B., et al., *Protein expression profiling of normal and neoplastic canine prostate and bladder tissue.* Vet Comp Oncol, 2007. **5**(2): p. 119-30.

31.   Roy, J., et al., *Comparative proteomic investigation of metastatic and non-metastatic osteosarcoma cells of human and canine origin.* PLoS One, 2017. **12**(9): p. e0183930.

32.   Asling, J., J. Morrison, and A.J. Mutsaers, *Targeting HSP70 and GRP78 in canine osteosarcoma cells in combination with doxorubicin chemotherapy.* Cell Stress Chaperones, 2016. **21**(6): p. 1065-1076.

33.   Hamed, H.A., et al., *OSU-03012 enhances Ad.7-induced GBM cell killing via ER stress and autophagy and by decreasing expression of mitochondrial protective proteins.* Cancer Biol Ther, 2010. **9**(7): p. 526-36.

34.   Booth, L., et al., *Multi-kinase inhibitors can associate with heat shock proteins through their NH2-termini by which they suppress chaperone function.* Oncotarget, 2016. **7**(11): p. 12975-96.

35.   Booth, L., et al., *AR-12 Inhibits Chaperone Proteins Preventing Virus Replication and the Accumulation of Toxic Misfolded Proteins.* J Clin Cell Immunol, 2016. **7**(5).

36.   Alvarez, F.J., et al., *3-Phosphoinositide-dependent protein kinase-1/Akt signalling and inhibition in a canine prostate carcinoma cell line.* Vet Comp Oncol, 2007. **5**(1): p. 47-58.

37.   Weng, S.C., et al., *Sensitizing estrogen receptor-negative breast cancer cells to tamoxifen with OSU-03012, a novel celecoxib-derived phosphoinositide-dependent protein kinase-1/Akt signaling inhibitor.* Mol Cancer Ther, 2008. **7**(4): p. 800-8.

38.   Wang, Y.C., et al., *Targeting endoplasmic reticulum stress and Akt with OSU-03012 and gefitinib or erlotinib to overcome resistance to epidermal growth factor receptor inhibitors.* Cancer Res, 2008. **68**(8): p. 2820-30.

39.   Booth, L., et al., *OSU-03012 interacts with lapatinib to kill brain cancer cells.* Cancer Biol Ther, 2012. **13**(14): p. 1501-11.

40.   West, N.W., et al., *OSU-03012 sensitizes breast cancers to lapatinib-induced cell killing: a role for Nck1 but not Nck2.* BMC Cancer, 2013. **13**: p. 256.

41.   Booth, L., et al., *OSU-03012 and Viagra Treatment Inhibits the Activity of Multiple Chaperone Proteins and Disrupts the Blood-Brain Barrier: Implications for Anti-Cancer Therapies.* J Cell Physiol, 2015. **230**(8): p. 1982-98.

42.   Selvarajah, G.T., et al., *Expression of epidermal growth factor receptor in canine osteosarcoma: association with clinicopathological parameters and prognosis.* Vet J, 2012. **193**(2): p. 412-9.

43.   Freeman, S.S., et al., *Copy number gains in EGFR and copy number losses in PTEN are common events in osteosarcoma tumors.* Cancer, 2008. **113**(6): p. 1453-61.

44.   Lee, J.A., et al., *Epidermal growth factor receptor: is it a feasible target for the treatment of osteosarcoma?* Cancer Res Treat, 2012. **44**(3): p. 202-9.

45.   Sevelda, F., et al., *EGFR is not a major driver for osteosarcoma cell growth in vitro but contributes to starvation and chemotherapy resistance.* J Exp Clin Cancer Res, 2015. **34**: p. 134.

46.   Sun, C., et al., *Inhibition of GRP78 abrogates radioresistance in oropharyngeal carcinoma cells after EGFR inhibition by cetuximab.* PLoS One, 2017. **12**(12): p. e0188932.

47.   Booth, L., et al., *GRP78/BiP/HSPA5/Dna K is a universal therapeutic target for human disease.* J Cell Physiol, 2015. **230**(7): p. 1661-76.

48.   Lewy, T.G., J.M. Grabowski, and M.E. Bloom, *BiP: Master Regulator of the Unfolded Protein Response and Crucial Factor in Flavivirus Biology.* Yale J Biol Med, 2017. **90**(2): p. 291-300.

49.   Kim, J.H., et al., *Endoplasmic reticulum chaperone GRP78 regulates macrophage function and insulin resistance in diet-induced obesity.* FASEB J, 2018. **32**(4): p. 2292-2304.

Development of a Workflow for the Discovery and Characterization of ER
Secretory Pathway Inhibitors: Phenotypic Screening to
Target Validation

CHAPTER 5

Xuemei Wan, Daphne R. Mattos, Jeffrey D. Serrill, Ian R. Humphreys, Christian
E. Badr, Dylan Nelson, Shinya Oishi, Kerry L. McPhail, and Jane E. Ishmael

Abstract

Almost one third of all proteins reside in, or transit through, the cellular secretory pathway. As this cellular compartment is responsible for the maturation and trafficking of many cell surface and secreted proteins, that are critical for sustaining cancer growth, the selecive inhibition of this pathway has the potential to reveal novel druggable targets for future cancer therapy. In the present study, we developed a workflow for the discovery of new inhibitors of protein secretion by combining a funcitonal assay, based on detection of a naturally secreted reoprter, with basic cell viability assays. This dual screening approach was amenable to High-Throughput Screening (HTS) and was used to screen 1000s of pure compounds and mixtures from synthetic and natural product libraries. Of the 3906 small molecules screened, 6 of them were recogizable as candidates for further evaluation as secretory pathway inhibitors. We also characterized the activity of several known natural product inhibitors of the secretory pathway to provide a framework for future target validation. We found that coibamide A decreases expression of the endoplasmic reticulum (ER) chaperone protein glucose regulated protein 78 (GRP78) in human umbilical vascular endothelial cells (HUVEC), human glioblastoma (U87-MG, U251) and prostate (Du145) cancer cells in a time-dependent manner and that loss of GRP78 may be a useful biomarker of secretory pathway inhibition in cell-based assays. Finally, we developed the use of a cellular thermal shift assay for the identification of compounds that bind the alpha subunit of the Sec61 translocon complex.

Introduction

In mammalian cells, one third of the proteome resides in, or is trafficked through, the secretory pathway. Nascent polypeptides, destined for the secretory compartment, are first moved into the lumen of the endoplasmic reticulum (ER) via a process known as co-translational translocaion which goes through a conserved channel known as the Sec61 translocon [1]. From the ER, the polypeptides complete multiple maturation steps required for correct folding such as undergoing glycosylation and disulfide bond formation. Properly folded proteins are trafficked to the Golgi complex and from there are moved to their final destination [2]. The natural features of cancer cells, such as high proliferation rates, high metabolic demands and aneuploidy, place increased demands on the ER and secretory functions of the cell [3]. Recent studies have revealed the critical contribution of the secretory pathway in cancer development, which raises the possibility that the secretory pathway can be targetted for therapeutic advantage in certain human cancers.

It is now clear that some microrganisms produce secretory pathway inhibitors. For example, the cyanobacterial natural product apratoxin A is an inhibitor of co-translational translocation and has anticancer properties [4]. Coibamide A, an N-methylated cyclic depsipeptide natural product structure discovered by Dr. Kerry McPhail, also appears to target the cellular secretory pathway. Coibamide A was first isolated from a cyanobacterial assemblage found in the Coiba National Park, Panama and displayed potent cytotoxicity at nanomolar concentrations against the National Cancer Institution-60 panel [5]. Towards the goal of determining the mechanism of coibamide action we previously reported that coibamide A inhibits the expression of vascular endothelial growth factor receptor 2 (VEGFR2), the secretion of VEGF A, and suppresses tumor growth in glioblastoma xenografts [6]. In addition, coibamide A induces autophagy and promotes cross-signaling between ATG5-dependent autophagy and caspase-dependent apoptosis [7] [8]. Recently we revealed that coibamide induces mTOR-independent autophagy without activation of a classic ER stress response [8]. This finding is significant as this lack of an ER stress response, potentially distinguishes the action of coibamide A from compounds that disrupt proteostasis within ER such as thapsigargin and

tunicamycin [8]. Taken together, these results indicate that coibamide A acts as an inhibitor of the secretory pathway with a mechanim that is similar to that of apratoxin A [6] [8].

The heterotrimeric Sec61 complex forms the structural core of the translocon channel [9]. As an ER resident chaperone and a member of heat shock protein family [10], glucose-regulated protein 78 (GRP78), also known as BiP, associates with Sec61 complex on the lumenal side of the channel and is the only soluble protein necessary and sufficient to control the closure of the translocon and engaged in the early stages of protein translocation [11]. Working with other ER chaperones, GRP78 binds to nascent proteins to prevent them from aggregation as most of them will be N-linked glycosylated [12]. GRP78 monitors the processing of highly branched glycans and forms disulfide bonds to stabilize the folded protein [13], and also targets unfolded proteins for degradation in a process called ER-associated degradation (ERAD) [14]. In past decades, genome wide and immunohistochemical analyses of clinical samples have shown that GRP78 is overexpressed in several tumors refractory to therapy like prostate cancer[15], breast cancer [16] and glioblastoma [17]. Increased level of GRP78 seems to be the key feature for cancer cells that chronically upregulate the UPR without however inducing apoptosis.

In the present study, we developed a workflow for the discovery of new secretion pathway inhibitors using the combination of a functional secretion assay, based on detection of the naturally secreted reporter *Gaussia luciferase* (Gluc), coupled with established cell viability assays. We also tested the activity of four known macrocyclic natural products to reveal patterns that can be used for profiling and future validation of potential inhibitors of Sec61 function. Comparative analysis of coibamide A, relative to other natural and synthetic compounds, supported the use of the workflow and indicated that several straightforward assays can be used to reveal biological activity consistent with a Sec61 inhibitor. Of the pure compounds tested, coibamide A was the only compound that appeared to target the co-translational translocation machinery.

Materials and Methods

Mammalian Cell Culture

All cells were maintained as adherent cultures under standard laboratory conditions at 37°C in an atmosphere of 5% CO_2. Human U251, U87-MG, and DU145 were cultured in Minimum Essential Media (Corning Cellgro) with 10% fetal bovine serum (FBS; VWR, Radnor PA), L-glutamine (2mM), and 1% penicillin and streptomycin. HUVEC cells were cultured in Medium 200PRF (Life Technologies Corp.) supplemented with Low Serum Growth Supplement (Life Technologies Corp.) as specified by the supplier.

Chemicals and Reagents

The isolation and purification of coibamide A [5] and apratoxin A [18] has been discribed. Geldanamycin was purchased from Medchemexpress LLC (Cat.NO.: HY-15230). Thapsigargin (Cat# T9033) was from Sigma Aldrich (St Louis, Missouri US). Bortezomib was purchased from Medchemexpress LLC (Cat.NO.: HY-10227). All compounds were reconstituted in 100% DMSO, aliquot and stored in amber borosilicate glass vials at -20°C for use in biological studies. Cell culture-grade DMSO was used as the vehicle for all treatments and final concentrations of DMSO for *in vitro* experiments never exceeded 0.1%.

Primary and secondary antibodies purchased from Cell Signaling Technology, Inc. (Danvers, MA, USA) included: BiP/GRP78 (#3177), HSP70 (#4873), HSP40 (#4868), GAPDH (#5174), Tie-2 (#4224). Antibodies to VCAM-1(#ab7224). Primary antibodies Sec61α (ab183046), BiP/GRP78 (for immunoccytochemistry studies; #21685) were from Abcam. General laboratory reagents for biological studies were obtained from VWR International (Radnor, PA).

Cell Viability Analysis

For CellTiter-Glo assays, cells were seeded at a density of 3000 cells/well in 100µL of complete medium in 96-well plates. After 18 hr, cells were treated with drugs or vehicle (0.1%DMSO). Cell viability was assessed using a CellTiter-Glo®

Luminescent Cell Viability Assay kit (Promega Corp., Madison, WI), with the viability of vehicle-treated cells defined as 100%.

Cell Lysis and Immunublot Analysis

Cell lysates were prepared using freshly made ice-cold Lysis Buffer containing 50nM Tris-HCl (PH7.5), 1mM EDTA, 1mM EGTA, 1% Triton X-100, 0.27 M Sucrose, 50mM sodium fluoride,1mM sodium orthovanadate, 5mM sodium pyrophosphate, 1mM PMSF and 1mM benzamidine. All cell lysates were cleared by centrifugation at 16,000xg for 20min at 4°C and the protein concentration was determined by bicinchoninic acid (BCA) method indicated by the manufacturer's recommendations (Thermo Fisher Scientific Inc.)

For immunoblot analysis, cell lysates were adjusted by protein concentration and equal amounts (50µg) separated by SDS-PAGE gel. Then proteins were transferred onto PVDF membrane (Thermo Fisher Scientific) in transfer buffer contains 25nM Tris, 192mM glycine, 10%methanol. Membranes were then blocked in 5%(m/v) non-fat milk in 50mM Tris-HCl, pH7.4, 150mM NaCl (TBS) with 0.05% Tween-20 (TBS-T), and incubated at 4°C for 16 hs with appropriate primary antibody in 5%(w/v) bovine serum albumin (BSA) in TBS-T. On the following day, membranes were washed with TBS-T for 2 x 5min, then incubated in appropriate HRP-conjugated secondary antibody for 1 h at room temperature. Membranes were then washed in TBS-T for 3 x 5min, and target proteins were detected by chemiluminescence (Amersham™ ECL™ Chemiluminescent Labeling and detection Reagents for Proteins, GE Healthcare), using either X-ray films or myECL™ Imager system (Thermo Scientific).

Immunofluorescence

U87-MG cells were seeded on slides coated with 0.1% gelatin in 6-well cell culture plates. After treatment, slides were washed with PBS, then fixed with Methanol for 10 min. After three washes with PBS, cells were permeabilizated with 0.1% Triton X-100 in PBS and incubated in room temperature for 15 min. For blocking, 10% goat serum were used for incubation for 30 min. After blocking, slides were incubated in desired concentration of primary antibody (GRP78 1:100, Sec61α

1:100) diluted in 0.1% BSA overnight at 4 °C. On the second day, wash the slides with PBS, add 1:200 of fluorescent dye-labeled secondary antibody along with nucleus (DAPI) and incubate for 90min at room temperature protected from light. After washing again with PBS, add the slides with mounting medium.

Cellular Thermal Shifting Assay

Assays were carried out according to a method previously decribed by Jafari and co-workers [19]. Briefly, to determine the apparent melting curve, U87-MG cells were seeded in 10 cm cell culture dishes, and treated with coibamide A, apratoxin A, OSU-03012 or vehicle (0.1% DMSO) for 1h. After treatment cells were harvested using trypsin and collected in 15 mL conical tubes. Whole cells were pelleted by gentle centrifugation at 300 x g for 3 min. Cell pellets were re-suspended in PBS supplemented with PMSF and benzamidine to a final cell density of ~2 million cells per mL. The cell suspension was distributed into PCR tubes (0.2 mL size), arranged in strips, with 100µl in each tube.

Cells were subjected to increasing temperatures in a Veriti[TM] 96-well thermal cycler (Thermo Fisher). PCR-tube strips with the first six temperature endpoints (45 - 60°C) were heated to the designated temperature for 3 min. Immediately after heating, tubes were removed and samples incubated at room temperature for an additional 3 min. After this 3 min incubation, samples were immediately snap-frozen in liquid nitrogen. The remaining samples were subjected to the same procedure at 4 additional temerature endpoints (60-72°C). All samples were subjected to two freeze-thaw cycles (using liquid nitrogen and a water bath set at 25°C) in order to ensure a uniform treatment of all tubes. Lysates were cleared by centrifugation at 18,000 x g for 20 min, at 4°C, and the supernatant (90µl) carefully transferred to a new tube. An aliquot of 4X laemmli reducing buffer (22µl) was added to each sample and all tubes were then heated to 90°C for 5 min in preparation for immunoblot analysis.

Gluc Secretory Activity Assay

For concentration-response assays, *Gaussia luciferase* (Gluc)-expressing U87-MG cells were seeded in 96-well plates at a density of 3,000 cells per well and

allowed to grow overnight. The next day, the growth medium was replaced with complete medium containing coibamide A (1µM - 0.1nM), aureobasidin A (10µM - 0.3 nM), cyclosporin (10 µM – 0.3 nM), or vanilomycin (10 µM – 0.3 nM) or vehicle (0.1% DMSO). Following 16 h treatments, aliquots (20 µL) of conditioned cell culture medium were removed from each well and transferred to 96-well white-walled plates. Coelenterazine (1.68 µM) was injected into each well to yield a final concentration of 1.2 µM, and luminescent signals were measured using a multi-mode microplate reader (BioTek Synergy HT) with Gen5® software and compared across conditions (3 sec wait, 0.5 sec integration time following coelenterazine injection). We defined the Gluc secretion of vehicle-treated cells as 100%.

Screening of a Synthetic Small Molecule Library

For primary screeingn of small molecules from the Oregon Translational Research and Development Institute (OTRADI) library, Gluc-expressing U87-MG cells were seeded in 96-well plates at a density of 3,000 cells per well and allowed to grow overnight. On the next day, column 1 of each 96-well plate was treated with 0.1% DMSO as negative (upper secretome limit) control, and column 12 treated with 100 nM apratoxin A as positive (lower secretome limit) control. Small molecules from the OTRADI library were injected by automated pin tool of 0.2µl for a final of 10µM. After 24h, 20 µL of conditioned cell culture medium was removed for analysis of Gluc secretion assay as described above and the culture plates returned to the incubator. Cell viability was assessed 24 h later, using a standard MTT viability, at the 48 h end-point. We defined the inhibition of Gluc secretion of vehicle-treated cells as 0%, and apratoxin A-treated cell as 100%. For cell viability assays, we defined the viability of vehicle-treated cells at 48 h as 100%.

Hits were defined as compounds that inhibited the signa/Gluc by more than three times that stardard deviation away from the mean inhibition of all the compounds across all plates with an estimated Z-factor >0.5. The estimated Z-factor is defined in terms of four parameters: the sample means ($\hat{\mu}$) and sample standard deviation ($\hat{\sigma}$) of both the positive (p) and negative (n) controls:

Estimated Z-factor = $1 - \dfrac{3(\hat{\sigma}_p + \hat{\sigma}_n)}{|\hat{\mu}_p - \hat{\mu}_n|}$

Fifiteen compounds met the criteria for secondary screening and advanced for concentration-response analyses. Gluc-expressing U87-MG cells were seeded in 96-well plates at a density of 3,000 cells per well and allowed to grow overnight as before. On the next day, cells were treated with a range of concentrations (10 μM - 0.3nM) using a Hewlett-Packard (HP) Tecan D300 Digital dispenser. After 24 h of treatment, the Gluc assay was conducted as descibed previously. The culture plates were returned to the incubator and cell viability was tested after 48 h using a MTT cell viability assay.

Data Analysis

Dose-response relationships were analyzed using GraphPad Prism Software, and EC_{50} values were determined by nonlinear regression analysis fit to a logistic equation. For immunoblot analysis, target protein signals were normalized to the intensity of controls (Tubulin or GAPDH) and quantified relative to control using ImageJ software (rsbweb.nih.gov/ij). Statistical significance of data derived from MTT viability assays was performed using a one-way analysis of variance (ANOVA) followed by a Student's *t*-test comparing untreated controls and treatment groups. *P*-values of 0.05 or less were considered statistically significant.

Results

Discovery of secretion inhibitors using a functional assay.

Previously Badr and co-authors [20] described a novel functional screening assay based on measurement of bioluminescense of a naturally secreted reporter, *Gaussia luciferase* (Gluc), from cultured cells. This assay was first used to identify small molecules that can sensitize brain tumor cells to cell death [20]. We generated Gluc-expressing human U87-MG glioblastoma cells by infection with a lentiviral vector encoding an expression cassette for *Gaussia luciferase* and CFP separated by an IRES element under the control of a CMV promotor [20]. Upon infection, Gluc was first expressed in the cells and then processed through the secretory pathway and released into the conditioned medium. Therefore, the secretory activity can be monitored by measuring bioluminescense generated by the reaction of *Gaussia luciferase* with substrate coelenterazine [20].

We utilized this whole-cell based Gluc secretion assay to screen for for new inhibitors of secretory function. Using a High Throughput Screening (HTS) approach we screened 3906 small molecules from the OTRADI library to look for compounds that inhibited Gluc secretion into the culture medium after a 24 h exposure. To gain additional information about the potential cytotoxicity of the compounds to glioblastoma cells, all cultures were returned to the incubator for an additional 24h for assessment of cell viability at 48 hr. The workflow of the entire screen of the 3906 compounds is summarized in Figure 5.1(A), and the result from the primary screen are presented as a scatter plot in Figure 1B. Fifteen hits were revealed form the primary screening. Hits were determined from the subset of plates with Z-Prime > 0.5, indicative of a robust assay, that inhibited Gluc secretion by more than three times the standard deviation (94.826% inhibition of Gluc secretion) away from the mean inhibition of all the compounds (Figure 5.1B). The 15 hits also displayed a moderate inhibition of cytotoxicity by 48 h (Table 5.1). In the secondary screening, we treat Gluc-U87 cells with increasing concentrations of each of the lead compounds (designated 1-15) ranging from 3 nM to 10 μM, and then measured the Gluc secretion and cell viability at 24 h and 48 h, respectively. Six of the hits displayed clear concentration-dependent inhibition of Gluc secretion, and 11 displayed micromolar potency as cytotoxic agents for future analyses

(Suplementary S5.1). These results served to validate the use of the Gluc assay for HTS and potential use for for the discovery of new secretory pathway inhibitors.

Profiling of known natural product structures in the Gluc secretion assay.

As we previously demonstrated the ability of coibamide A to decrease expression of membrane-bound receeotors and secreted ligands, such as VEGFR2 and VEGF-A [6], we tested the ability of Gluc to inhibit Gluc secretionin. In these assays, coibamide A potently inhibited cellular secretory activity, after relatively short (16 h) exposures (Figure 5.2A), without affecting cell viability (Figure 5.2B). We used this assay to compare the action of coibamide A to other natural product macrocycles. The ability of coibamide A (0.1nM - 1µM) to inhibit Gluc secretion was compared with vanilomycin (1 nM - 10 µM), aureobasidin A (0.3 nM-3 µM) and cyclosporin A (1 nM - 10 µM),. Both coibamide A and vanilomycin displayed potent inhibition of the secretory pathway after 16h (Figure 5.2), however vanilomycin also inhibited up to 50% of cell viablity at the same time point (16 h). In contrast, the immunosuppresor cyclosporin and antifungal antibiotic aureobasidin A failed to inhibit either secretory function or viability (Figure 5.2). and, in separate experiments, remained essentially non-toxic after 72 h (Figure 5.2). In contrast, both coibamdie A and vanilomycin killed more than 80% of cells after 72 h (Figure 5.2C; Table 5.2). The results indicate that cell viability was not affected in the short treatment period (16 h), and that the observed inhibition of secretory activity was unlikley to occur as a secondary consequence in dying cells. This differential response between Gluc secretion and cell viability revealed a pattern of activity consistent with our previous assignment of coibamdie A as a likely secretory pathway inhibitor [6].

Coibamide A decreases GRP78 expression in a concentration- and time - dependent manner

We previously determined that coibamide A does not induce a typical ER stress response in cultured mouse embryonic fibroblasts [8], raising the possibility that secretory pathway inhibitors may induce a specific pattern of cell stress. Using normal HUVECs as a model cell type, we exposed cells to a range of coibamide A concentrations (1nM, 10nM, 100nM and 1µM) for 24 h. Immunoblot analysis of

HUVEC lysates revealed slight decreases in GRP78 expression at low concentrations of coibamide A, and undetectable levels of GRP78 protein following concentrations of 10 nM - 1 μM. On the other hand, the cytosolic chaperone proteins HSP70 and HSP40 were upregulated in a concentration-dependent manner. As a resident chaperone protein in ER lumen, GRP78 plays an important role in folding proteins that are entering the secretory pathway. In order to expand our investigation of coibamide A target proteins, we examined coibamide-treated HUVEC lysates for the cell adhesion molecule vascular cell adhesion molecule 1 (VCAM-1) and tyrosine kinase receptor Tie 2. We found that in HUVECs models, both Tie2 and VCAM-1 began to disappear after 24h exposure to coibamide A in a concentration-dependent manner (Figure 5.3A-B).

To expand our analysis of cell stress signaling in response to coibamide A, we selected three human cancer cell lines (U87-MG and U251-MG glioblastoma and DU145 prostate cancer cell), which have high endogenous GRP78 expression. As anticipated from studies in HUVECs, GRP78 expression decrease after 12 h, then almost disappeared by 24 h in all of the three cell lines. In contrast, total levels of HSP70 and HSP40 are correspondingly induced in a time-dependent manner (Figure 4 A-F). The inhibition of GRP78 expression by coibamide A was also studied using immunocytochemistry in U87-MG cells to visualize both proteins. After a 24 h exposure to coibamide A, GRP78 (green) expression was dramatically decreaesd, whereas Sec61α (red) showed no significant change (Figure 5). In addition, consistent with recent studies, the immunofluorescence reveals that GRP78 is up-regulated in cancer cells not only in ER but also in the cytosol and close to the plasma membrane.

Profiling of the heat shock proteins in response to known natural product structures

To study the effect of coibamide A on cell stress, we compared the action of coibamide A to that of the well characterized natural product HSP90 inhibitor geldanamycin [21], to thapsigargin as a known inducer of ER stress [22], and to apratoxin A which has been revealed to target the Sec61α subunit of the Sec61 translocon complex [23]. While thapsigargin induced a large increase in GRP78

expression after 24 h, coibamide A and apratoxin A induced statistically significant decreases in GRP78. On the other side, while the thapsigargin treated group induced little change in terms of changes in the cell stress indicator heat shock proteins HSP70 or HSP40, cells treated with coibamide A, apratoxin A or geldanamycin all showed increased HSP70 and HSP40 (Figure 5.6A, B). This result indicates that coibamide A works in a different mechanism of action than HSP90 inhibitor geldanamycin, and was most similar to apratoxin A.

Coibamide A induces Proteasome-dependent degradation of GRP78.

We then investigated whether GRP78 was being subject to degradation upon being exposed to coibamide A. Proteasome-dependent degradation is the main pathway for cellular degradation of proteins. We utilized the proteasome inhibitor bortezomib to address the involvement of this pathway. As shown in immunoblot, bortezomib alone caused a massive amount of protein ubiquitination while doesn't change the endogenous level of GRP78. However, when U87-MG cells were treated with coibamide A and bortezomib in combination, then harvest the in-soluble lysate by sonication, we captured a dramatically large amount of GRP78 (Figure 5.6C, D). This rescue of GRP78 immunoreactivity, by co-treatment of coibamide A with bortezomib, indicates that a large fraction of GRP78 undergoes proteosomal degradation in response to coibamide treatment and was retained in cytosol in the presence of bortezomib.

Biochemical analysis of the Sec61α subunit of the translocon in response coibamide A.

Recently apratoxin A was shown to target the Sec61 translocon complex [24]. As our previous studies provide evidence that coibamide A has the similar mechanism of action as apratoxin A [6] [8], we used a biochemical method to investigate the binding target of coibamide A. In the present study, we used a cellular thermal shift assay (CETSA) following with immunoblot analysis to detect if there is any thermal stabilization of the alpha subunit of the Sec61 protein complex upon coibamide A or apratoxin A treatment in cells. We first screened lysates from several human cell types to test the quality and specificity of a commercially available anti-Sec61α antibody. Lysates were generated from human embryonic kidney 293 (HEK293)

cells, U87-MG glioblastoma, human HeLa cervical cancer cells, and human H3122 lung cancer cells and probed in parallel. This analysis showed a uniform clear detection of Sec61α at the predicted protein size in all of the four cell lysates (Figure 5.7A), indicating that this antibody is suitable for use in CETSAs.

In theory, unbound proteins denature, aggregate and precipitate at elevated temperatures, whereas ligand-bound proteins remain more stable and can be detected in solution by immunoblot analysis. [19] In our initial melting curve experiments in intact U87-MG cells, in the absence (vehicle) and presence of coibamide A in Figure 5.7B and Figure 5.7C, we observed a series of identical patterns for GRP78/BiP, α-tubulin, GAPDH and Sec61β at increasing temperatures from 45 °C to 72 °C, indicating that none of those proteins are bound by coibamide A, or at least coibamide A didn't cause any thermal stabilization of those proteins. Then we expanded the experiment to compare the action of coibamide A, apratoxin A and a celecoxib derivative OSU-03012 and concentrated on potential changes in Sec61α, the core subunit of the Sec61 translocon protein complex. Whereas Sec61α mostly disappeared at 57 °C to 60 °C in vehicle- and OSU-03012-treated cells, this protein was still detectable at 60°C of temperature in coibamide A treated cells and at 63 °C to 66 °C of temperature in apratoxin A-treated cells (Figure 5.7 D,E). These results suggest that both coibamide A and apratoxin A stabilize the Sec61α subunit at elevated temperatures but may do so to a different extent. This results strongly indicates that Sec61α is the direct target of both coibamide A and apratoxin A.

Discussion

In the present study, we validated a method that is amenable to high-throughput screening assay whereby a functional Gluc secretory assay can be combined with a standard cell viability assay to screen for inhibitors of the cellular secretory pathway. We utilized this workflow to identify 6 new candidates from a synthetic small molecule library that could be studied for their potency in secretory inhibition. In mammalian cells, almost one third of proteins reside in or transit through the secretory pathway. Secretory proteins are segregated from the cytosol and translocated across the endoplasmic reticulum (ER) membrane [1]. Nascent peptide chain are co-translationally translocated through the ER membrane at sites termed translocons [25]. From ER, these polypeptides go through folding, glycosylation, disulfide bond formation to get matured and then are transported through Golgi to reach their destination such as secretome or plasma membrane proteins. The interruption of ER proteostasis would trigger unfolded protein response (UPR), and the fall of restoring ER homeostasis induces cell death.

Cancer cells have a high demand of metabolic and proliferation rates, require particularly robust ER and secretory machineries. The increased demand for the secretory functions in cancer cells changes the ER homeostasis and consequently induces constitutive UPR activity [3]. ER stress is a gatekeeper of tumor progression in the early stage, and its activation controls the fate of malignant cells facing glucose shortage [26] [27]. On the other side, the differentiation and stress response factor XBP-1 drives multiple myeloma pathogenesis [28]. Moreover, secretory proteins like cytokines, extracellular matrix (ECM) proteins and integrins control the tumor-stroma interactions. The inhibition of secretory pathway function has previously been shown to result in cell ECM destabilization and an increase in cancer dissemination and inhibition of invasion [3]. Finally, ER chaperones have critical functions outside of the simply facilitating protein folding that it promotes oncogenesis and tumor immunogenicity [29]. Because of it's multiple roles in cancer development, the secretory pathway has been identified as a novel target in cancer therapy.

Therapeutic intervention might be possible at many levels in the secretory pathway in cancer cells, such as inhibiting of the entry of co-translationally translocation at translocon, modulating the secretion of selected proteins, targeting ER chaperones, increasing proteostasis unbalance and modulating UPR [3]. In eukaryotes, the conserved Sec-dependent pathway is used for the translocation of secretory proteins. At the beginning of the secretion pathway, the Sec61 translocon is a dynamic protein complex that consists of a central Sec61α subunit and two smaller peripheral subunits Sec61β and γ [30]. The lateral gate of Sec61α allows opening of the channel towards the lipid bilayer for lipid insertion of transmembrane domains [31]. The dominant mode operated by the Sec pathway is co-translational translocation, which couples ribosomal protein synthesis directly to protein translocation through the channel. This process has multiple steps that needs dynamic interactions between many factors. A group of natural and synthetic agents have recently been discovered to affect different steps of the translocon mechanisms. Mycolactone induces an irreversible conformational change in Sec61α [32]. Exotoxin A modulates translocon gating similar to calmodulin [33]. More interestingly, several cyclic depsipeptides have been found to be co-translational translocation inhibitors. HUN-7293 and its derivatives contransin and CAM741 interfere with signal peptide insertion at the translocon [34] [35]. Fungal cyclic decadepsipeptide Decatransin and secondary metabolite from marine cyanobacterium apratoxin A inhibit translocation into the ER lumen and can prevent growth of tumor cells [36] [24].

In validating the screen, coibamide A and valinomycin stood out as potent inhibitors of secretory function whereas cyclosporin A and aureobasidin A showed no activity is this assay. Coibamide A and valinomycin did, however, show a different profile. Coibamide A and valinomycin inhibited more than 70% of Gluc secretion in as fast as 16 h, however valinomycin simultaneously decreased U87-MG cell viability by almost 50%. These findings support previous studies that indicate valinomycin has some activity as a Sec61 inhibitor, but also has off-target effects as a potent disrupter of potassium transport. Valinomycin is a macrocyclic depsipeptide that isolated from an Actinomycete culture. It is not only a potassium anionophore but also a signal peptide-specific inhibitor of hamster prion protein (PrP) translocation [37]. However, human PrP was not affected by valinomycin,

due to the differences in the signal peptides of these two homologous proteins. Our finding that valinomycin displays potent secretory inhibition and also cytotoxicity raise the possibility that it causes a rapid secretory disruption maybe alone with other mechanisms, resulting the cell death. Our findings also suggest that our dual screening approach is sensitive enough to detect potential differences between the mechanism of action of valinomycin and coibamide A.

On the other side, coibamide A caused fast secretory inhibition that could not be attributed to a rapid decrease in cell viability. This sign indicates that the secretory pathway is an early, or first, target affected by coibamide A, but raises the question of how coibamide A causes cell death. By the study in HUVECs, two human glioblastoma cells (U87-MG, U251), and one prostate cancer cells (DU145), we revealed a consistent pattern alone these cell lines that, the immunoactivity of ER chaperone proteins GRP78 was mostly decreased after exposure to coibamide A. In the mean time, cytosolic chaperone HSP70 and co-chaperone protein HSP40 were up-regulated. The GRP78 plays multiple roles in ER function. It protects cells from ER stress crash and supports the unfolded protein response as a survival mechanism. Reduced GRP78 can thus result in cell death under ER stress conditions, which are typical for solid tumor because of the high metabolic demand. In addition, GRP78 performs several functions in both co- and post-translational translocation, such as driving translocon gating and assisting with insertion of precursor peptides into the channel [38] [39]. Therefore, loss of GRP78 impedes the translocation of polypeptides into ER. Those nascent peptides aggregate in the cytosol and inducing a rapid loss of proteostasis, and a compensatory up-regulation of cytosolic chaperones such as HSP70 and co-chaperone HSP 40. The HSP70 family of proteins controls all aspects of cellular proteostasis such as nascent protein chain folding, protein import into organelles, recovering of proteins from aggregation, and assembly of multi-protein complexes. In malignantly transformed cells, the HSP70 family can be induced to protect cells from the proteotoxic stress associated with abnormally rapid proliferation and cytostatic drugs [40]. The fact that ER stress inducer thapsigargin, and HSP90 inhibitor geldanamycin gave different patterns in terms of GRP78 and HSP70 expression indicates the diverse mechanisms between them and coibamide A or apratoxin A.

Only coibamide A and apratoxin A can decrease the expression of GRP78 and induce a dramatic proteotoxicity.

In chapter 4, we discussed that high basal expression of GRP78 and distribution to cellular compartments outside then ER is increasingly associated with several treatment-resistant human and canine cancers. GRP78 may also participate in oncogenic signaling in some aggressive cancers [41] [42]. Here we not only detect the decrease of GRP78 after treatment by coibamide A, but also revealed that protease-dependent degradation is involved in coibamide A induced down-regulation of GRP78. Moreover, the results of immunofluorescence studies showed a comprehensive decrease of GRP78 protein both inside and outside of ER, we have adequate evidence to conclude coibamide A not only inhibits the biosynthesis of GRP78 but also caused degradation of existing GRP78. Until now coibamide A displays an apratoxin A-like actions in cells. In cellular thermal shift assay, both coibamide A and apratoxin A induced the thermal stabilization of translocon protein sec61α. This result strongly indicates that Sec61α subunit is the direct binding target of coibamide A and apratoxin A. Now total synthesis of coibamide A has been achieved. Based on the characteristic inhibitory profile of coibamide A, valinomycin and apratoxin A, after some pharmaceutical optimism, these secretory inhibitors can be exploited for the development of new therapeutic and anticancer applications.

In summary, we developed a workflow (Figure 5.8) for the discovery of new secretion pathway inhibitors. Among the pure compounds we tested, coibamide A was the only compound that appeared to target the co-translational translocation machinery.

Acknowledgments

Author Contributions: J.E.I. conceived and designed the experiments; K.L.M. contributed materials and edited the manuscript; X.W., J.D.S.,,D.R.M. and I.R.H. performed the experiments; J.D.S., X.W and J.E.I. analyzed the data and wrote the manuscript.

References

1. Walter, P. and A.E. Johnson, *Signal sequence recognition and protein targeting to the endoplasmic reticulum membrane.* Annu Rev Cell Biol, 1994. **10**: p. 87-119.
2. De Raedt, T., et al., *Exploiting cancer cell vulnerabilities to develop a combination therapy for ras-driven tumors.* Cancer Cell, 2011. **20**(3): p. 400-13.
3. Dejeans, N., et al., *Addicted to secrete - novel concepts and targets in cancer therapy.* Trends Mol Med, 2014. **20**(5): p. 242-50.
4. Liu, Y., B.K. Law, and H. Luesch, *Apratoxin a reversibly inhibits the secretory pathway by preventing cotranslational translocation.* Mol Pharmacol, 2009. **76**(1): p. 91-104.
5. Medina, R.A., et al., *Coibamide A, a potent antiproliferative cyclic depsipeptide from the Panamanian marine cyanobacterium Leptolyngbya sp.* J Am Chem Soc, 2008. **130**(20): p. 6324-5.
6. Serrill, J.D., et al., *Coibamide A, a natural lariat depsipeptide, inhibits VEGFA/VEGFR2 expression and suppresses tumor growth in glioblastoma xenografts.* Invest New Drugs, 2016. **34**(1): p. 24-40.
7. Hau, A.M., et al., *Coibamide A induces mTOR-independent autophagy and cell death in human glioblastoma cells.* PLoS One, 2013. **8**(6): p. e65250.
8. Wan, X., et al., *ATG5 Promotes Death Signaling in Response to the Cyclic Depsipeptides Coibamide A and Apratoxin A.* Mar Drugs, 2018. **16**(3).
9. Gorlich, D., et al., *A mammalian homolog of SEC61p and SECYp is associated with ribosomes and nascent polypeptides during translocation.* Cell, 1992. **71**(3): p. 489-503.
10. Hendershot, L.M., *The ER function BiP is a master regulator of ER function.* Mt Sinai J Med, 2004. **71**(5): p. 289-97.
11. Hamman, B.D., L.M. Hendershot, and A.E. Johnson, *BiP maintains the permeability barrier of the ER membrane by sealing the lumenal end of the translocon pore before and early in translocation.* Cell, 1998. **92**(6): p. 747-58.
12. Otero, J.H., B. Lizak, and L.M. Hendershot, *Life and death of a BiP substrate.* Semin Cell Dev Biol, 2010. **21**(5): p. 472-8.
13. Glembotski, C.C., *The role of the unfolded protein response in the heart.* J Mol Cell Cardiol, 2008. **44**(3): p. 453-9.
14. Brodsky, J.L., *Cleaning up: ER-associated degradation to the rescue.* Cell, 2012. **151**(6): p. 1163-7.
15. Daneshmand, S., et al., *Glucose-regulated protein GRP78 is up-regulated in prostate cancer and correlates with recurrence and survival.* Hum Pathol, 2007. **38**(10): p. 1547-52.
16. Scriven, P., et al., *Activation and clinical significance of the unfolded protein response in breast cancer.* Br J Cancer, 2009. **101**(10): p. 1692-8.
17. Pyrko, P., et al., *The unfolded protein response regulator GRP78/BiP as a novel target for increasing chemosensitivity in malignant gliomas.* Cancer Res, 2007. **67**(20): p. 9809-16.
18. Thornburg, C.C., et al., *Apratoxin H and apratoxin A sulfoxide from the Red Sea cyanobacterium Moorea producens.* J Nat Prod, 2013. **76**(9): p. 1781-8.

19.   Jafari, R., et al., *The cellular thermal shift assay for evaluating drug target interactions in cells.* Nat Protoc, 2014. **9**(9): p. 2100-22.

20.   Badr, C.E., T. Wurdinger, and B.A. Tannous, *Functional drug screening assay reveals potential glioma therapeutics.* Assay Drug Dev Technol, 2011. **9**(3): p. 281-9.

21.   Prodromou, C., et al., *Identification and structural characterization of the ATP/ADP-binding site in the Hsp90 molecular chaperone.* Cell, 1997. **90**(1): p. 65-75.

22.   Thastrup, O., et al., *Thapsigargin, a tumor promoter, discharges intracellular Ca2+ stores by specific inhibition of the endoplasmic reticulum Ca2(+)-ATPase.* Proc Natl Acad Sci U S A, 1990. **87**(7): p. 2466-70.

23.   Paatero, A.O., et al., *Apratoxin Kills Cells by Direct Blockade of the Sec61 Protein Translocation Channel.* Cell Chem Biol, 2016. **23**(5): p. 561-566.

24.   Huang, K.C., et al., *Apratoxin A Shows Novel Pancreas-Targeting Activity through the Binding of Sec 61.* Mol Cancer Ther, 2016. **15**(6): p. 1208-16.

25.   Johnson, A.E. and M.A. van Waes, *The translocon: a dynamic gateway at the ER membrane.* Annu Rev Cell Dev Biol, 1999. **15**: p. 799-842.

26.   Huber, A.L., et al., *p58(IPK)-mediated attenuation of the proapoptotic PERK-CHOP pathway allows malignant progression upon low glucose.* Mol Cell, 2013. **49**(6): p. 1049-59.

27.   Denoyelle, C., et al., *Anti-oncogenic role of the endoplasmic reticulum differentially activated by mutations in the MAPK pathway.* Nat Cell Biol, 2006. **8**(10): p. 1053-63.

28.   Carrasco, D.R., et al., *The differentiation and stress response factor XBP-1 drives multiple myeloma pathogenesis.* Cancer Cell, 2007. **11**(4): p. 349-60.

29.   Luo, B. and A.S. Lee, *The critical roles of endoplasmic reticulum chaperones and unfolded protein response in tumorigenesis and anticancer therapies.* Oncogene, 2013. **32**(7): p. 805-18.

30.   Van den Berg, B., et al., *X-ray structure of a protein-conducting channel.* Nature, 2004. **427**(6969): p. 36-44.

31.   Gogala, M., et al., *Structures of the Sec61 complex engaged in nascent peptide translocation or membrane insertion.* Nature, 2014. **506**(7486): p. 107-10.

32.   McKenna, M., R.E. Simmonds, and S. High, *Mechanistic insights into the inhibition of Sec61-dependent co- and post-translational translocation by mycolactone.* J Cell Sci, 2016. **129**(7): p. 1404-15.

33.   Schauble, N., et al., *Interaction of Pseudomonas aeruginosa Exotoxin A with the human Sec61 complex suppresses passive calcium efflux from the endoplasmic reticulum.* Channels (Austin), 2014. **8**(1): p. 76-83.

34.   Mackinnon, A.L., et al., *An allosteric Sec61 inhibitor traps nascent transmembrane helices at the lateral gate.* Elife, 2014. **3**: p. e01483.

35.   Harant, H., et al., *The translocation inhibitor CAM741 interferes with vascular cell adhesion molecule 1 signal peptide insertion at the translocon.* J Biol Chem, 2006. **281**(41): p. 30492-502.

36.   Junne, T., et al., *Decatransin, a new natural product inhibiting protein translocation at the Sec61/SecYEG translocon.* J Cell Sci, 2015. **128**(6): p. 1217-29.

37. Kim, J., et al., *Specific inhibition of hamster prion protein translocation by the dodecadepsipeptide valinomycin.* Exp Cell Res, 2013. **319**(13): p. 2049-57.

38. Schauble, N., et al., *BiP-mediated closing of the Sec61 channel limits Ca2+ leakage from the ER.* EMBO J, 2012. **31**(15): p. 3282-96.

39. Dierks, T., et al., *A microsomal ATP-binding protein involved in efficient protein transport into the mammalian endoplasmic reticulum.* EMBO J, 1996. **15**(24): p. 6931-42.

40. Radons, J., *The human HSP70 family of chaperones: where do we stand?* Cell Stress Chaperones, 2016. **21**(3): p. 379-404.

41. Lee, A.S., *Glucose-regulated proteins in cancer: molecular mechanisms and therapeutic potential.* Nat Rev Cancer, 2014. **14**(4): p. 263-76.

42. Milovancev, M., et al., *Comparative analysis of the surface exposed proteome of two canine osteosarcoma cell lines and normal canine osteoblasts.* BMC Vet Res, 2013. **9**: p. 116.
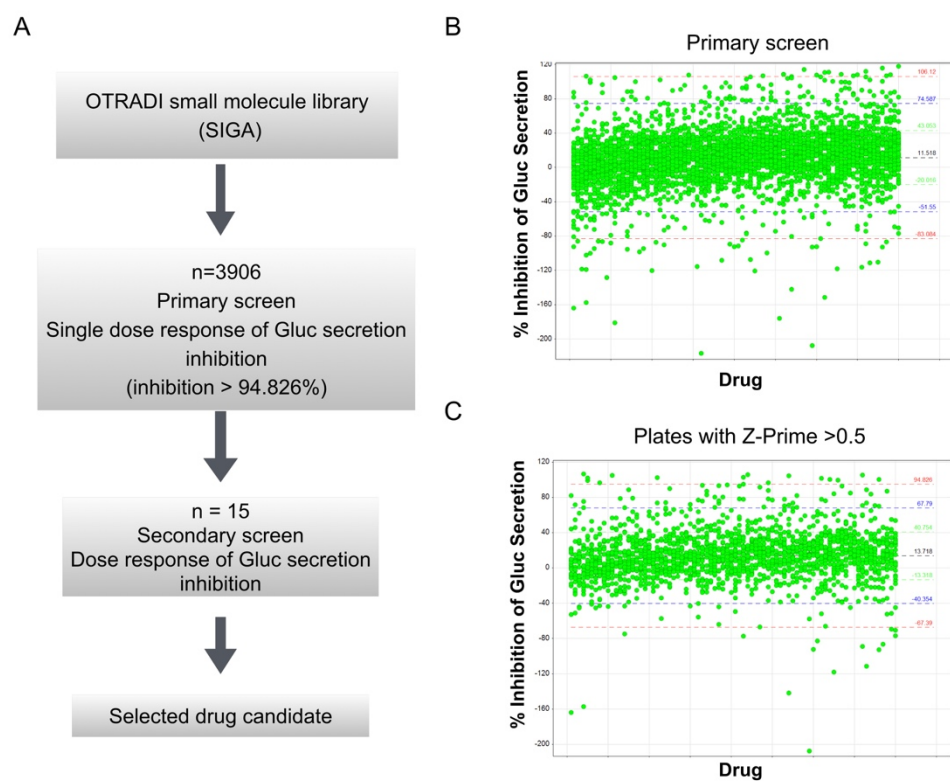
Figure 5.1. Gluc functional screening assay.

(A) A general flowchart showing the steps of screening assay. (B) Scatter plot of the 3,906 compounds tested(upper) or only 1965 compounds in plates with Z-Prime >0.5 (lower). Results are presented as percentage of Gluc expression in which the negative control (0.1%DMSO) was set at 0% and positive control 100nM Apratoxin A was set at 100%.
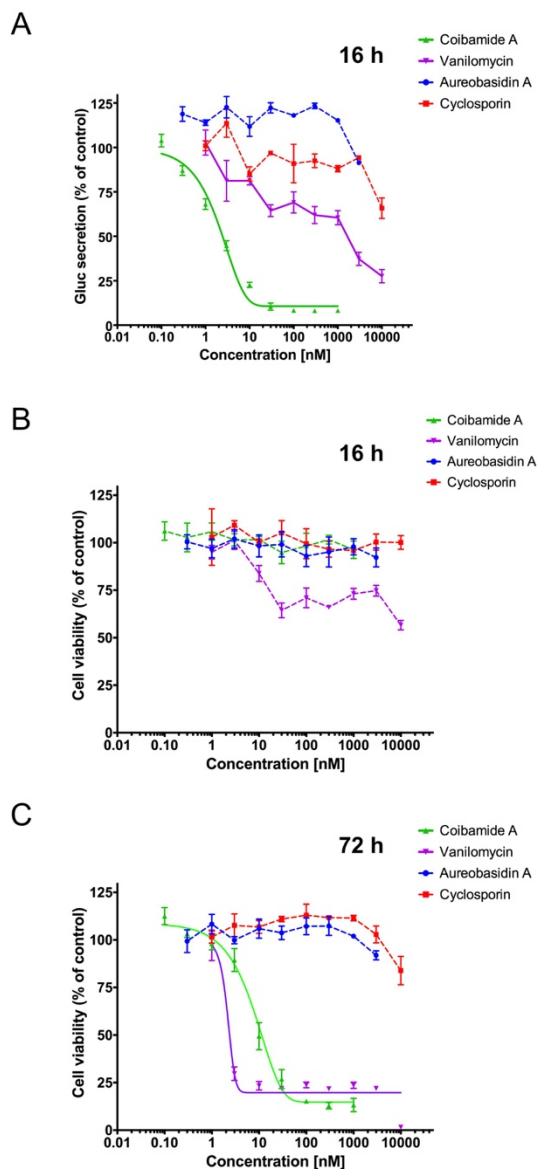
Figure 5.2. Gluc secretion and cell viability inhibition of natural products.

Coibamide A, vanilomycin, aureobasidin A and cyclosporin A – induced inhibition of Gaussia luciferase (Gluc) secretion (A) and cell viability (B)(C) in U87-MG glioblastoma cells. Gluc-infected U87-MG and normal U87-MG cells were seeded at a density of 3000 cells/well, treated the following day with increasing concentrations of coibamide A (0.1nM - 1μM), vanilomycin (1nM - 10 μM), aureobasidin A (0.3nM-3μM), or cyclosporin A (1nM - 10 μM) for indicated time in serum-enriched medium, and assessed for their secretory activity using the substrate coelenterazine (1.2 μM final concentration) to Gluc-infected U87-MG and cell viability using Celltiter Glo to Gluc-infected U87-MG (16 h) and U87-MG cells (72hr). Figure is representative from three independent experiments.
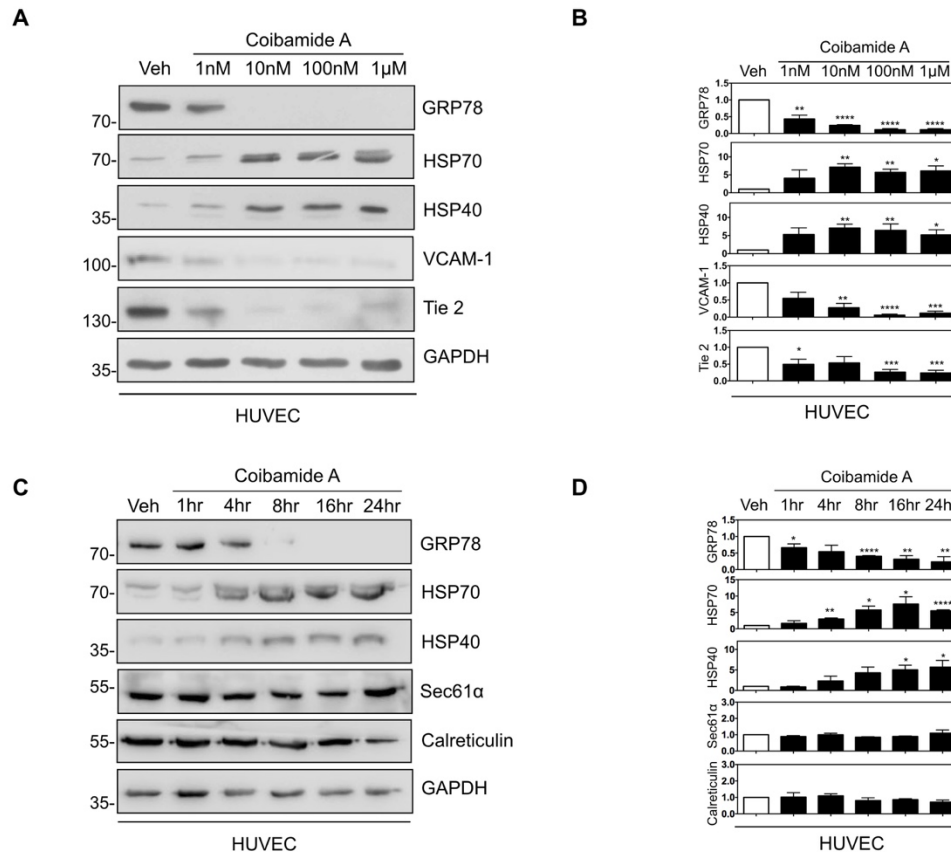
Figure 5.3. Coibamide A decreased GRP78/BiP and induces cell stress in HUVECs in a dose and time dependent manner.

(A) Immunoblot analysis of GRP78, HSP70, HSP40, vascular cell adhesion protein 1 (VCAM-1) and tyrosine-protein kinase receptor 2 in HUVECs. Cells were incubated in complete media with 0.1%DMSO (vehicle), 1nM, 10nM, 100nM and 1uM coibamide A for 24 h. Whole cell lysates were harvest. Figure is representative from three independent experiments. (B) Histograms show quantification of immunoblot data of (A) from three independent experiments, normalized to GAPDH and relative to vehicle lysates (* P< 0.05, ** P < 0.01, *** P < .001, compared to vehicle, N = 3). (C) Immunoblot analysis of ER resident proteins GRP78, sec61α, calreticulin, and cytosolic cell stress marker heat shock protein 70 and 40 (HSP70, HSP40) in human umbilical vein endothelial cells (HUVEC). Cells were incubated in complete media with 0.1%DMSO (vehicle) for 24 h or 30nM coibamide A for 1, 4, 8, 16 or 24 h. Whole cell lysates were harvest. Figure is representative from three independent experiments. (D) Histograms show quantification of immunoblot data of (C) from three independent experiments, normalized to GAPDH and relative to vehicle lysates (* P< 0.05, ** P < 0.01, *** P < .001, compared to vehicle, N = 3).
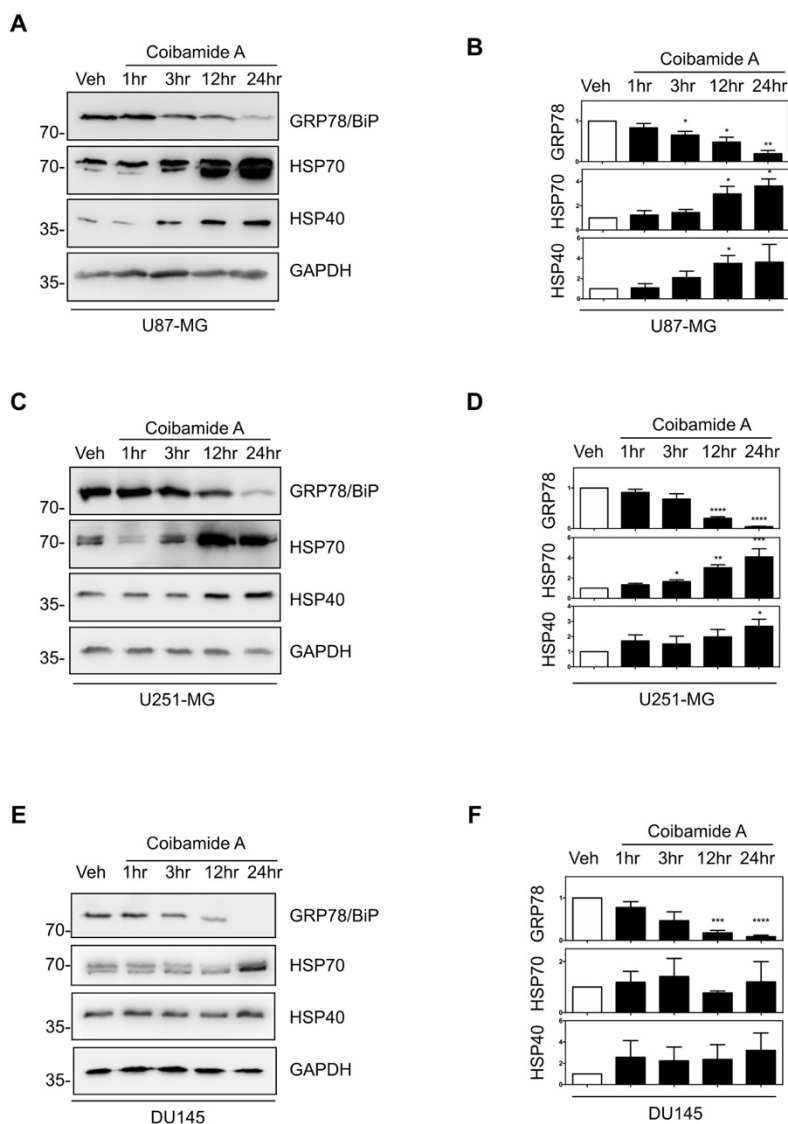
Figure 5.4. Coibamide A inhibits GRP78 expression and induce cytosolic cell stress in cancer cell lines in a time-dependent manner.

(A)(C)(E) Immunoblot analysis of GRP78, heat shock protein 70 and 40 expressions in human U87-MG glioblastoma cells, U251 glioblastoma cells (B) and DU145 prostate cancer cells (E). Cells were incubated in complete media with 0.1% DMSO (vehicle) for 24 h or 30nM coibamide A for 1 h, 3 h, 12 h or 24 h. Figures are representatives from three independent experiments. (B)(D)(F) Histograms show quantification of immunoblot data from three independent experiments, normalized to GAPDH and relative to vehicle lysates (** P < 0.01, *** P < .001, compared to vehicle, N=3).
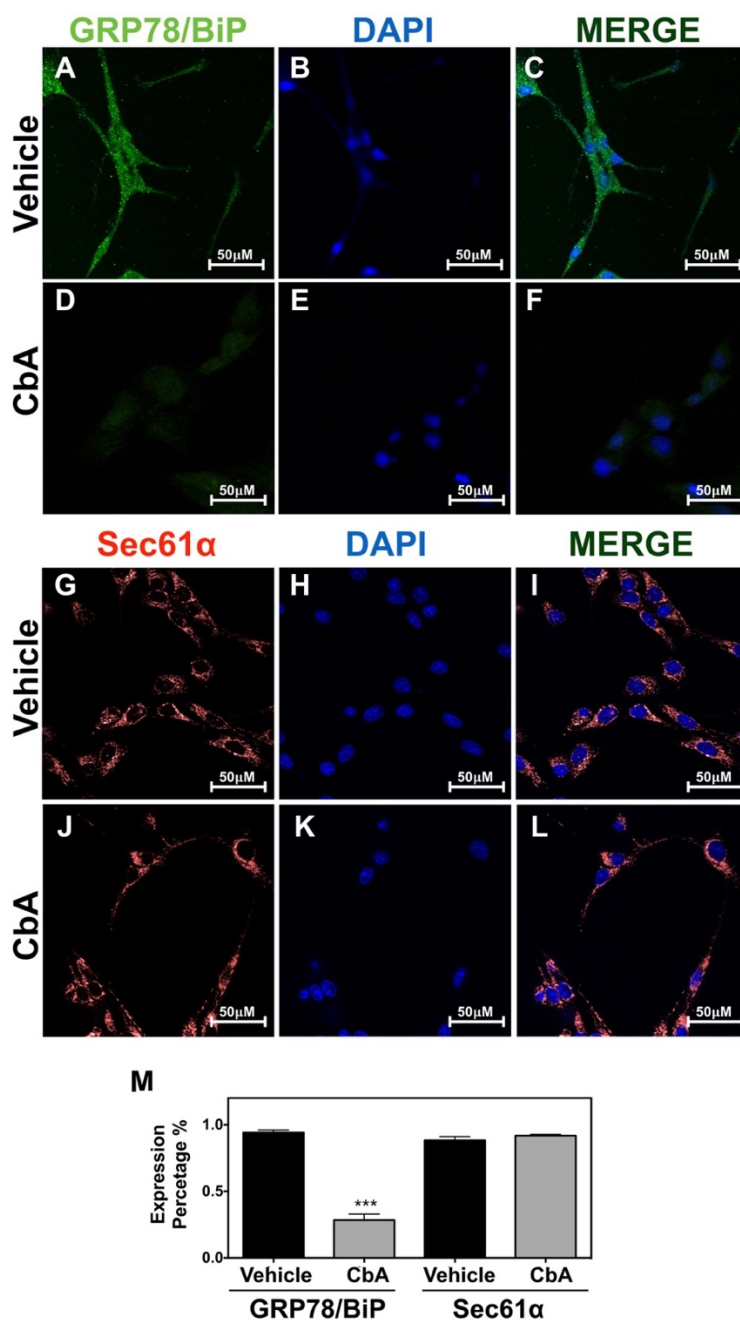
Figure 5.5. Immunofluorescence analyses of GRP78 and sec61α expression in U87-MG after treatment of coibamide A.

Cells were harvest after 24 h exposure of 30nM coibamide A and incubated with primary GRP78 antibody or sec61 α and secondary cy2 antibody(green) or cy3 antibody(red), in respect. DAPI(blue) was used as a nuclear counterstain. Bar represents 50μm. Figures are representatives from three independent experiments.
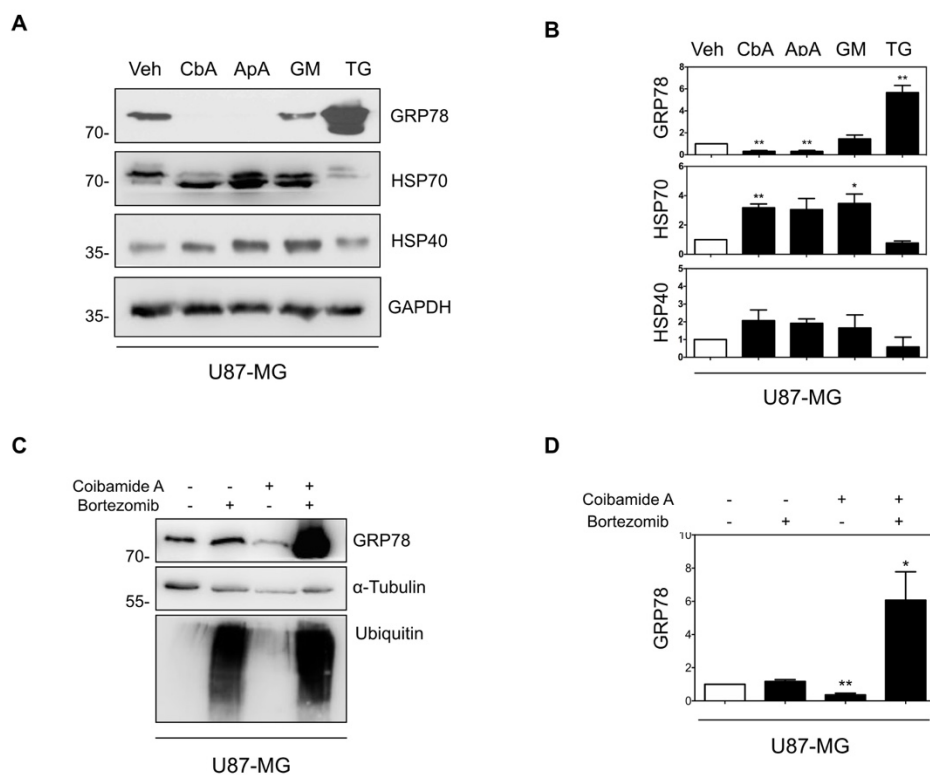
Figure 5.6. ER stress or HSP90 inhibition is not implicated in the reduction of GRP78/BiP level by coibamide A.

(A) Immunoblot analysis of GRP78/BiP, heat shock protein 70 and 40 expressions in glioblastoma cells (U87-MG). Cells were incubated in complete media with 0.1%DMSO (vehicle), 30nM coibamide A, 30nM apratoxin A, 300nM geldanamycin, 3uM thapsigargin for 24 h. Whole cell lysate was harvest. (B) Histograms show quantification of immunoblot data from three independent experiments, normalized to GAPDH and relative to vehicle lysates (** P < 0.01, *** P < .001, compared to vehicle). (C) Proteasome-dependent degradation is involved in coibamide A induced downregulation of GRP78/BiP. Immunoblot analysis of GRP78/BiP and ubiquitin in glioblastoma U87-MG cells. Cells were incubated in complete media with 0.1%DMSO (vehicle), 25nM bortezomib or 30nM coibamide A for 24 h. Cell lysates then was harvest. Figures are representatives from three independent experiments.
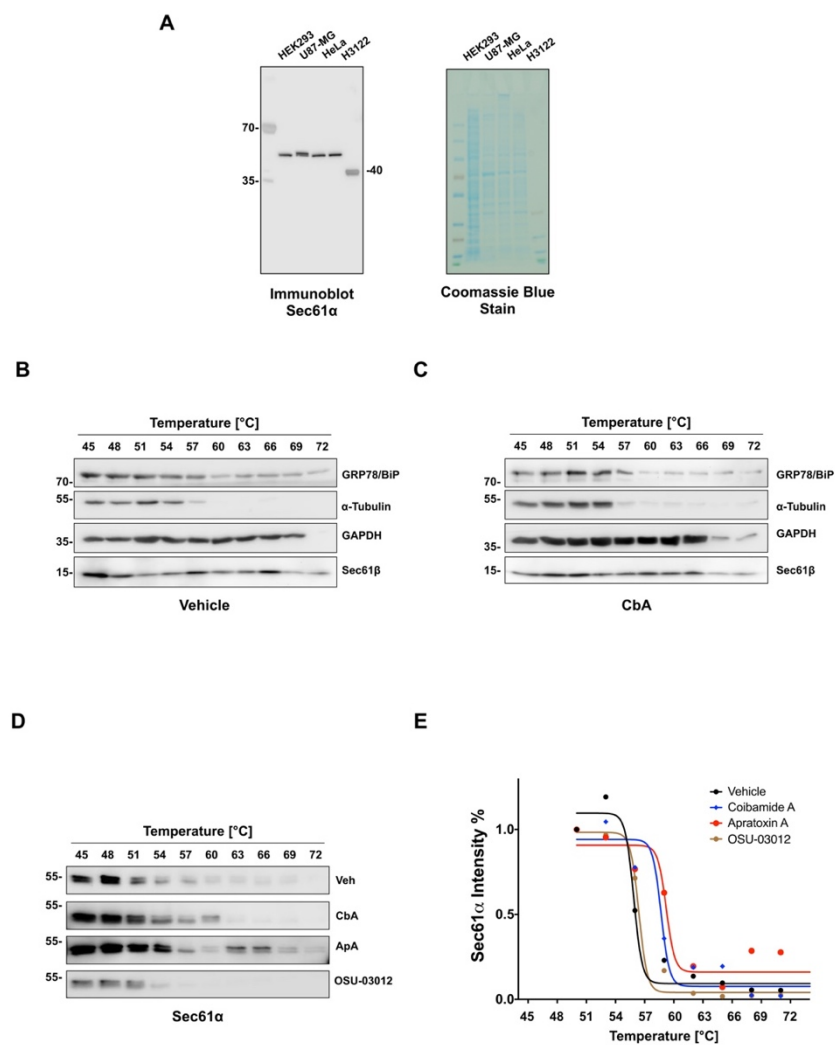
Figure 5.7. Cellular Thermal Shift Assay on U87-MG cells.

(A) Immunoblot analysis of human embryonic kidney HEK293, human U87-MG glioblastoma, HeLa cervical cancer and H3122 lung cancer cells. Two identical gels were running side-by-side, the gels were either stain by coomassie blue or transferred to membrane, and the whole membrane was probed for sec61α proteins. (B)(C) Immunoblot analysis of intact U87-MG cells treated by vehicle (0.1% DMSO) or 300nM coibamide A for 1 h. Cells were incubated in indicated temperature and the loaded on gels to analysis immunoactivity of indicated proteins. (D) Immunoblot analysis of U87-MG cells exposed to vehicle (0.1% DMSO), 1µM coibamide A, apratoxin A or OSU-03012 for 1 h. Cells were incubated in indicated temperature and the loaded on gels to analysis immunoactivity of sec61α. (E) The apparent melting curve analyzed from (D) measuring relative sec61α intensity compare to band intensity under temperature of 45 Celsius. The figure is a representative of three independent experiments.
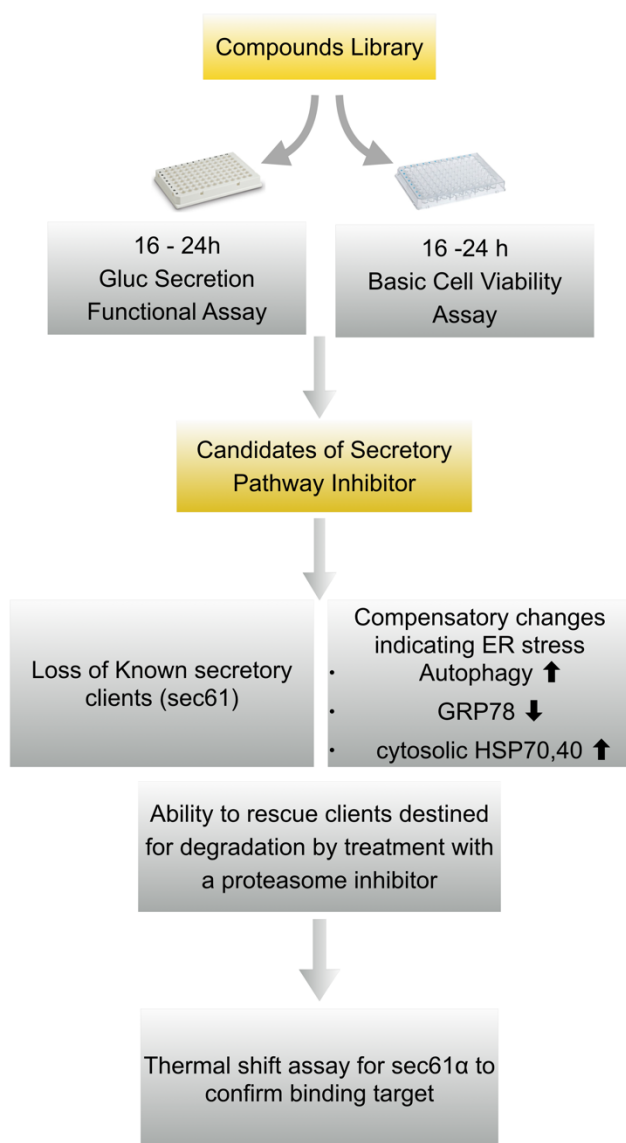
Figure 5.8. A workflow for the discovery of new inhibitors of protein secretion.
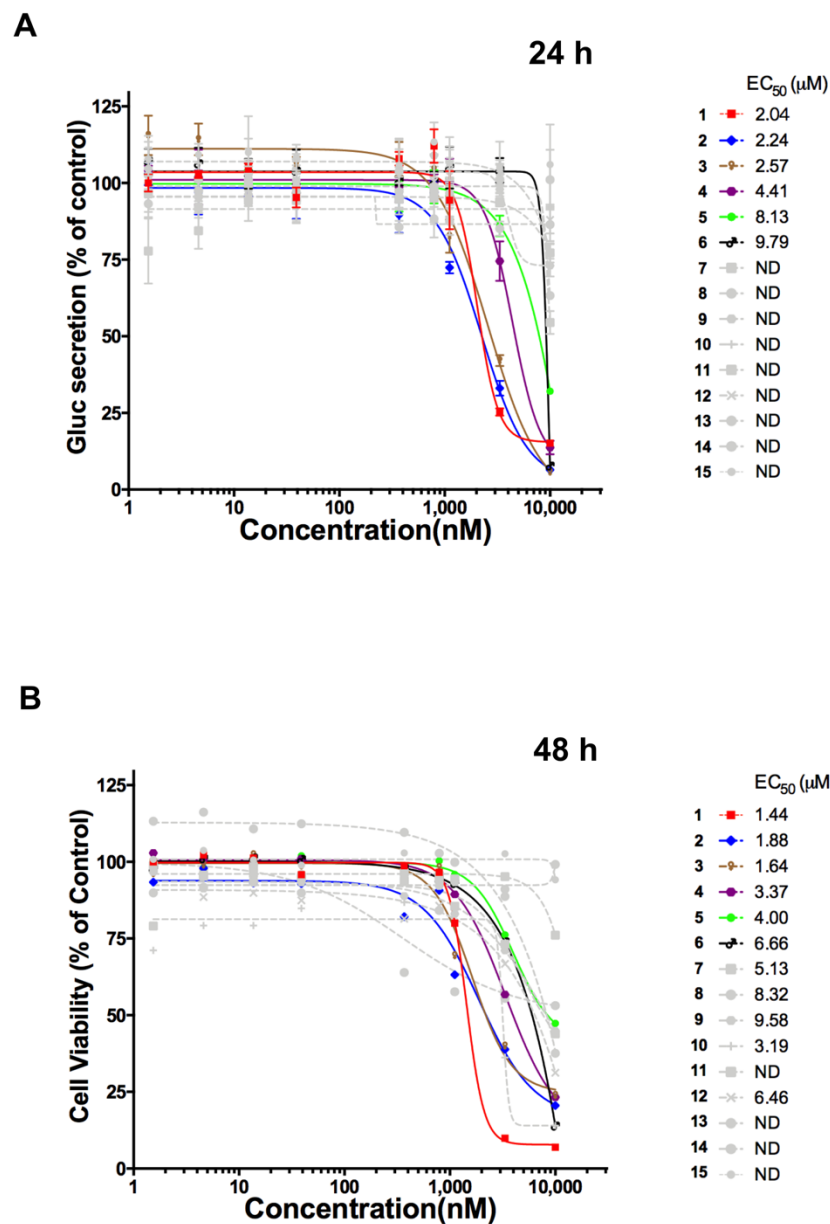
Supplementary S5.1 Dose response curses of Gluc secretion and cell viability of Gluc-U87 treated by hits 1 -15.

Cell were seeded at density of 3,000 cells/well, and treated by hits 1-15 from a range of 3nm-10μM. Gluc secretion was measured at 24 h. Cell viability was measured at 48 h. Figures are representatives from three independent experiments.
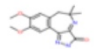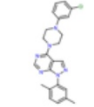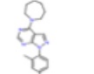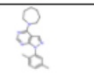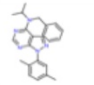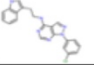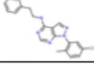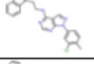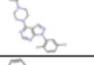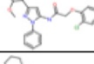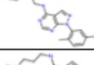
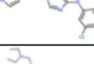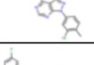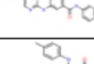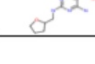| ID	Structure	Library ID	PubChem CID	MW	Inhibition of Gluc secretion (%)	Survival(%)
1		OTR-0169930-001	701785	287.31	102.0	39.3
2		OTR-0241111-001	17017315	418.92	105.8	39.5
3		OTR-0241072-001	17017336	341.84	99.1	44.7
4		OTR-0241121-001	17017322	321.42	104.3	34.6
5		OTR-0241131-001	17017318	371.48	100.3	40.2
6		OTR-0241037-001	17017213	388.85	96.8	35.9
7		OTR-0240905-001	7205433	363.84	100.4	58.1
8		OTR-0240895-001	17017492	402.88	99.6	38.3
9		OTR-0240920-001	17017381	404.9	104.9	35.8
10		OTR-0240419-001	16030793	433.89	101.5	42.5
11		OTR-0240679-001	16033909	367.88	96.5	40.1
12		OTR-0240872-001	16033976	367.84	102.8	40.7
13		OTR-0240901-001	17017485	358.87	105.4	24.2
14		OTR-0241169-001	50826567	469.51	102.3	35.7
15		OTR-0240400-001	3801214	344.37	95.0	48.8

Table 5.1. Summary of 15 hits from screening from small molecule library.

Table of 15 hits from plates with Z-prime >0.5 with ORADI ID, Pubchem ID, molecular weight (MW), percentage of 48hr survival, and percentage of inhibition of Gluc secretion in 16 h. A "hit" is a compound that inhibited the signal by more than three times the standard deviation away from the mean inhibition of all the compounds in the subsets of plates with Z-Prime >0.5.

Compound	EC$_{50}$ (nM) ± SEM (16 h)		EC$_{50}$ (nM) ± SEM (72 h)
	Gluc secretion	Cell Viability	Cell Viability
Coibamide A	4.3 ± 1.5	>1,000	10.5 ± 1.1
Vanilomycin	3166 ± 897	> 10,000	8.2 ± 3.1
Aureobasidin A	>3,000	>3,000	>3,000
Cyclosporin	>10,000	>10,000	>10,000

Table 5.2. Coibamide A, vanilomycin, aureobasidin A and cyclosporin A – induced inhibition of Gaussia luciferase (Gluc) secretion and cell viability in U87-MG glioblastoma cells.

GENERAL CONCLUSION

CHAPTER 6

Xuemei Wan

Cancer is a group of diseases involving abnormal cell growth with the potential to invade or spread to other parts of the body (*"Defining Cancer". National Cancer Institute. Retrieved 28 March 2018).* The hallmarks of cancer were proposed by Douglas Hanahan and Robert Weinberg from 2000. The hallmarks include sulf-sufficiency in growth signals, evading apoptosis, and abnormal metabolic pathways [1]. In the needs of invading and metastasis, cancer cells have both abnormally up-regulated metabolism and secretion activity, making these two systems potential targets in cancer treatment.

The marine natural product mandelalide A has been recently found to be a direct inhibitor of ATP synthase. We revealed that mandelalide A induces transient activation of AMP-activated protein kinase pathway in LKB1-dependent manner in several cancer cells. Mandelalide A induces synergistic affect in combination with first-line antitumor agents erlotinib and paclitaxel on EGFR mutant non-small cell lung cancer cells. Clinically used mitochondrial inhibitors like metformin and phenformin have been studied for potential cancer metabolism-based therapeutics to selectively target LKB1-deficient tumors [2]. As a more potent anti-proliferative mitochondrial inhibitor, after further in vivo study, mandelalide A could be the next drug as an adjuvant chemotherapy reagents for clinical use.

Two other marine natural products Coibamide A and apratoxin A were found to use autophagy-related protein 5 (ATG5) to promote death signaling [3]. Mouse embryonic fibroblasts (MEFs) with functional autophagy are more sensitive to coibamide A, whereas ATG5-/- deficient MEFs displayed delayed decrease of cell viability to coibamide A treatment. Our understanding of autophagy and lysosomal functions have been greatly enhanced by the discovery of natural product structures that can serve as chemical probes to reveal new patterns of signal transduction in cells. Coibamide A and apratoxin A appear to be examples of cytotoxic natural products that promote cross-signaling between ATG5-dependent autophagy and caspase-dependent apoptosis.

Glucose regulated proteins are stress-inducible molecular chaperones that belong to the heat shock protein (HSP) family. GRP78 is found in the endoplasmic reticulum (ER), a critcal organelle for regulation of secretory protein quality control.

GRP78 facilitates protein folding and assembly, as well as the export of misfolded proteins for degradation. Promising agents are being developed to target GRP78 as novel anticancer therapeutics. We discovered GRP78 is an indirect target of coibamide A, and the decrease of GRP78 induced a compensatory up-regulation of cytosolic chaperone heat shock protein 70 and 40. Even though more research is needed to validate and explain the specificity of GRP78 by coibamide A, our results raise the possibility of coibamide A to be used as clinically useful GRP78 inhibitor.

High basal expression of GRP78, and distribution to cellular compartments outside the endoplasmic reticulum (ER), is increasingly associated with several treatment-resistant human cancers. We characterized GRP78 expression in canine osteosarcoma cells under basal conditions and in response to treatment of an indirect GRP78 inhibitor OSU-03012. These results suggest that advances in detection and targeting of GRP78 may eventually benefit a sub-set of both canine and human patients. Recently studies have found that GRP78 can be actively translocated to other cellular locations and assume novel functions that control signaling, proliferation, invasion, apoptosis and immunity. Mouse models further identified their specific roles in tumorigenesis, metastasis and angiogenesis. (Reviewed in [4]). In the view of dramatic reduction of GRP78 caused by coibamide A and apratoxin A, it would be valuable to discover the direct signaling changes that are controlled by GRP78 after treated by coibamide A. For example, GRP78 plays a critical role in limiting Ca^{2+} exit from ER to cytosol. Calcium leakage from Sec61 translocon caused by loss of GRP78 may be very pronouced that it makes ER susceptible to ER stress or even apoptosis [5] [6]. We predicted that the loss of calcium homeostasis to be a determinant cell death triggger that caused by coibamide A, which in future would be validated by a calcium imaging study on living cells.

As mentioned before, the secretory pathway is a novel target in cancer therapy. We developed a workflow for discovery of secretion inhibitors by combining a functional Gluc secretion assay with recognized cell viability assays. We used this workflow to identify small molecules as potential inhibitors of secretory function, and revealed similar activity for known natural products coibamide A and

valinomycin. Further study for the candidates would be needed to reveal whether the secretory inhibition is caused by direct or indirect mechanism. The parallel measurements of secretory function and cell viability is a reasonable way to distinguish a direct secretory inhibition and an effect caused by cell death signaling and provides an efficient method for future screening of synthetic and natural product libraries.

Using a cellular thermal shift assay, we identified the translocon protein Sec61α as the likley direct binding target of coibamide A and apratoxin A. This result is consistent to our previous study which shows a group of secretory proteins (VEGFA, VEGFR2 [7], VCAM) were inhibited by coibamide A. What is needed to be determined is whether this binding of this translocon protein causes a non-specific inhibition of secretory pathway or a selective block of client proteins. This assay may have great potential for future validation of Sec61-interactinhg prioteins as it is amenable for small scale studies on cultured cells with basic laboratory equipment. This is particularly significant for the study of natural products where the scope and scale of any biological evaluation is typically limited by the availabilty of small quantities of field-collected material in the early stages of investigation before synthetic routes are established.

The secretome in cancer cells has been revealed to have differenct signiture than non-tumorous cells. In a study of the protein composition of the secretomes of 16 primary and established cell lines of pancreatic ductal adenocarcinoma, 112 proteins, including IL10, VCAM1, exhibited significantly different abundances[8]. The advanced secretome signiture of cancer cells raised the possibility of using coibamide A-like secretory inhibitors as future thereaputic strategy in cancer treatment. Future study on the scale of secretory inhibition by coibamide A using proteomic approaches need to be done to reveal the specificity of coibamide A activity.

Reference

1. Hanahan, D. and R.A. Weinberg, *The hallmarks of cancer.* Cell, 2000. **100**(1): p. 57-70.
2. Shackelford, D.B., et al., *LKB1 inactivation dictates therapeutic response of non-small cell lung cancer to the metabolism drug phenformin.* Cancer Cell, 2013. **23**(2): p. 143-58.
3. Wan, X., et al., *ATG5 Promotes Death Signaling in Response to the Cyclic Depsipeptides Coibamide A and Apratoxin A.* Mar Drugs, 2018. **16**(3).
4. Lee, A.S., *Glucose-regulated proteins in cancer: molecular mechanisms and therapeutic potential.* Nat Rev Cancer, 2014. **14**(4): p. 263-76.
5. Johnson, G.G., et al., *The deadly connection between endoplasmic reticulum, Ca2+, protein synthesis, and the endoplasmic reticulum stress response in malignant glioma cells.* Neuro Oncol, 2014. **16**(8): p. 1086-99.
6. Lang, S., et al., *Sec61 complexes form ubiquitous ER Ca2+ leak channels.* Channels (Austin), 2011. **5**(3): p. 228-35.
7. Serrill, J.D., et al., *Coibamide A, a natural lariat depsipeptide, inhibits VEGFA/VEGFR2 expression and suppresses tumor growth in glioblastoma xenografts.* Invest New Drugs, 2016. **34**(1): p. 24-40.
8. Mustafa, S., et al., *Comparison of the tumor cell secretome and patient sera for an accurate serum-based diagnosis of pancreatic ductal adenocarcinoma.* Oncotarget, 2017. **8**(7): p. 11963-11976.